UC Berkeley
UC Berkeley Electronic Theses and Dissertations

Title

Optogenetic stimulation, and control or promotion of epileptiform activity, in a mean field model of the human cortex

Permalink

https://escholarship.org/uc/item/16m0w1m3

Author

Selvaraj, Prashanth

Publication Date

2015

Peer reviewed|Thesis/dissertation

eScholarship.org Powered by the California Digital Library
University of California

Optogenetic stimulation, and control or promotion of epileptiform activity, in a mean field model of the human cortex

by

Prashanth Selvaraj

A dissertation submitted in partial satisfaction of the

requirements for the degree of

Doctor of Philosophy

in

Engineering – Mechanical Engineering

in the

Graduate Division

of the

University of California, Berkeley

Committee in charge:

Professor Andrew J. Szeri, Chair
Professor Bruno Olshausen
Professor Jamie Sleigh
Professor Mohammad-Reza Alam

Spring 2015

Optogenetic stimulation, and control or promotion of epileptiform activity, in a mean field model of the human cortex

Copyright 2015
by
Prashanth Selvaraj

Abstract

Optogenetic stimulation, and control or promotion of epileptiform activity, in a mean field model of the human cortex

by

Prashanth Selvaraj

Doctor of Philosophy in Engineering – Mechanical Engineering

University of California, Berkeley

Professor Andrew J. Szeri, Chair

Epilepsy is a neural network disorder that manifests when certain elements (neuron types, subnetworks) malfunction or fail. Epileptiform activity, in turn, is characterized by the excessive synchronous firing of populations of neurons. In this dissertation, we present a mathematical model of the human cortex based on the activity of populations of neurons best captured at the meso-scale to study epileptic seizure dynamics. We then investigate further developments of the use of a spatially, temporally and cell type specific stimulation technique called optogenetics to trigger or to inhibit epileptiform activity in the cortical model.

Optogenetics involves the genetic modification of a host neuron to express light activated ion channels. To incorporate this method of stimulation into the meso-scale cortical model, we first develop a scale free mathematical model of optogenetic channel dynamics, which enables study of micro-scale level optogenetic activity at the meso-scale. We then integrate the optogenetic model into the meso-scale cortical model to study the combined dynamics of cortico-optogenetic activity in time and two spatial dimensions. Through this combined model, we explore the efficacy of optogenetic stimulation in an open loop configuration to inhibit epileptic seizures. Next, we close the loop using techniques of classical control theory, and investigate the controllability of seizures in two parameter spaces that correspond well with patient seizure data. By basing our control effort on measurements of cortical activity that are clinically relevant, we aim to provide a physiologically safe and efficient way of seizure inhibition. We also study the dynamics of the combined cortico-optogenetic model using bifurcation analysis. We then explore the use of optogenetic stimulation as an excitatory technique to drive seizure like activity in a normally functioning cortical model. All of this makes a strong case for the consideration of optogenetics as a highly specific cortical stimulation modality in seizure research.

Finally, we present preliminary results from work that describes the link between cortical metabolic demands and cortical activity. A quantitative definition of this link will aid in reconciling the different temporal scales of electrode measurements and imaging techniques like functional magnetic resonance imaging, while also providing a clearer picture of the role of glucose

and oxygen metabolism in multiple states of cortical activity, such as normal sleep, awake, and seizure states.

Contents

Contents **i**

List of Figures **iii**

List of Tables **viii**

1 Introduction **1**
- 1.1 Epilepsy and seizures 1
- 1.2 Optogenetics 2
  - 1.2.1 Optogenetics and epilepsy 4
- 1.3 Applied control theory 4
- 1.4 2D cortical model 6
- 1.5 Seizure like activity in the model cortex 8
- 1.6 Layout of this dissertation 10

2 Open loop optogenetic control **12**
- 2.1 Meso scale optogenetics model 12
- 2.2 Open loop control 15
  - 2.2.1 Constant illumination 16
  - 2.2.2 Pulsed Illumination 18
- 2.3 Robustness of open loop optogenetic stimulation 20
  - 2.3.1 Stochastic inputs 20
  - 2.3.2 Seizure hotspot 20
  - 2.3.3 Changes in cortical model parameters 22
- 2.4 Summary of original contributions 24

3 Closed loop Optogenetic control **25**
- 3.1 Development of the control law 25
  - 3.1.1 Triggering and deploying control 27
  - 3.1.2 Tuning the controller 28
- 3.2 Seizures in the P_{ee}-Γ_e space 29
  - 3.2.1 Seizures with $\Gamma_e = 0.00066$ and $\alpha = 1.15$ 29

3.2.2 Seizures with Γ_e = 0.0008 and $\alpha = 1.6$ 32
3.2.3 Robust control 33
3.3 Seizures in the g_e-Γ_i space 34
3.4 Summary of original contributions 36

4 The ODE Model 37
4.1 The ODE model 38
4.2 Bifurcations in the P_{ee}-Γ_e space 39
4.2.1 Seizures in parameter space 42
4.3 Seizures in the g_e-Γ_i space 42
4.4 Summary 43

5 Stimulating seizures using optogenetics 45
5.1 Optogenetic stimulation of the excitatory population in a normally functioning model cortex 45
5.2 Constant illumination 46
5.3 Pulsed illumination 49
5.4 Seizure stimulation in parameter space using the ODE model 50
5.5 Summary of original contributions 52

6 Cortical metabolic demands 53
6.1 Calculating energy demands of the model cortex 54
6.1.1 Model for ATP consumption 54
6.1.2 Calculating glucose consumption ($\mathrm{CMR_{glc}}$) from calculated ATP consumption 55
6.2 Preliminary results 55

7 Conclusion 57
7.1 Summary 57
7.2 Future work 58

Bibliography 61

List of Figures

1.1 Block diagram showing proportional, integral and differential (PID) control applied to a dynamical system. 5

1.2 Propagation of seizure waves in a 2D model of cortex which measure $1400 \times 1400\, mm^2$. Snapshots taken from time t = $0.5s$ to t = $1s$. The spiral waves are tracking the values of the mean soma potential of the excitatory population (h_e) in mV. Stochastic fluctuating inputs readily trigger a seizure wave when the model cortex is put in a state susceptible to seizures, which is characterized here by the baseline parameters of [49] for normal cortical function, except for $P_{ee} = 548.0$ and $\Gamma_e = 0.8 \times 10^{-3}$. 10

1.3 Seizure wave propagation in a two dimensional meso scale model of the human cortex, with $P_{ee} = 548.0$, $\Gamma_e = 0.66 \times 10^{-3}$ and $\alpha = 1$. The model cortex measures $700 \times 700\, mm^2$. Figure 1.3a shows the variation of the mean soma potential of the excitatory population at a point in the cortex, while figure 1.3b illustrates travelling waves in time and space in a one dimensional slice of the 2D cortical model. The color bar in fig. 1.3b shows mean soma potential values in mV. 11

2.1 Transition from one optogenetic state to another in the 4 state model for ChR2 channels. 13

2.2 Illumination profiles for light intensity of 1 mW/mm^2. The light is turned on and off for 0.01s until 0.1s in the pulsed illumination profile shown in fig. 2.2b 14

2.3 Semi-log plot showing variation of conductance with constant and pulsed light intensity for an ion channel density of 10^9ChR2's$/m^2$. △– - 1 mW/mm^2, – - 0.100 mW/mm^2, •– - 0.01 mW/mm^2. If the conductance were multiplied by the clamped voltage value of -70 mV, it would reproduce the plot of current vs. time in [31]. 14

2.4 Optogenetic seizure control using constant illumination of intensity 20 mW/mm^2. The model cortex measures $700 \times 700\, mm^2$, with $P_{ee} = 548.0$, $\Gamma_e = 0.66 \times 10^{-3}$ and $\alpha = 1.15$. Fig. 2.4a shows the variation of mean soma potential of the excitatory population, while the arrow indicates control being turned on at 0.5s. The color bar in fig. 2.4b shows mean soma potential values in mV. 17

2.5 Firing rates for the excitatory and inhibitory population with optogenetic control applied at 0.5s 17

2.6 Optogenetic seizure control using pulsed illumination of intensity 40 mW/mm^2 with pulses that are switched on and off for 0.005s. The model cortex measures 700×700 mm^2, with $P_{ee} = 548.0$, $\Gamma_e = 0.66 \times 10^{-3}$ and $\alpha = 1.15$. Fig. 2.6a shows the variation of mean soma potential of the excitatory population, and the arrow in the figure indicates control is turned on at 0.5s. The color bar in fig. 2.6b shows mean soma potential values in mV. 18

2.7 Optogenetic control applied at 0.5s using 0.05s pulsed illumination. Synchronous behavior persists even after control is applied, but the amplitude of seizure waves is decreased. Parameters: $P_{ee} = 548.0$, $\Gamma_e = 0.00066$, $\alpha = 1.15$, expression density $= 10^4$ ChR2s/m^2, Intensity = 40 mW/mm^2. 19

2.8 Pulsed optogenetic control using 0.08s pulses applied at 0.5s. Frequency of seizure waves has decreased, but amplitude of oscillations is invariant. Parameters: $P_{ee} = 548.0$, $\Gamma_e = 0.00066$, $\alpha = 1.15$, expression density $= 10^4$ ChR2s/m^2, Intensity = 40 mW/mm^2 - pulsed illumination with 0.08 s pulses. 19

2.9 More uniform seizures produced with low noise. Control switched on at 0.5s successfully inhibiting seizures. Parameters: $\alpha = 0.05$, $\Gamma_e = 0.0008$, $P_{ee} = 548.0$, expression density $= 10^4$ ChR2s/m^2, Intensity = 40 mW/mm^2 - constant illumination. 20

2.10 Higher α causes noisier oscillations, however, control is still successful in diminishing synchronous activity when applied at 0.5s. Parameters: $\alpha = 5$, $\Gamma_e = 0.00066$, $P_{ee} = 548.0$, expression density $= 10^9$ ChR2s/m^2, Intensity = 60 mW/mm^2 - constant illumination. 21

2.11 Gaussian distribution of P_{ee} (seizure hotspot) with a *gyri* to *sulci* area ratio of 1:2. Red lines running across the model cortex represent *gyri* populated with optogenetic channels. 21

2.12 Seizure hotspot with maximum P_{ee} at the center of the model cortex. with a *gyri* to *sulci* ratio of 1:2. Parameters: $P_{ee} = 548.0$, $\Gamma_e = 0.001$, $\alpha = 1.6$, expression density $= 2 \times 10^9$ ChR2s/m^2, Intensity = 20 mW/mm^2 - constant illumination. 22

2.13 Change in the long range connectivity N_j^{α} to demonstrate efficacy of the controller when the connectivity is changed . Parameters: $P_{ee} = 548.0$, $\Gamma_e = 0.00066$, $\alpha = 1.15$, expression density $= 10^9$ ChR2s/m^2, Intensity = 60 mW/mm^2 - constant illumination, $N_e^{\alpha} = 5000$, $N_i^{\alpha} = 3000$. 23

2.14 Change in the neurotransmitter rate constant T_e to demonstrate efficacy of the controller when the connectivity is changed . Parameters: $P_{ee} = 548.0$, $\Gamma_e = 0.00066$, $\alpha = 1.15$, expression density $= 10^9$ ChR2s/m^2, Intensity = 60 mW/mm^2 - constant illumination, $T_e = 20$, $T_i = 2.6$. 23

2.15 Change in the neurotransmitter rate constant T_i to demonstrate efficacy of the controller when the connectivity is changed . Parameters: $P_{ee} = 548.0$, $\Gamma_e = 0.00066$, $\alpha = 1.15$, expression density $= 10^9$ ChR2s/m^2, Intensity = 60 mW/mm^2 - constant illumination, $T_e = 12.0$, $T_i = 4.0$. 24

3.1 Seizures in the P$_{ee}$-Γ_e space. P$_{ee}$ is gradually increased then decreased in time with a maximum value of 548.0 as shown in fig. 3.1c. Γ_e is held constant at 0.00066 with α = 1.15. All other parameters are similar to baseline parameters in [49]. 30

3.2 Effect of closed loop optogenetic control on seizures in the P$_{ee}$-Γ_e space using a temporal modulation of P$_{ee}$ in time shown in fig. 3.1c. Γ_e is held constant at 0.00066 with α = 1.15. All other parameters are similar to baseline parameters in [49]. Figures 3.2a and 3.2c show the variation with time of h_e and intensity, respectively at the same point. The red dot-dash line in figure 3.2c indicates the open loop intensity required to suppress a fully formed seizures at $P_{ee} = 548.0$. Gains used: $K_P = 3.0$ and $K_I = 0.12$. . 31

3.3 Seizures in the P$_{ee}$-Γ_e space. P$_{ee}$ is gradually increased then decreased in time with a maximum value of 548.0 as shown in fig. 3.3c. Γ_e is held constant at 0.0008 with α = 1.6. All other parameters are similar to baseline parameters in [49]. 32

3.4 Effect of closed loop optogenetic control on seizures in the P$_{ee}$-Γ_e space using a temporal modulation of P$_{ee}$ in time shown in fig. 3.3c. Γ_e is held constant at 0.0008 with $\alpha = 1.6$. All other parameters are similar to baseline parameters in [49]. Figures 3.4a and 3.4c show the variation with time of h_e and intensity, respectively at the same point. The red dot-dash line in figure 3.4c indicates the open loop intensity required to suppress a fully formed seizures at $P_{ee} = 548.0$. Gains used: $K_P = 0.4$ and $K_I = 3.6$. . 33

3.5 Effect of closed loop optogenetic control on seizures in the P$_{ee}$-Γ_e space using a temporal modulation of P$_{ee}$ in time shown in fig. 3.3c. Γ_e is held constant at 0.00066 with $\alpha = 1.15$. All other parameters are similar to baseline parameters in [49]. This seizure is similar to the one presented in section 3.2.1. Figures 3.5a and 3.5c show the variation with time of h_e and intensity, respectively at the same point. The red line in figure 3.5c indicates the open loop intensity required to suppress fully formed seizures presented in section 3.2.2. The red dot-dash line in figure 3.2c indicates the open loop intensity required to suppress a fully formed seizures at $P_{ee} = 548.0$, $\Gamma_e = 0.0008$, and $\alpha = 1.6$. Gains used: $K_P = 0.4$ and $K_I = 3.6$, which are the same gains used to suppress the robust seizure presented in section 3.2.2. 34

3.6 Seizures in the $\tilde{g}_e$-Γ_i space using a variation of $\tilde{g}_e$ in time with a maximum value of -12.5 as shown in figure 3.6c. Γ_i is held constant at 0.085. All other parameters are similar to baseline parameters in [49]. 35

3.7 Effect of closed loop optogenetic control on seizures in the $\tilde{g}_e$-Γ_i space. $\tilde{g}_e$ is varied in time with a maximum value of -12.5 as shown in figure 3.6c. Γ_i is held constant at 0.085 with $\alpha = 1.6$. All other parameters are similar to baseline parameters in [49]. Figures 3.7a and 3.7c show the variation with time of $\tilde{h}_e$ and intensity, respectively at the same point. The red dot-dash line in figure 3.7c indicates the open loop intensity required to suppress a fully formed seizures at $g_e = -12.5$. Gains used: $K_P = 1.0$ and $K_I = 0.64$. 35

4.1 Comparison between the full SPDE model and the simpler ODE model. **Left:** Response diagram for the hyperexcited cortex with subcortical input $P_{ee} = 548.0$. Amplitude of noise from stochastic subcortical inputs was reduced by an order of magnitude to 0.1 to demonstrate the effect of spatial terms on the dynamics of the model. The red jagged lines indicate maximum and minimum values of h_e over 2 seconds for different Γ_e, which is the influence of the synaptic input on the mean soma potential of the excitatory population, using the SPDE model. Black lines indicate the bifurcation diagram for the ODE model. Dashed and solid lines indicate unstable and stable fixed points, respectively. Maximum and minimum values of h_e during stable (dot-dashed) and unstable (dashed) limit cycles arising from a subcritical Hopf bifurcation (asterisk) are also shown. **Right:** Comparison of the SPDE and ODE models in parameter space, with grey regions indicating seizure causing areas. As one might expect, the stochastic inputs in the SPDE model enhance the seizure area (indistinct boundary marked in grey) in parameter space when compared to the ODE model (darker region with sharp boundaries). Here, we use $\alpha = 1.6$ which corresponds to the amplitude of noise used with the SPDE model elsewhere in the manuscript. 40

4.2 Bifurcation analysis using an unstimulated cortex (figure 4.2a) and a cortex stimulated with light of constant 10 mW/mm^2 intensity in the open loop configuration (figure 4.2b). Asterisks indicate subcritical Hopf bifurcations that lead to unstable limit cycles. Time integration of the combined cortico optogenetic model with PI control to track the maximum and minimum values of the excitatory mean soma potential is shown in figure 4.2c. The red triangle ($P_{ee} = 710$), which is shifted further away from the first blue Hopf bifurcation ($P_{ee} = 548.0015$) in figure 4.2a, indicates the start of oscillatory activity despite closed loop control being triggered. The dashed black lines in fig. 4.2c indicate minimum and maximum values of $\tilde{h}_e$ during oscillatory activity arising despite the use of closed loop control. Gains used $K_P = 3.0$ and $K_I = 0.12$. 41

4.3 From left to right: Seizure prone areas in the $\mathrm{P}_{ee} - \Gamma_e$ parameter space with no control, using open loop control with an illumination of 1.9 mW/mm^2, and PI control using $K_P = 3.0$ and $K_I = 0.12$. Here, dark regions represent values of P_{ee} and Γ_e which produce oscillations in the mean soma potential h_e. These results were obtained using the dimensionless ODE system of equations. 42

4.4 Seizure prone areas in the $\tilde{g}_e - \Gamma_i$ parameter space with no optogenetic stimulation. Here, dark regions represent values of $\tilde{g}_e$ and Γ_i which produce oscillations in the mean soma potential h_e. The grayscale shading indicates the variation in h_e during oscillatory behavior. These results were obtained using the dimensionless ODE system of equations. 43

5.1 Propagation of seizure waves in a 2D model of a normally functioning human cortex when optogenetic stimulation is applied to a 280×280 mm^2 patch in the centre of the cortex. Snapshots are taken from time t = 0.5s to t = 1s. The traveling waves are tracking the values of the mean soma potential of the excitatory population (h_e) in mV. Normal cortical function is characterized here by the baseline parameters of [49] with $P_{ee} = 11.0$ and $\Gamma_e = 0.0012$. The model cortex is stimulated with a constant light intensity of 50 mW/mm^2 at 0.5s. 47

5.2 Optogenetic stimulation of a normally functioning cortex with an illumination source of constant intensity. Figures 5.2a - 5.2c are for a stimulation intensity of 30 mW/mm^2 and figures 5.2d - 5.2f are for a stimulation intensity of 60 mW/mm^2. 48

5.3 Optogenetic stimulation of a normally functioning cortex with an illumination source of constant intensity. Figures 5.3a - 5.3c are for a stimulation intensity of 50 mW/mm^2 and figures 5.3d - 5.3f are for a stimulation intensity of 60 mW/mm^2. 49

5.4 Top left: effect of optogenetic stimulation on oscillatory behavior in the Γ_e - P_{ee} parameter space, using a 60 mW/mm^2 illumination intensity (grey) and in an unstimulated cortex (black). The red dot indicates Γ_e = 0.0012 and P_{ee} = 11.0, which are used in the full SPDE system simulations shown in figures 5.1 - 5.3. Top right: Bifurcation diagram for the underlying deterministic ODE system showing the variation of h_e for different illumination intensities. Dashed and solid lines indicate unstable and stable fixed points, respectively. Maximum and minimum values of h_e during stable (dot-dashed) and unstable (dashed) limit cycles arising from a subcritical Hopf bifurcation (asterisk) are also shown. Bottom: Frequency of seizure waves for a given illumination intensity. 51

6.1 Mean soma potential of the excitatory population and energy consumption in terms of number of ATP per second per unit volume in the model cortex during normal function. The mean firing rate of the excitatory population is calculated using the mean soma potential via a sigmoid function as described in [58]. The ATP consumption of signaling events, in turn, is directly calculated from the firing rate using equation 6.3. Non-signaling events have a total ATP consumption rate of 2.9372×10^{16} per second per cm^3 which remains constant. Total ATP consumption in figure 6.1b includes both signaling and non-signaling events. Parameters: $P_{ee} = 11.0$, $\gamma_e = 0.0012$, $\alpha = 1.15$. . . 56

List of Tables

1.1 Dimensionless variables and parameters of the SPDE meso-scale cortcial model used throughout this dissertation, and taken from [49]. For the dimensional form of the model, and accompanying descriptions and values of parameters, please see [96]. . . . 9

2.1 Rate constant values for the meso scale optogenetic model of ChR2 embedded in the cell membrane [31]. 13

Acknowledgments

First, I would like to thank my advisor, Andrew Szeri, for his guidance, advice, patience and unrelenting support over the past few years. I would also like to thank Walter Freeman, Heidi Kirsch, and Jamie Sleigh for their collaborations, generosity and invaluable insights into my work. Thank you to my dissertation committee - Bruno Olshausen, Jamie Sleigh, and Mohammad-Reza Alam - for their time, support and suggestions. Thank you to Mark Kramer for help with, and advice on, my work and computational neuroscience. I would also like to thank Allyson Goldberg for patiently reading multiple drafts of various sections of my dissertation, and Vera Dadok for her suggestions and insights.

Finally, thank you to friends and colleagues from 6112 Etcheverry Hall, the department of Mechanical Engineering, and the Redwood Center for Theoretical Neuroscience.

This work was partially supported by the National Science Foundation through the research grant CMMI 1031811. Any opinions, findings, conclusions, or recommendations expressed in this publication are those of the author and do not necessarily reflect the views of the National Science Foundation.

Chapter 1

Introduction

1.1 Epilepsy and seizures

Epilepsy is a chronic, non-communicable disorder that manifests as seizures, which are characterized by abnormal or excessive synchronous neuronal activity in the brain. It is a condition that will affect about 1 in 100 people worldwide, and about 1 in 10 people will suffer a seizure in their lifetime [100]. While epilepsy can arise in any person at any age, it more commonly occurs in the elderly and children with causes that include but are not limited to genetic conditions, head injuries and brain tumors [101].

Under the most recent International League Against Epilepsy (ILAE) revised terminology of classification of seizures and epilepsies developed between 2011 and 2014, epileptic seizures can be broadly classified as either focal, generalized or unknown seizures [41]. Focal seizures are ictal (relating to seizures) events originating in neural networks limited to one cerebral hemisphere. Focal seizures are characterized according to one or more features that fall under the categories of aura, motor, autonomic, and dyscognitive [41]. On the other hand, generalized seizures simultaneously originate within, and rapidly engage, bilaterally distributed networks, and can be further classified as tonic-clonic, absence, clonic, tonic, atonic, and myoclinic generalized seizures [41]. Finally, unknown seizures are seizures that cannot be categorized as either focal, generalized or both for lack of sufficient evidence. Epileptic spasms are an example of unknown seizures [41].

In this work, we will be looking at focal seizures that generalize at the network level. However, the defining feature of focal seizures is that they originate at a focus in a small group of neurons [43], and so it is important to understand epileptic neural activity at the level of single neurons or small groups of neurons first. Here, we present a concise description of how seizures develop at the level of single neurons, but a more detailed description can be found in the book by Kandel et al. [43].

Neurons are electrically and chemically excitable cells with a voltage gradient maintained across their cellular membrane (called membrane potential) because of differences in extracellular and intracellular ion concentration. Neurons are said to be in a state of rest when not transmitting signals, and have a negative membrane potential in the resting state. A neuron is said to be hyperpolarized when the membrane potential is further decreased by the influx of anions or the efflux of cations, and is said to be depolarized if the ion flux is reversed. Sufficient depolarization results in an action potential, which results in a discharge of ions (transmittance of an electrical signal). Now neurons located in the seizure focus exhibit a synchronized electrical response called the paroxysmal depolarizing shift (PDS), which consists of a sudden, large (20-40 mV) and long-lasting (50-200 ms) depolarization that triggers a train of action potentials at the peak of the PDS [43]. The PDS is followed by an afterhyperpolarization (AHP), which limits the duration of the PDS. While the PDS is primarily dependent on excitatory inputs, the AHP is primarily dependent on inhibitory inputs from surrounding interneurons. Focal seizures develop when the PDS is able to gradually overcome the surrounding inhibition, eliminate the AHP, and spread past the original focus.

There are many factors occurring at different scales that lead to excessive excitation of cells or the decrease in surrounding inhibition, and the different etiologies of seizures make diagnosis and treatment of this disorder complicated tasks. Physical trauma, stroke and tumors are examples of causes that may be more easily identifiable than those responsible for idiopathic (unknown cause) seizures. About 70% of people suffering from epileptic seizures can be treated with anti-epileptic drugs (AEDs) [101]. For the remaining 30% with medically refractory, more commonly focal-onset epilepsy, surgical removal of the epileptogenic zone is a treatment option [12], as are implanted neurostimulators such as the vagus nerve stimulator [84]. Options on the horizon include closed-loop devices that sense the onset of a seizure and deliver local therapy to interrupt the seizure's spread and/or to reduce its intensity. For example, the firing pattern of neurons near the epileptogenic zone can be altered by the application of an external electric field. *In vitro* experiments on rat cortex [78] showed it is possible to modulate the behavior of seizure like waves, while *in vivo* experiments on rats [30] showed that stimulation using proportional feedback temporarily inhibited seizure waves. Electrical cortical stimulation was modeled *in silica* [48] using various methods of feedback control, and charge balanced control was ensured in subsequent work [58]. However, while brain electrical stimulation (BES) offers an alternative, vagus nerve stimulation using electrical pulses is the only FDA approved BES technique, and these methods only have a success rate comparable to medication at best. Also, the physiological methods by which seizures are prevented or reduced with current BES techniques are unknown, leading to concerns over long term use. Finally, the cortex contains both excitatory and inhibitory cells, but BES techniques target only a small fraction of excitatory cells, suggesting significant untapped potential. Further, drug delivery cannot be isolated to localized regions of the brain.

To address these limitations, we explore the idea of a new, targeted treatment modality focused on using light activated ion channels to inhibit epileptiform activity.

1.2 Optogenetics

In 1979, Sir Francis Crick stressed the importance of independently stimulating the different cell types that form the complex architecture of the mammalian brain to provide insight into the relationship between specific neural activity and abstract brain functions such as cognition, memory and emotions. Twenty years later, he suggested using light as a modality for such precise and accurate neural stimulation. It took a few more years for his ideas to develop into a technology called optogenetics, which uses genetically induced light-sensitive ion channels to control neurons. Since then the field of optogenetics has come a long way, being named 'Method of the year' in 2010 [24], and today, optogenetics is one of the most valuable research tools in neuroscience, offering unparalleled specificity in the stimulation of individual neurons and neural circuits.

The key to the specificity of optogenetics is the genetic modification of a cell type to render it sensitive to light. The first step is the identification of an opsin, a protein that forms the visual pigment rhodopsin that converts light of a particular wavelength into an electrochemical signal. Opsins have different ion conductance properties and can have reaction rates ranging from milliseconds to minutes [65]. Certain rhodopsins like channelrhodopsin-2 (ChR2), which is sensitive to blue light, pump cations into neurons [66], depolarizing them (excitation), while natronomonas pharaonis halorhodopsin (NpHR) is sensitive to yellow light, and works as an anion pump that hyperpolarizes neurons (inhibition) [106]. The next step is to deliver a gene that encodes these opsins to a host cell. Examples of delivery methods include the use of benign viruses to carry the opsin gene to cells (viral vectoring), and the use of transgenic animals that express these opsins from birth. These methods safely render a neuron light sensitive without changing its overall function.

Selective opsin expression, selective ion conductivity [81] and a rapid response time ensure that optogenetics also offers unparalleled temporal and spatial specificity in the targeted stimulation of distinct neurons and neuron networks in a particular brain region [105]. Other methods, such as lesioning and electrical stimulation offer good temporal resolution, but are invasive, and collectively influence all cell types within the stimulated region - thus blurring individual neuron contributions to specific brain functions. Similarly, pharmacological methods can target specific families of neurons, but they lack the temporal sensitivity that other stimulation methods offer. Additionally, recent innovations like injectable, wireless, cellular-scale optoelectronics [47] provide a minimally invasive method of delivering light to the brain. In this way, optogenetics offers recourse to the shortcomings of other stimulation methods, and in the future, has the potential to be an extremely effective therapeutic tool to treat neurological diseases in human beings.

However, the technique is already proving to be invaluable, even without use in humans. Research with optogenetics in animal models has already advanced understanding of various psychiatric and neurological disorders. Ahmari et al. [3] triggered obsessive compulsive disorder (OCD) behavior in mice by selectively stimulating certain neurons using optogenetics. Chen et al. [14] used optogenetic stimulation in rats to show how particular neurons controlled drugseeking behaviors. Kravitz et al. [50] regulated motor symptoms of Parkinson's disease in mice using optogenetic control of basal ganglia circuitry. Beyond these examples, optogenetics has also been used to deconstruct sleep-wake circuitry [2], to research the cortical balance of inhibition and excitation and its effect on social behavior [105], in psychiatric studies of the anti-depressant effect of cortical stimulation [21], and in the treatment of schizophrenia [73]. Hence, although this method is not yet used experimentally or therapeutically in human beings, it is already enhancing understanding of neural activity in animal models, which greatly facilitates comprehension of human brain function.

1.2.1 Optogenetics and epilepsy

Optogenetics offers another modality of seizure control, albeit with higher spatial, temporal and cell type specificity than any other method of stimulation [105]. The control of seizures using closed loop optogenetic control has been demonstrated in rats [102; 72] and in mice [51], where hyperpolarising excitatory neurons or depolarising inhibitory neurons in the hippocampus or the thalamus leads to the suppression of seizure waves. Previous work has shown how seizure control in a mathematical model of the human cortex can be achieved by inhibiting the excitatory population in [58], albeit with an electric field and not optogenetic stimulation. Here, we present a method of seizure suppression where we depolarize the inhibitory cells in a model of the human cortex using ChR2 channels. The firing of the inhibitory cells suppresses the firing of excitatory cells, and this subsequently leads to the disruption of pathological synchronous firing of cortical neurons.

We specifically look at targeting the inhibitory population for two reasons. One, inhibitory neuron types and neural circuits might be responsible for certain types of cortical disorders and function. For example, GABAergic inhibition is decreased in some types of epilepsy [20; 19]. Depolarising inhibitory neurons more frequently via optogenetic stimulation is one possible way to address this decrease in inhibition. In this work, we use a mathematical model of the human cortex with averaged inhibition that does not take into account specific subtypes of inhibitory neurons, but it does allow us to explore the efficacy of optogenetic depolarisation of the inhibitory neuron population.

Two, recent advances in delivering light to deeper cortical layers aids in the targeting of cells that do not synapse at the surface of the cortex. The distribution of inhibitory neurons in mammalian cortices is non-uniform, with the majority of inhibitory neurons embedded well below the cortical surface [45]. If light could only be delivered to the surface of the cortex, the obvious choice to suppress seizures would be to target pyramidal (excitatory) neurons using optogenetics. However, recent work [11] and [16] has shown light can penetrate at least 1 mm or more beneath the cortical surface giving access to a number of other neuron types that can be found in larger numbers in layers 2-6 of the cortex.

1.3 Applied control theory

Control theory involves the study of dynamical systems with the aim of making these systems behave a certain way, i.e. control them. Control is achieved through a controller, which monitors the output of the system (measured signal), and compares the measured signal with a desired output signal. The error arising from the difference between the measured and desired signals is applied as feedback to the input of the system, with the goal of reducing the error in the output. If the system is based on a linear relationship between the input and the output, control is achieved easily. However, most systems are non-linear and require an iterative process of measuring the error and correcting the input signal until the desired output is achieved. We now present terms and ideas from control theory related to this dissertation, however, there are numerous books on control theory that offer more in depth insight into the subject, e.g. the books by Franklin et al. [29] and Doyle et al. [26].

In some applications, like laundry dryers that work on timers, feedback is not necessary to apply control to the system. This type of control, where the control effort is predetermined and fixed throughout the operation of the system, is called open loop control. However, if the same dryer were to measure the degree of dampness of the laundry in it, and adjust the temperature and duration of a drying cycle based on the dampness, it would now be using closed loop control. In this case, the control effort is calculated using a 'control law', which determines the adjusted input in terms of the measured output. Some of the most widely used control laws are based on the proportional, integral and differential (PID) calculation of control effort from the error in the measured signal, and variations of the PID system like proportional integral (PI), proportional differential (PD), and proportional (P) control.

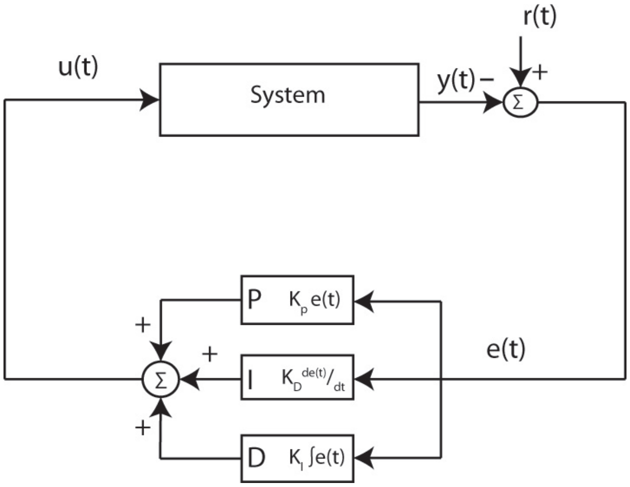

Figure 1.1: Block diagram showing proportional, integral and differential (PID) control applied to a dynamical system.

The working of a PID controller is shown in figure 1.1. The error $e(t)$ between the output of the system $y(t)$ and the reference/desired signal $r(t)$ is calculated and input to the controller, where the control effort $u(t)$ is obtained by summing up the proportional, integral and differential components as shown in equation 1.1.

$$u(t) = K_P e(t) + K_I \int e(t) + K_D \frac{de(t)}{dt} \tag{1.1}$$

Using these principles of classical control theory, we explore the use of optogenetic stimulation in both the open and closed loop formats to inhibit seizure waves in the model cortex. In the open loop configuration, a predetermined intensity of light is used to illuminate the neurons in a seizing model human cortex. This allows us to study and determine the efficacy of optogenetics as a seizure inhibition strategy. In the closed loop configuration we use the proportional integral (PI) mode of control (the differential term is set to zero). By basing our control strategy on electrode like measurements of the same spatial and temporal scales as the cortical model, we propose a method of seizure inhibition that is biologically relevant and efficient in the use of energy required to effect control - criteria that have to be satisfied for the use of any control strategy in humans over long periods of time.

1.4 2D cortical model

Despite the differences in etiologies and physiologies, all epileptic seizures are characterized by the excessive synchronous firing of a large number of neurons [27]. This activity is captured well at the mesoscale, which involves the averaged activity of millions of neurons. Electrocorticogram (ECoG) readings, and especially much easier to administer electroencephalogram (EEG), provide the most helpful tests to identify idiopathic seizures [68]. These two techniques are used to observe cortical activity at the mesoscale.

To simulate electrical activity in the human cortex ideally, one would have to model the connections between individual neurons taking into account the characteristics of each neuron (location, connections to other neurons, pyramidal or stellate etc.). However, given the limits of computing capacity, and variation between individuals, it would be extremely difficult to model a network consisting of all of these neurons even if the complicated physiology were well defined. In light of this, Liley at el. [55] proposed a mathematical model of the cortex based on the columnar arrangement of cortical neurons, which was first discovered by Santiago Ramón y Cajal towards the end of the 19th century. A detailed description of the model can be found in [55], however, we present the basic ideas underlying the model in what follows.

The mathematical model simulates the variation of the averaged soma potentials of excitatory and inhibitory, h_e and h_i, respectively, by heuristically averaging neural activity at the microscopic level over columnar volumes with diameters just under the spatial scales of EEG and ECoG readings. The result of this spatial averaging is the fundamental unit of the model - an averaged neuron, which includes both neuronal and non-neuronal (e.g. neuroglia) components. Motivated by cortical phsyiology, the mathematical model also incorporates interaction between neural populations via action potentials. These interactions include two types of connections: (1) local feedback and feedforward connections within and between excitatory and inhibitory populations, and (2) long range excitatory connections that synapse on both the excitatory and inhibitory populations. The long range connections are assumed to be isotropic and homogeneous, and decrease exponentially with distance. These assumptions were made for lack of experimental data and to simplify the model. The model also takes into account subcortical inputs (e.g. inputs from the hippocampus and thalamus) that can be both excitatory or inhibitory in nature, and act on both populations.

Since this formulation was originally presented by Liley et al., the mesoscale model of the cortex has been shown to model the mesoscopic electrical behavior recorded from the human cortex during sleep [59; 22], anesthesia [35; 10] and seizures [48; 23]. Various methods of feedback control were demonstrated to suppress seizures simulated using the cortical model [49], which resulted in a biologically relevant method of closed loop control [58] to treat medically refractory epilepsy.

In its full form, the meso-scale mathematical model of the human cortex is characterized by a set of 8 non-linear stochastic partial differential equations (SPDEs), and is written in the following way:

$$\frac{\partial \tilde{h}_e}{\partial \tilde{t}} = 1 - \tilde{h}_e + \Gamma_e(h_e^0 - \tilde{h}_e)\tilde{I}_{ee} + \Gamma_i(h_i^0 - \tilde{h}_e)\tilde{I}_{ie} \tag{1.2}$$

$$\frac{\partial \tilde{h}_i}{\partial \tilde{t}} = 1 - \tilde{h}_i + \Gamma_e(h_e^0 - \tilde{h}_i)\tilde{I}_{ei} + \Gamma_i(h_i^0 - \tilde{h}_i)\tilde{I}_{ii} \tag{1.3}$$

$$\left(\frac{1}{T_e}\frac{\partial}{\partial \tilde{t}} + 1\right)^2 \tilde{I}_{ee} = N_e^{\beta}\tilde{S}_e\left[\tilde{h}_e\right] + \tilde{\phi}_e + P_{ee} + \tilde{\Gamma}_1 \tag{1.4}$$

$$\left(\frac{1}{T_e}\frac{\partial}{\partial \tilde{t}} + 1\right)^2 \tilde{I}_{ei} = N_e^{\beta}\tilde{S}_e\left[\tilde{h}_e\right] + \tilde{\phi}_i + P_{ei} + \tilde{\Gamma}_2 \tag{1.5}$$

$$\left(\frac{1}{T_e}\frac{\partial}{\partial \tilde{t}} + 1\right)^2 \tilde{I}_{ie} = N_i^{\beta}\tilde{S}_i\left[\tilde{h}_i\right] + P_{ie} + \tilde{\Gamma}_3 \tag{1.6}$$

$$\left(\frac{1}{T_e}\frac{\partial}{\partial \tilde{t}} + 1\right)^2 \tilde{I}_{ii} = N_i^{\beta}\tilde{S}_i\left[\tilde{h}_i\right] + P_{ii} + \tilde{\Gamma}_4 \tag{1.7}$$

$$\left(\frac{1}{\lambda_e}\frac{\partial}{\partial \tilde{t}} + 1\right)^2 \tilde{\phi}_e = \frac{1}{\lambda_e^2}\nabla^2\tilde{\phi}_e + \left(\frac{1}{\lambda_e}\frac{\partial}{\partial \tilde{t}} + 1\right) N_e^{\alpha}\tilde{S}_e\left[\tilde{h}_e\right] \tag{1.8}$$

$$\left(\frac{1}{\lambda_i}\frac{\partial}{\partial \tilde{t}} + 1\right)^2 \tilde{\phi}_i = \frac{1}{\lambda_i^2}\nabla^2\tilde{\phi}_i + \left(\frac{1}{\lambda_i}\frac{\partial}{\partial \tilde{t}} + 1\right) N_i^{\alpha}\tilde{S}_e\left[\tilde{h}_e\right] \tag{1.9}$$

Here, all variables have been non dimensionalized and are functions of time $\tilde{t}$, and the two spatial dimensions $\tilde{x}$ and $\tilde{y}$. Throughout this dissertation, tildes are used to denote non-dimensionalized variables in the meso-scale cortical model. Also, 'mean' values of any variable denote spatial averages unless otherwise specified. The subscripts e and i represent excitatory and inhibitory populations respectively, and variables with two subscripts represent the transfer of an electrical signal from one population to another. The mean soma potential for a neuronal population is represented by the $\tilde{h}$ state variable, $\tilde{I}$ represents the postsynaptic activation due to local, long-range, and subcortical inputs. $\tilde{\phi}$ represents long range (corticocortical) inputs.

The firing rate of each neuron population is given by the sigmoid function $\tilde{S}_{e,i}$, and is assumed to be dependent on the mean soma potential of the population, $\tilde{h}_{e,i}$, the inflection point of the sigmoid function, $\tilde{\theta}_{e,i}$, and the slope at the inflection point of the sigmoid function, $\tilde{g}_{e,i}$.

$$\tilde{S}_{e,i} = \frac{1}{1 + exp[-\tilde{g}_{e,i}(\tilde{h}_{e,i} - \tilde{\theta}_{e,i})]} \tag{1.10}$$

The stochastic subcortical inputs are defined as,

$$\tilde{\Gamma}_1 = \alpha_{ee}\sqrt{P_{ee}}\xi_1[\tilde{x},\tilde{t}] \tag{1.11}$$

$$\tilde{\Gamma}_2 = \alpha_{ei}\sqrt{P_{ei}}\xi_2[\tilde{x},\tilde{t}] \tag{1.12}$$

$$\tilde{\Gamma}_3 = \alpha_{ie}\sqrt{P_{ie}}\xi_3[\tilde{x},\tilde{t}] \tag{1.13}$$

$$\tilde{\Gamma}_4 = \alpha_{ii}\sqrt{P_{ii}}\xi_4[\tilde{x},\tilde{t}] \tag{1.14}$$

$$\tag{1.15}$$

Here, we set $\alpha_{ee} = \alpha_{ei} = \alpha_{ie} = \alpha_{ii} = \alpha$ as in the stochastic simulations of spatioadiabatic one-dimensional cortex [97]. Additionally, α is the amplitude of the Gaussian white noise sources with mean zero and δ-function correlations denoted by ξ_k. While physiologically shaped brown noise is more appropriate [10], it is typical to assume Gaussian white noise [95; 97]. Values and explanations for all other parameters and variables can be obtained in table 1.1.

1.5 Seizure like activity in the model cortex

In prior work, our group has shown this model and EEG or ECoG data from a patient undergoing seizure are in good agreement on the average frequency of maximum power and the speed of spatial propagation of voltage peaks [49]. Also, the variables of the mean field model are spatially averaged properties of neuron populations, and can be related to EEG and ECoG measurements which represent the spatially averaged extracellular local field potential (LFP). The sign reversed LFP, in turn, is proportional to the spatially averaged excitatory soma membrane potential, h_e, which is one of the variables used in the SPDEs. It has been shown that increasing the subcortical input results in h_e mimicking ECoG data obtained from a seizing cortex [49]. In this dissertation, we look at tonic-clonic seizures characterized by runaway excitation, and this makes the meso scale model ideal for this study.

The evolution and propagation of seizure waves in a one dimensional cortical model has been shown in previous work [58] and [49]. The 1D model has been extended to a 2D model by using the two dimensional Laplacian ($\partial^2/\partial x^2 + \partial^2/\partial y^2$) instead of just one second order spatial derivative, leading to the long range connections scaled by a spatial decay in two dimensions. Fig. 1.2 depicts an example, showing the propagation of seizure waves in a two dimensional cortex of size 1400 mm × 1400 mm.[1] Seizure waves originate at a focus in response to stochastic fluctuations and propagate outwards in spiral waves. This is in good agreement with the results for the multi neuron integrate and fire network model in [103]. Fig. 1.3a shows the variation of the mean soma potential of the excitatory cell population at a point in the cortex. The cortex starts exhibiting synchronous behavior at around 0.2s. Fig. 1.3b shows travelling seizure waves in a 1D slice of the 2D model cortex.

---

[1] The average human cortex has dimensions of 500×500 mm^2 if it were laid open like a sheet. However, the spiral seizure waves have a radius of curvature that is too large to be appreciated within a domain of the size of an average human cortex, and because cortical dynamics is scale-free, we have used a larger cortical domain to illustrate them.

Symbol	**Definition**	**Description**	**Typical value**
$\tilde{h}_{e,i}$	$h_{e,i}/h^{rest}$	Spatially averaged soma potential of neuron populations	-
$h^0_{e,i}$	$h^{rev}_{e,i}/h^{rest}$	Reversal potential	-
$\tilde{I}_{ee,ei}$	$\frac{I_{ee,ei}*\gamma_e}{G_e exp(1) S^{max}}$	Post-synaptic activation due to excitatory inputs	-0.643, 1.29
$\tilde{I}_{ie,ii}$	$\frac{I_{ie,ii}*\gamma_i}{G_i exp(1) S^{max}}$	Post-synaptic activation due to inhibitory inputs	-
$\tilde{\phi}_{e,i}$	$\phi_{e,i}/S^{max}$	Long range (corticocortical) input to *e* and *i* populations	-
$\tilde{\Gamma}_{e,i}$	$\frac{G_{e,i} exp(1) S^{max}}{\gamma_{e,i}\lvert h^{rev}_{e,i} - h^{rest}\rvert}$	Dimensionless space	-
$T_{e,i}$	$\tau\gamma_{e,i}$	Neurotransmitter rate constant	12.0, 2.6
$\lambda_{e,i}$	$\tau\overline{\upsilon}\Lambda_{ee,ei}$	Inverse length scale for corticocortical connections	11.2, 18.2
$P_{ee,ei}$	$p_{ee,ei}/S^{max}$	Excitatory subcortical inputs to the *e* and *i* populations	11.0, 16.0
$P_{ie,ii}$	$p_{ie,ii}/S^{max}$	Inhibitory subcortical inputs to the *e* and *i* populations	16.0, 11.0
$N^{\alpha}_{e,i}$	-	Number of distant (corticocortical) connections from excitatory population to *e* and *i* populations	4000, 2000
$N^{\beta}_{e,i}$	-	Number of local connections from *e* and *i* populations	3034, 536
$\tilde{g}_{e,i}$	$g_{e,i}h^{rest}$	Slope at inflection point of sigmoid function $\tilde{S}_e$	-19.6, -9.8
$\tilde{\theta}_{e,i}$	$\theta_{e,i}/h^{rest}$	Inflection point for sigmoid function $\tilde{S}_e$	0.857, 0.857
$\tilde{t}$	t/τ	Dimensionless time	-
$\tilde{x}$	$x/(\tau\overline{\upsilon})$	Dimensionless space	-

Table 1.1: Dimensionless variables and parameters of the SPDE meso-scale cortcial model used throughout this dissertation, and taken from [49]. For the dimensional form of the model, and accompanying descriptions and values of parameters, please see [96].

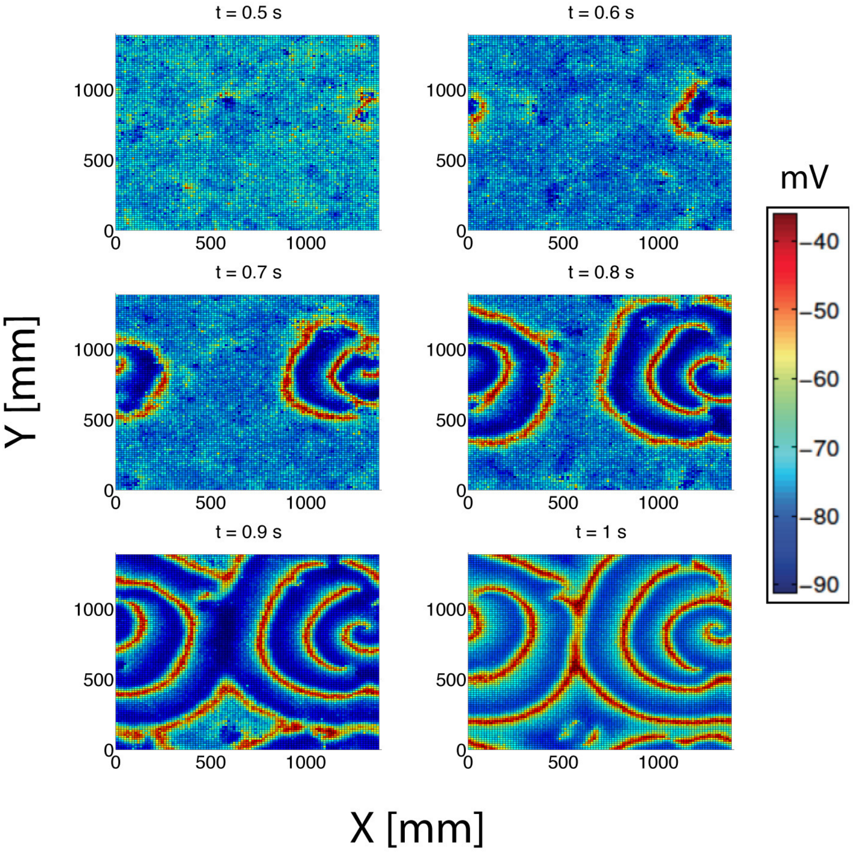

Figure 1.2: Propagation of seizure waves in a 2D model of cortex which measure $1400 \times 1400\ mm^2$. Snapshots taken from time $t = 0.5s$ to $t = 1s$. The spiral waves are tracking the values of the mean soma potential of the excitatory population (h_e) in mV. Stochastic fluctuating inputs readily trigger a seizure wave when the model cortex is put in a state susceptible to seizures, which is characterized here by the baseline parameters of [49] for normal cortical function, except for $P_{ee} = 548.0$ and $\Gamma_e = 0.8 \times 10^{-3}$.

1.6 Layout of this dissertation

In this chapter, we have presented the development of a meso scale mathematical model of the human cortex, and how it may be used to model the origin and propagation of seizure waves. This model provides the basis for studying seizure initiation and propagation, and the testing of various seizure control strategies. Next, in chapter 2, we adapt to the meso scale a model of the dynamics of ChR2 channels in the cortex, and their behavior when illuminated with either constant or pulsed light is studied. In chapter 3, we explore the efficacy of closed loop optogenetic control in inhibiting seizures in two parameter spaces of the mathematical model that have been shown to correspond well with seizures observed in patients [23]. We analyse the effect of open and closed loop optogenetic stimulation on the dynamics of the mathematical model of the human cortex us-

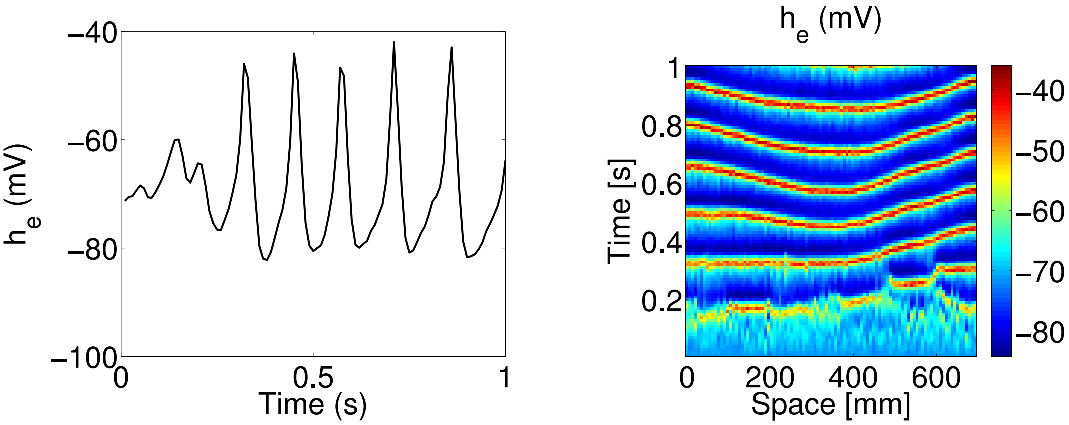

(a) Mean soma potential at a point in the model cortex (b) 1D slice of the 2D model cortex

Figure 1.3: Seizure wave propagation in a two dimensional meso scale model of the human cortex, with $P_{ee} = 548.0$, $\Gamma_e = 0.66 \times 10^{-3}$ and $\alpha = 1$. The model cortex measures $700 \times 700\ mm^2$. Figure 1.3a shows the variation of the mean soma potential of the excitatory population at a point in the cortex, while figure 1.3b illustrates travelling waves in time and space in a one dimensional slice of the 2D cortical model. The color bar in fig. 1.3b shows mean soma potential values in mV.

ing bifurcation analysis in chapter 4. In chapter 5, we further exploit the specificity of optogenetic stimulation to depolarize the excitatory population, which induces seizures in a normally functioning model cortex, and lays the groundwork for studying the etiology of the seizure state using optogenetics. In chapter 6, we present a quantitative method of calculating the metabolic demands of the human cortex, which will help in understanding the role of cortical metabolic dynamics in disorders like seizures. We conclude by summarising the contributions of this dissertation, and by offering insights into future work in chapter 7.

Chapter 2

Open loop optogenetic control of seizure like activity in the model cortex

In this chapter, we present a model that describes the activity of channelrhodopsin-2 (ChR2), a protein that functions as a light activated ion channel when expressed by neurons, at the meso scale. By expressing the dynamics of ChR2 at the meso scale, we are able to study the plausibility of using ChR2 ion channels as a means to control seizure like activity in the model cortex described in chapter 1. We explore the robustness of this method of stimulation, and its efficacy as a seizure control method while being physiologically safe when used in an open loop configuration. Much of this material was previously published in [85].

2.1 Meso scale optogenetics model

The meso scale optogenetics model described here is based on the four state model of Channelrhodopsin-2 (ChR2) cells first proposed by [66]. This model was able to reproduce qualitatively the ChR2 photocurrents obtained from experimental measurements. It takes into account the fact that the recovery rates under constant illumination and in the dark are different, and is thus able to simulate the characteristic peak-plateau behavior and degraded transient response for subsequent stimulus. Building on this and a ChR1 model [34], a 4 state model for ChR2 channels was proposed and the effect of the change in conductance on a neuron described by a cable model, which contains active Hodgkin−Huxley type elements, was studied [31].

The 4 state model has two open states ($O1$ and $O2$) and two closed states ($C1$ and $C2$). These states do not actually represent the physical energy levels of ChR2, but instead describe a functional model that is a good representation of the behavior of ChR2 ion channels when illuminated with light. The conductivity in the $O1$ state is more than in the $O2$ state, but the $O2$ state has a longer life time. Conversion from one state to the other can be achieved through both light and thermal excitation. Figure 2.1 illustrates the possible transitions from one state to another. The equations describing the 4 state model are based on those of [31].

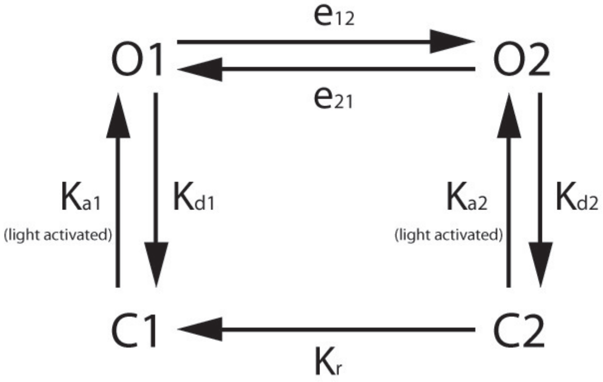

Figure 2.1: Transition from one optogenetic state to another in the 4 state model for ChR2 channels.

$$\frac{dN_{O1}}{dt} = K_{a1}.N_{C1} - (K_{d1} + e_{12}).N_{O1} + e_{21}.N_{O2} \tag{2.1}$$

$$\frac{dN_{O2}}{dt} = K_{a2}.N_{C2} + e_{12}.N_{O1} + (K_{d2} + e_{21}).N_{O2} \tag{2.2}$$

$$\frac{dN_{C2}}{dt} = K_{d2}.N_{O2} - (K_{a2} + K_r).N_{C2}, \tag{2.3}$$

Equations 2.1-2.3 describe the number of channels in each open and closed state, represented by N_{Oi} and N_{Ci} respectively. K_{ai} are the rates of transition from the closed states, $C1$ and $C2$, to the open states $O1$ and $O2$ respectively. Conversely, K_{di} are the closing rates from the open states to the closed states. K_r is the thermal recovery rate from $C2$ to $C1$. e_{12} and e_{21} are the transition rates from $O1$ to $O2$ and vice versa. The values for all rate constants can be found in table 2.1.

Table 2.1: Rate constant values for the meso scale optogenetic model of ChR2 embedded in the cell membrane [31].

Rate constant	Transition from	Value ($\times 10^3 s^{-1}$)
K_{a1},K_{a2}	C1 to O1, C2 to O2	0.5Φ, 0.12Φ
K_{d1},K_{d2}	O1 to C1, O2 to C2	0.1, 0.05
e_{12},e_{21}	O1 to O2, O2 to O1	$.011 + .005 log(\Phi/0.024)$, $0.008 + 0.004 log(\Phi/0.024)$
K_r	C2 to C1	1/3000

$\Phi(t)$ is the photon flux per ChR2. K_{ai} is given by the quantum efficiency times the photon flux, $\varepsilon_i.\Phi(t)$.

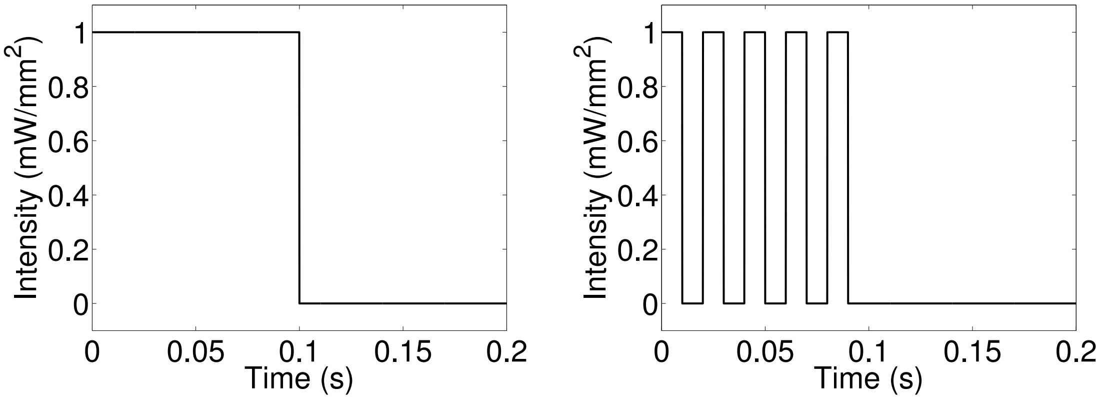

(a) Constant illumination (b) Pulsed illumination

Figure 2.2: Illumination profiles for light intensity of 1 mW/mm^2. The light is turned on and off for 0.01s until 0.1s in the pulsed illumination profile shown in fig. 2.2b

Fig. 2.2 shows the two kinds of illumination profiles we use for optogenetic actuation, and fig. 2.3 depicts the corresponding optogenetic conductance for a given illumination using a constant cell membrane voltage of -70 mV. For both constant and pulsed illumination, light intensities of 1 mW/mm^2, 0.1 mW/mm^2 and 0.01 mW/mm^2 have been used. The pulsing of light has a markedly different effect on a cortical model without a voltage clamp, and this is demonstrated in the next section. Here, we use a fourth order Runge Kutta method to solve equations 2.1-2.3.

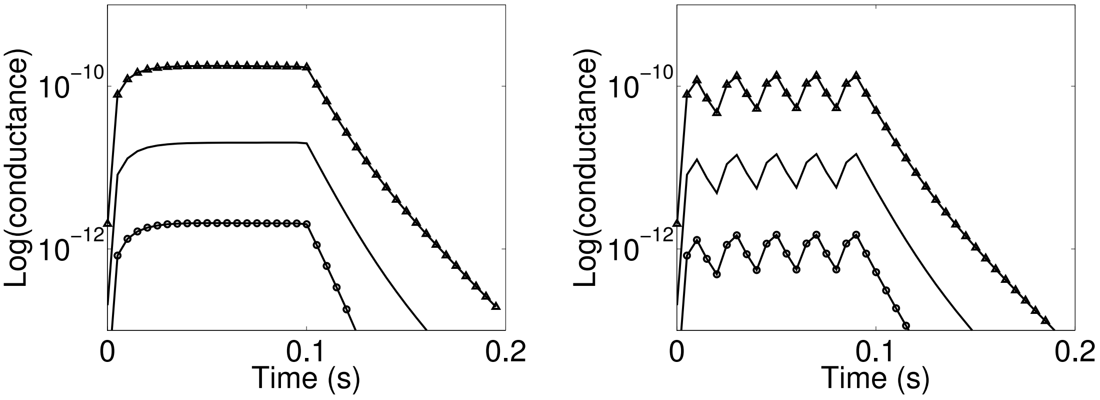

(a) Constant illumination (b) Pulsed Illumination

Figure 2.3: Semi-log plot showing variation of conductance with constant and pulsed light intensity for an ion channel density of 10^9ChR2's$/m^2$. △– - 1 mW/mm^2, – - 0.100 mW/mm^2, •– - 0.01 mW/mm^2. If the conductance were multiplied by the clamped voltage value of -70 mV, it would reproduce the plot of current vs. time in [31].

Fig. 2.3a shows the difference between the conductance of optogenetic channels illuminated by 1 mW/mm^2, 0.1 mW/mm^2 and 0.01 mW/mm^2 light intensities. The peak to plateau ratio of the conductance is decreased as intensity decreases. Also, the peak and plateau values decrease as the intensity is decreased. Similar behavior is observed in the case with pulsed illumination. Fig. 2.3b shows the conductance has sharper spikes when a lower intensity is used. However, with a higher intensity, the peak conductance value decreases less rapidly at the highest point before dropping off again when the light is turned off. Both constant and pulsed illumination profiles produce a sharp rise in conductance value before it reaches a steady state after about 50 ms.

2.2 Open loop control

In [85], we presented a strategy for integrating the preceding model into the meso-scale cortical dynamics. The computational domain for our meso scale cortical model is broken up into 100×100 cells which corresponds to a total area of 700×700 mm^2. To adapt the optogenetic model to the meso scale, the values of N_{Oi} and N_{Ci} have been normalized with the total number of ChR2 channels per representative neuron, and now represent the fraction of channels in each state per representative neuron. The sum of these fractions equals unity, and is described in eq.2.4.

$$N_{O1} + N_{O2} + N_{C1} + N_{C2} = 1. \tag{2.4}$$

By multiplying these fractions with the expression density (ion channels per unit area of cell membrane) and the area of each representative neuron, we obtain the total number of ion channels per representative neuron, and consequently, the total conductance of all the ion channels per representative neuron. It should be noted that while we are dealing with chemical dynamics at the molecular scale to describe the state of optogenetic channels, it is reasonable to scale the idea up to the meso scale that describes the cortex because the cortical model represents a population of spatially averaged neurons. In this study, we have not taken into account the light cone [11] emitted by each light source and the variation in illumination intensity they produce over a given area. Instead, we model the average intensity throughout a representative neuron with no overlap between two light cones.

We now introduce open loop control using optogenetic ion channels.

$$\frac{\partial \tilde{h}_i}{\partial \tilde{t}} = 1 - \tilde{h}_i + \Gamma_e(h_e^0 - \tilde{h}_i)\tilde{I}_{ei} + \Gamma_i(h_i^0 - \tilde{h}_i)\tilde{I}_{ii} - u, \tag{2.5}$$

Eqn. 2.5 is a modification of eqn. 1.3 that includes the control term u. ChR2 channels are cation pumps that conduct Na^+, Ca^{2+} , H^+ and K^+ ions. The control term is defined as

$$u = h_i.G_{ChR2}.R_m. \tag{2.6}$$

This formulation is dependent on the mean soma potential of the inhibitory population, and the mean membrane resistance of these cells represented by R_m is obtained from voltage clamp experiments and has a value of $7.1G\Omega$ [97]. The conductance of ChR2 channels is given by,

$$G_{ChR2} = G_{max}.g_{ChR2}.\frac{(1-exp(-h_i/U_0))}{h_i/U_1}.N_{ChR2}, \tag{2.7}$$

where h_i is the membrane potential for the inhibitory population, G_{max} is the maximum conductance of optogenetic channels in the $O1$ state, g_{ChR2} is the total conductance of the optogenetic channels in the $O1$ and $O2$ states defined by $(g_{O1}.N_{O1} + g_{O2}.N_{O2})$. U_0 and U_1 are empirical constants with values of $40mV$ and $15mV$ respectively. N_{ChR2} is the number of ChR2 channels per cortical macrocolumn.

2.2.1 Constant illumination

In what follows, the use of optogenetic channels to inhibit seizure waves is illustrated. In figures 2.4 and 2.6, control is actuated at 0.5s by illuminating the cortex with light of 470 *nm*. From eq. 2.7 it can be seen that the net conductance produced for a given light intensity is directly proportional to the number of ChR2 channels expressed. Here, we have used a channel expression density (number of ChR2 channels per unit area) of $\sim 10^9/\mathrm{m}^2$ in order to use illumination intensities that correspond to experiments [11]. Fig. 2.4 uses a constant light intensity source of 20 mW/mm^2 to illuminate the cortex.

The time scale at which the dynamics of the meso scale cortex occurs is slower than the time scale of the optogenetic channel dynamics. We used a two step predictor corrector numerical method to solve the set of SPDEs, and a first order forward Euler method to solve the optogenetic ODEs at each point in the domain[1].

The mechanism for seizure control using this approach is as follows. When ChR2 expressed by the inhibitory cell population is activated with light, cations are pumped from the extra-cellular space into the inhibitory cells, which depolarizes them. This changes the mean soma potential and the firing rate of the inhibitory population, which in turn changes the mean soma potential of the excitatory population through the influence of the postsynaptic activation due to the inhibitory population ($\tilde{I}_{ie}$). The firing rate of a representative neuron is determined by its mean soma potential, so by changing the mean soma potential, the firing rate can be changed as well. The seizures discussed here are caused by runaway excitation, so by increasing the firing rate of the inhibitory population the firing rate of excitatory cells, which fire synchronously during epileptic seizures, can be inhibited, breaking the synchronicity and inhibiting seizure waves.

---

[1] The fourth order solver is more accurate in producing results that match experimental observations of conductance, but the first order method takes less computation time to solve the equations. Because the optogenetic channels function at a faster time scale, and because we are only interested in time scales of the cortical model, the use of the simpler first order method is justified.

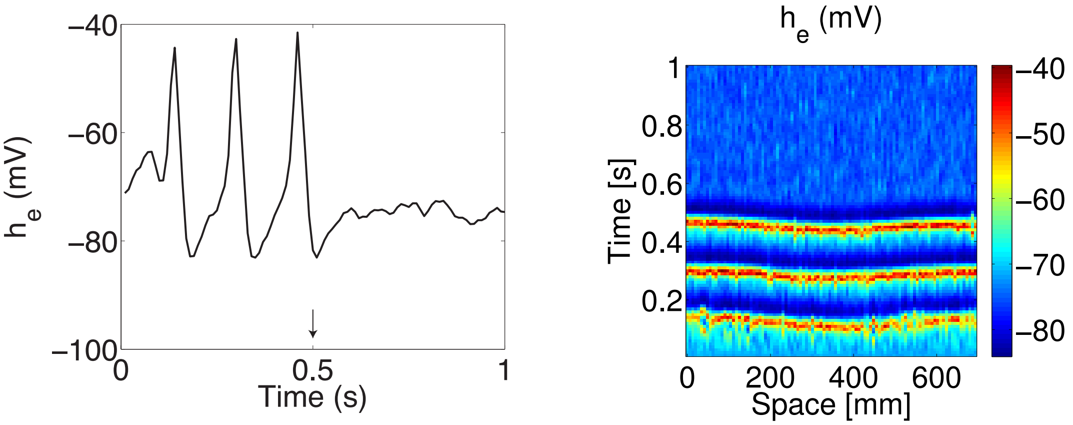

(a) Mean soma potential at a point in the model cortex (b) 1D slice of the 2D model cortex

Figure 2.4: Optogenetic seizure control using constant illumination of intensity 20 mW/mm^2. The model cortex measures 700×700 mm^2, with $P_{ee} = 548.0$, $\Gamma_e = 0.66 \times 10^{-3}$ and $\alpha = 1.15$. Fig. 2.4a shows the variation of mean soma potential of the excitatory population, while the arrow indicates control being turned on at 0.5s. The color bar in fig. 2.4b shows mean soma potential values in mV.

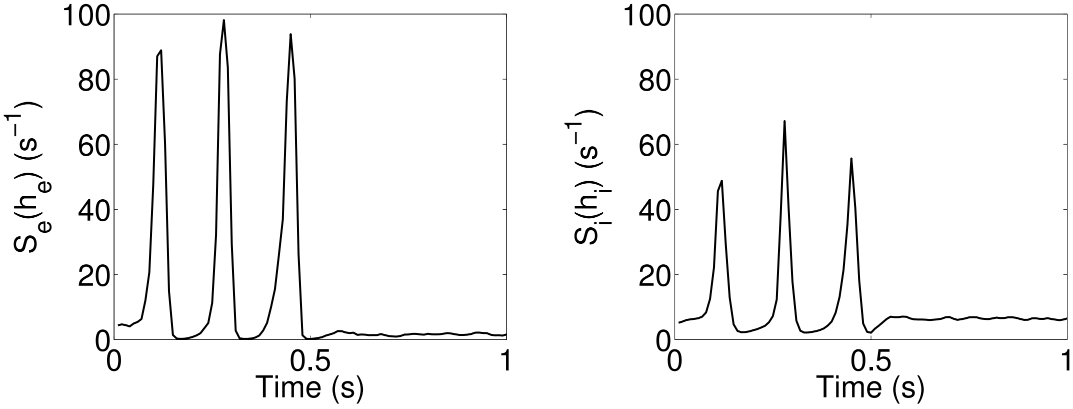

(a) Excitatory population (b) Inhibitory population

Figure 2.5: Firing rates for the excitatory and inhibitory population with optogenetic control applied at 0.5s

Fig. 2.5, shows how the baseline value of firing rate for the inhibitory population is higher than that of the excitatory population after optogenetic control is applied at 0.5s. It should be noted here that Fig. 2.5 depicts the firing rate of a representative neuron in the mean field model, and not the spiking of an individual neuron.

2.2.2 Pulsed Illumination

Optogenetic control using pulsed illumination depends on the intensity and the pulsing profile. Figure 2.6 uses a pulsed light source of 40 mW/mm^2 with pulses that are switched on and off for 0.005s. This leads to a successful breakdown of all synchronous behavior, as in fig. 2.6. With the shorter pulses the dark periods (0.005s) are not long enough for most of the optogenetic channels to close, and this results in behavior similar to constant illumination where the majority of the channels are open.

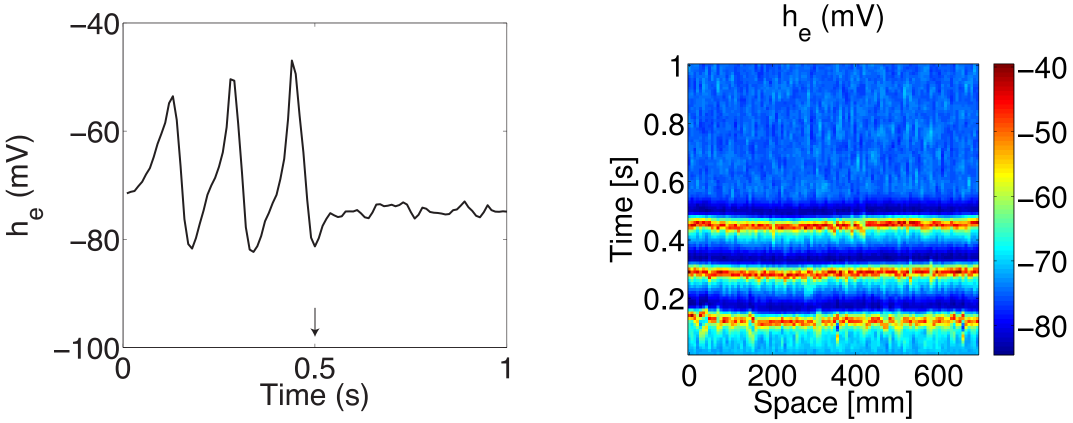

(a) Mean soma potential at a point in the model cortex

(b) 1D slice of the 2D model cortex

Figure 2.6: Optogenetic seizure control using pulsed illumination of intensity 40 mW/mm^2 with pulses that are switched on and off for 0.005s. The model cortex measures 700×700 mm^2, with $P_{ee} = 548.0$, $\Gamma_e = 0.66 \times 10^{-3}$ and $\alpha = 1.15$. Fig. 2.6a shows the variation of mean soma potential of the excitatory population, and the arrow in the figure indicates control is turned on at 0.5s. The color bar in fig. 2.6b shows mean soma potential values in mV.

In figures 2.7 and 2.8 we use two different pulsing profiles with the same peak intensity (40 mW/mm^2) used to generate fig. 2.6, where 0.005s pulses were used.

Fig. 2.7 was generated using light pulses that are turned on and off for 0.05s. While the amplitude of the seizure waves is decreased considerably, it is seen that synchronous behavior persists despite control being applied at 0.5s. This is because the dark regions of the pulsing profile, where the ion channels tend to close, is long enough to reduce control to a low value where it does not have a considerable effect on the seizing cortex. However, the frequency of the pulsing still ensures the oscillations are not fully developed because control does not go to zero during the dark regions on account of the gradual decay of channel conductivity.

Figure 2.8 was generated using light pulses that are turned on for 0.08s and turned off for the same duration. In this case, seizure waves have not been inhibited, but the frequency has been reduced. This can be accounted for by the duration of the dark periods of pulsing (0.08s), which is long enough to close the ion channels completely leading to zero control. During the dark periods,

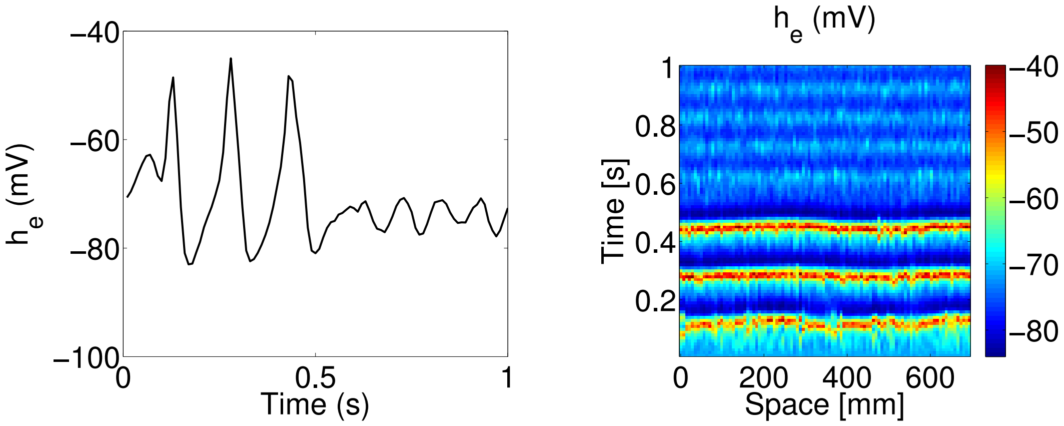

(a) Mean soma potential at a point (b) 1D slice of the 2D model cortex

Figure 2.7: Optogenetic control applied at 0.5s using 0.05s pulsed illumination. Synchronous behavior persists even after control is applied, but the amplitude of seizure waves is decreased. Parameters: $P_{ee} = 548.0$, $\Gamma_e = 0.00066$, $\alpha = 1.15$, expression density $= 10^4$ ChR2s/m^2, Intensity $= 40$ mW/mm^2.

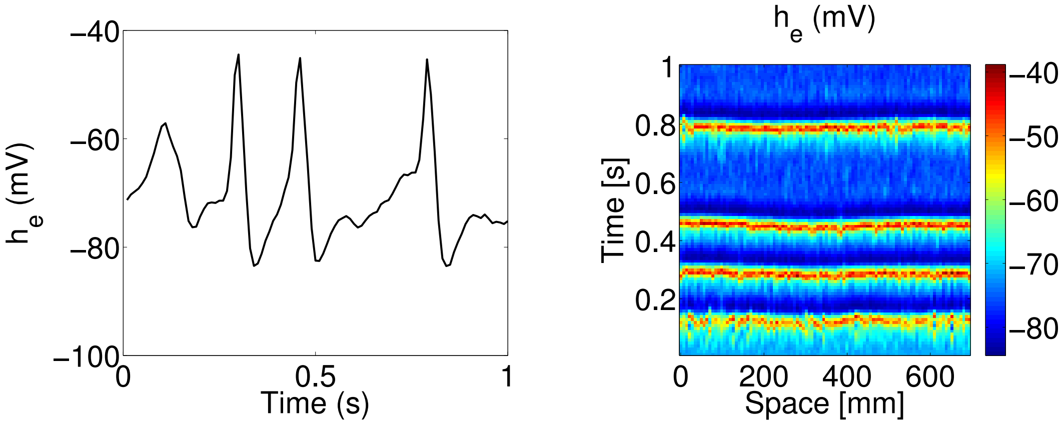

(a) Mean soma potential at a point in the model cortex (b) 1D slice of the 2D model cortex

Figure 2.8: Pulsed optogenetic control using 0.08s pulses applied at 0.5s. Frequency of seizure waves has decreased, but amplitude of oscillations is invariant. Parameters: $P_{ee} = 548.0$, $\Gamma_e = 0.00066$, $\alpha = 1.15$, expression density $= 10^4$ ChR2s/m^2, Intensity $= 40$ mW/mm^2 - pulsed illumination with 0.08 s pulses.

the cortex starts seizing again, but the seizures are inhibited completely during the illuminated periods of pulsing.

2.3 Robustness of open loop optogenetic stimulation

In this section we explore the robustness of the control approach to changes in different aspects of the model. The parameters for the meso scale model are varied within ranges provided in [10] and [55].

2.3.1 Stochastic inputs

The subcortical input contributes to the postsynaptic activation through constant P_{ij} and stochastic inputs defined by

$$\tilde{\Gamma} = \alpha\sqrt{P_{ij}}\xi[\tilde{x},\tilde{t}]$$

where α is a scaling parameter for the stochastic inputs and ξ is zero mean, Gaussian white noise in time and space.

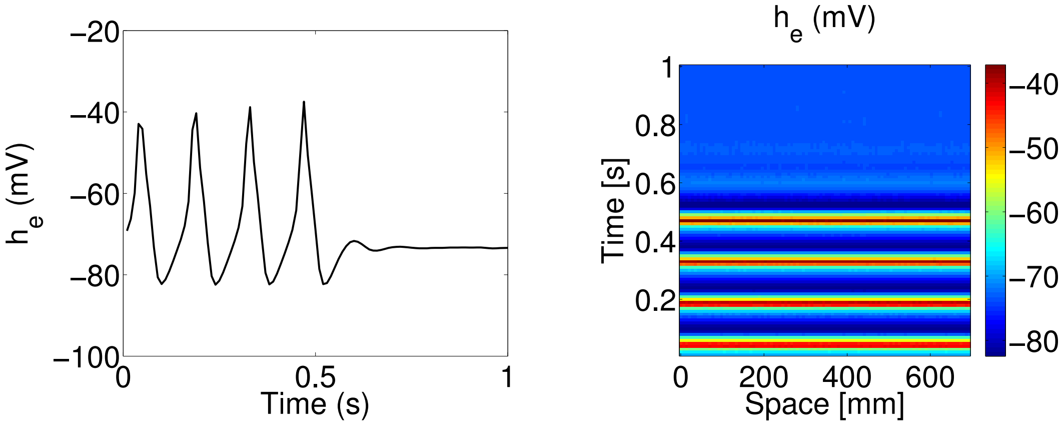

(a) Mean soma potential at a point in the model cortex (b) 1D slice of the 2D model cortex

Figure 2.9: More uniform seizures produced with low noise. Control switched on at 0.5s successfully inhibiting seizures. Parameters: $\alpha = 0.05$, $\Gamma_e = 0.0008$, $P_{ee} = 548.0$, expression density $= 10^4$ ChR2s/m^2, Intensity $= 40$ mW/mm^2 - constant illumination.

Figures 2.4, 2.9 and 2.10 demonstrate the efficacy of the optogenetic control method for different stochastic inputs over two orders of magnitude of noise. Seizure waves are successfully inhibited for α values of 0.05, 1.15 and 5, using the same expression density and constant illumination for all three cases.

2.3.2 Seizure hotspot

While the cortex has been laid out like a flat sheet in the figures presented here, it is made up of a number of folds in reality. The crests of these folds are called *gyri* (s. *gyrus*), while the intervening

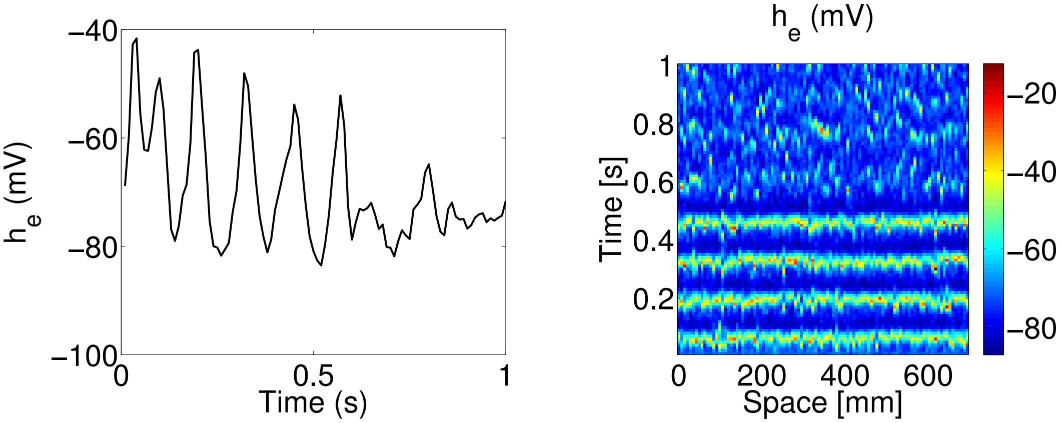

(a) Mean soma potential at a point in the model cortex (b) 1D slice of the 2D model cortex

Figure 2.10: Higher α causes noisier oscillations, however, control is still successful in diminishing synchronous activity when applied at 0.5s. Parameters: $\alpha = 5$, $\Gamma_e = 0.00066$, $P_{ee} = 548.0$, expression density $= 10^9$ ChR2s/m^2, Intensity $= 60$ mW/mm^2 - constant illumination.

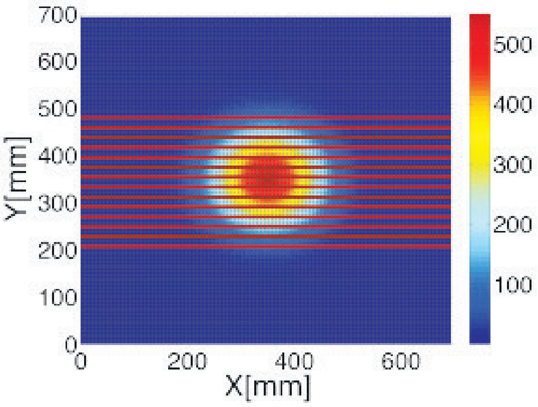

Figure 2.11: Gaussian distribution of P_{ee} (seizure hotspot) with a *gyri* to *sulci* area ratio of 1:2. Red lines running across the model cortex represent *gyri* populated with optogenetic channels.

grooves are called *fissures* or *sulci* (s. *sulcus*) [43]. When optogenetic channels are expressed in the cortex, the ones on the *gyri* have a better chance of being illuminated.

In order to account for this reduction in the number of channels being illuminated, fig. 2.12 only has channels expressed in a third of the cortical surface area. The sites of optogenetic expression are in strips running across the cortex (representing *gyri*) separated by strips of zero optogenetic channel expression (representing *sulci*). We have also included a seizure hotspot by using a Gaussian distribution for P_{ee} with a maximum value of 548.0. Seizure waves arise where the value of P_{ee} is high enough and travel outward until the level of excitation is too low to support them. It should also be noted that the channel expression only covers the hotspot area of the model cortex as shown in fig. 2.11.

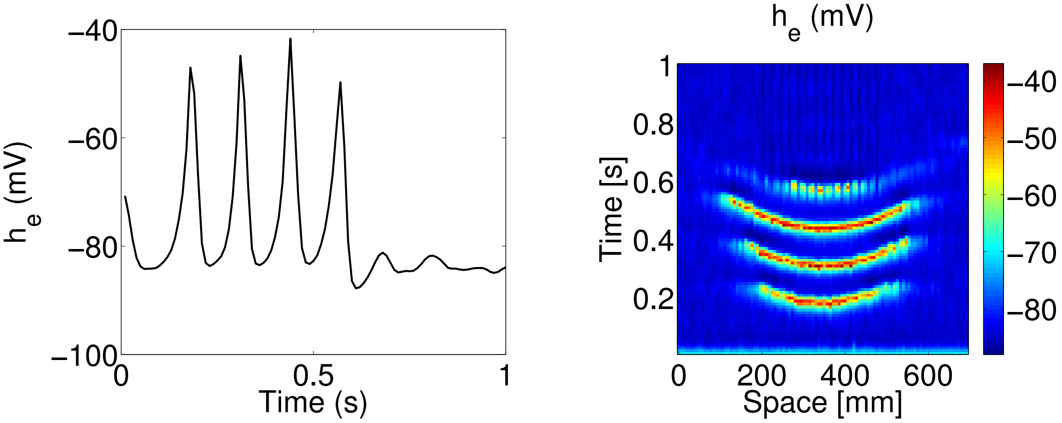

(a) Mean soma potential at a point in the model cortex (b) 1D slice of the 2D model cortex

Figure 2.12: Seizure hotspot with maximum P_{ee} at the center of the model cortex. with a *gyri* to *sulci* ratio of 1:2. Parameters: $P_{ee} = 548.0$, $\Gamma_e = 0.001$, $\alpha = 1.6$, expression density $= 2 \times 10^9$ ChR2s/m^2, Intensity $= 20$ mW/mm^2 - constant illumination.

Fig. 2.12 shows the application of optogenetic control at 0.5s to a cortex that has a *gyri* to *sulci* ratio of 1:2. The expression density has been increased by a factor of 2, but the control is successful in inhibiting seizures. As a first attempt to account for the geometry of the cortex and the ability to illuminate it, fig. 2.12 demonstrates the efficacy of using optogenetics as a control method.

2.3.3 Changes in cortical model parameters

The parameters of the meso scale model are taken to remain constant during our simulations. However, the cortex is more plastic. To account for this plasticity, parameters like the number of long range connections between cell populations and the neurotransmitter rate constants were changed within their physiological bounds [55], and the effect of optogenetic control on the model seizing cortex was studied.

The long range connections are critical to a seizing cortex [72]. In fig. 2.13 the number of long range connections from the excitatory cells to other excitatory or inhibitory cells was changed from the normative values of $N_e^\alpha = 4000$ and $N_i^\alpha = 2000$ [49], where *e* and *i* represent the excitatory and inhibitory populations respectively, to the extrema of their ranges [55]. It is seen that the model cortex can be driven to seizures only if both N_e^α and N_i^α are increased because it results in a model cortex predisposed to higher long range excitatory inputs. To this end, we used $N_e^\alpha = 5000$ and $N_i^\alpha = 3000$ connections for our simulations, and the seizing cortex was successfully brought under control using a constant illumination intensity of 60 mW/mm^2.

In figures 2.14 and 2.15 the neurotransimtter rate constants T_e and T_i are changed to 20 and 4 respectively from the normative values of 12 and 2.6. These rate constants incorporate the effects

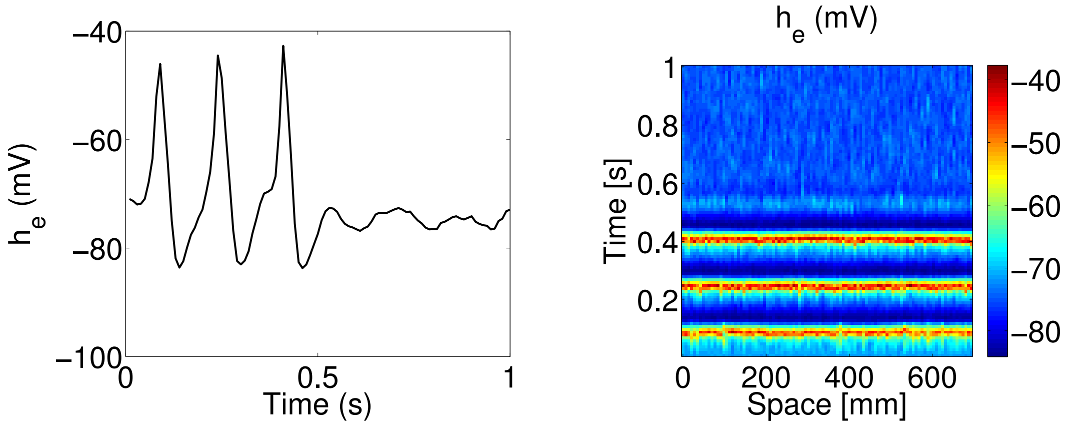

(a) Mean soma potential at a point in the model cortex (b) 1D slice of the 2D model cortex

Figure 2.13: Change in the long range connectivity N_j^α to demonstrate efficacy of the controller when the connectivity is changed . Parameters: $P_{ee} = 548.0$, $\Gamma_e = 0.00066$, $\alpha = 1.15$, expression density $= 10^9$ ChR2s/m^2, Intensity $= 60$ mW/mm^2 - constant illumination, $N_e^\alpha = 5000$, $N_i^\alpha = 3000$.

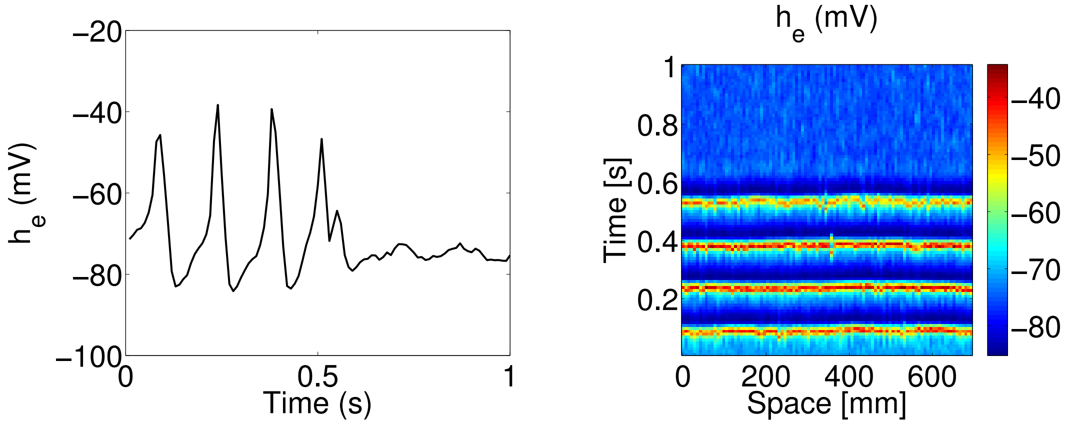

(a) Mean soma potential at a point in the model cortex (b) 1D slice of the 2D model cortex

Figure 2.14: Change in the neurotransmitter rate constant T_e to demonstrate efficacy of the controller when the connectivity is changed . Parameters: $P_{ee} = 548.0$, $\Gamma_e = 0.00066$, $\alpha = 1.15$, expression density $= 10^9$ ChR2s/m^2, Intensity $= 60$ mW/mm^2 - constant illumination, $T_e = 20$, $T_i = 2.6$.

of passive dendritic cable delays and neurotransmitter kinetics on the time course of somatically recorded postsynaptic spike activity in a neuron [55]. Again, seizures are produced in the cortical model, but they are successfully inhibited when optogenetic control is applied at 0.5s.

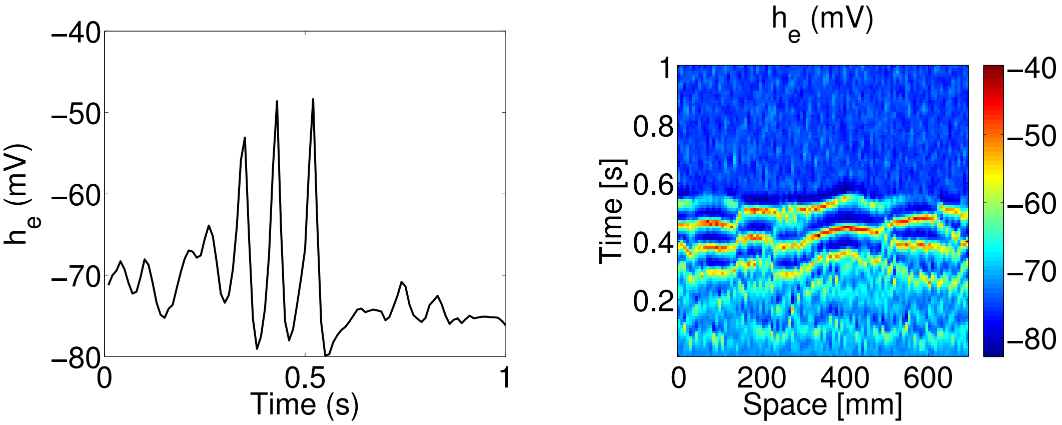

(a) Mean soma potential at a point in the model cortex (b) 1D slice of the 2D model cortex

Figure 2.15: Change in the neurotransmitter rate constant T_i to demonstrate efficacy of the controller when the connectivity is changed . Parameters: $P_{ee} = 548.0$, $\Gamma_e = 0.00066$, $\alpha = 1.15$, expression density $= 10^9$ ChR2s/m^2, Intensity $= 60$ mW/mm^2 - constant illumination, $T_e = 12.0$, $T_i = 4.0$.

2.4 Summary of original contributions

In this chapter, we presented a scale free model for the dynamics of Channelrhodopsin-2 (ChR2), which is an optogenetic channel that pumps cations into the host neuron when illuminated with blue light of wavelength 470 *nm*. The scale free ChR2 model facilitates integration of channel dynamics, which takes place physiologically at the micro-scale, into network models like the meso-scale human cortical model used in this dissertation. We showed how higher light intensities result in higher channel conductances, and demonstrated the capacity of open loop optogenetic stimulation to suppress seizures that manifest in the model human cortex from different pathways.

However, while open loop optogenetic stimulation demonstrates how cortical seizures can be successfully inhibited if a high enough illumination intensity is used, it does not use light energy optimally, which is a necessary condition for the efficient and cost-effective use of optogenetics as a seizure control strategy. Additionally, prolonged exposure to high intensities of light has been shown to cause irreversible tissue damage in animal models [11], so we have to minimize the time the cortex is illuminated with high intensities to ensure tissue safety. In light of this, we propose a method of feedback control that satisfies these requirements.

Chapter 3

Closed loop optogenetic control of seizure like activity in the model cortex

In the previous chapter, we demonstrated the use of optogenetics as an effective control modality for cortical seizures in the context of the meso-scale cortical model. The ion conductance of ChR2 is dependent on the intensity of light used, and the membrane potential of the cell population expressing these channels as demonstrated by equations 2.1-2.7. This results in intricate dynamics between the effects of optogenetic stimulation on the cortex, and vice versa. Higher intensities yield higher conductances as shown in fig. 2.3, while higher membrane potentials reduce conductivity of these ion channels (eq. 2.7). Channel conductivity is greatly reduced as the reversal potential of the neuron is approached because of its dependence on membrane potential. External modulation of the conductance of these channels is thus only possible via the intensity of light illuminating the channels. Taking these characteristics of channel dynamics into consideration, we present a method of closed loop feedback optogenetic control of seizures in the model human cortex.

3.1 Development of the control law

To design a feedback loop that provides optimal optogenetic stimulation, the light intensity has to be based on a measured variable in the combined cortical-optogenetic model. We have chosen to use the signal sensed at the surface of the cortex by an electrode, $\tilde{h}_m$ [58], for two reasons. Firstly, the length scales involved in the meso-scale model of the cortex used here are similar to the sizes of commercial electrode arrays. Secondly, it is a mean-field model, which means all variables in the model are spatially averaged properties of neuron populations. EEG/ECoG measurements are based on the ensemble behavior of many neurons, and the mesoscale model is suited to capturing such behavior.

The measured signal from the surface of the cortical model, $\tilde{h}_m$, is a function of the extracellular currents in the tissue, and not of the intracellular soma potential [69]. Taking this into account, Lopour & Szeri [58] defined $\tilde{h}_m$ using the following two equations:

$$\tilde{h}_m = (h_0^e - \tilde{h}_e)\tilde{I}_m \tag{3.1}$$

$$\begin{aligned}\left(\frac{1}{T_m}\frac{\partial}{\partial \tilde{t}} + 1\right)^2 \tilde{I}_m = F\big(& -0.413 \times N_e^\beta \tilde{S}_e - 0.092 \times N_i^\beta \tilde{S}_i \\ & -0.458 \times \tilde{\phi}_e + 0.034 \times (P_{ee} + \tilde{\Gamma}_1) - 0.004 \times (P_{ie} + \tilde{\Gamma}_3)\big)\end{aligned} \tag{3.2}$$

where $\tilde{h}_m$ is the potential measured by a cortical surface electrode, $\tilde{I}_m$ is the current measured at the cortical surface, h_0^e is the reversal potential of the excitatory population, $N_{e,i}^\beta$ are the number of synaptic connections from the excitatory and inhibitory populations, respectively, $\tilde{S}_{e,i}$ are the firing rates of the excitatory and inhibitory populations, respectively, P_{ee} and P_{ie} are the subcortical inputs from the excitatory and inhibitory populations to the excitatory population, and $\tilde{\phi}_e$ is the long range corticocortical input from the excitatory population. Please see chapter 1 for the full set of equations that describe the dynamics of the meso-scale cortical model and associated parameters. F is a positive gain parameter that helps convert the right side of equation 3.2, which is based on voltages, to currents, which is the basis of the left side of the equation. It also scales the magnitude of the synaptic inputs to ensure an appropriate amount of influence over the electrode measurement $\tilde{I}_m$. In equation 3.2, we use $F = 10^{-3}$. Additionally, we include the mean offset of the measured signal, which gives us a net positive signal. This is in contrast to EEG readings, for example, where the mean offset is subtracted to obtain a signal with mean zero. The theory behind the measured signal, mean offset, equations 3.1 and 3.2, and the constants, coefficients and parameters used in these equations is explained in detail in [58].

To calculate intensity, E, that should enable successful control - i.e. the ‘control law’ - we use the concept of proportional and integral (PI) control. As we are dealing with a highly non-linear and stochastic system, PI control offers a simple, but effective way to calculate the control effort based on the measured potential $\tilde{h}_m$:

$$E = K_P \tilde{h}_m + K_I \int_{t-\tau}^{t} \tilde{h}_m dt \tag{3.3}$$

The first term of eq. 3.3 represents proportional control, where K_P is proportional gain. This component of the control effort calculates a contribution to the intensity of light to be used based on the current value of measured potential. Spikes in intensity with highs past the physiological limit, and lows tending to zero, will lead to unsafe and ineffective control. To avoid this, we lower K_P to ensure peak values of intensity are safe for cortical tissue, and add a second term based on the integral of $\tilde{h}_m$ over a short duration of time, τ. Throughout this chapter, we use $\tau = 0.2$s. This contribution is modulated by K_I, which is the integral gain term in eq. 3.3, and addresses shortfalls in intensity, and synaptic delays between cell populations that lead to continued seizure activity.

It should be noted that equation 3.3 is slightly different from the traditional form of PI control, where the control effort is based on minimizing the error in the measured signal. Error would be calculated based on the difference between amplitude of the expected (or desired) signal and the measured signal. However, the mathematical model of the human cortex consists of a highly stochastic, non-linear system of PDEs, and in the example simulations we present in this work, the values of parameters associated with the model change over time - e.g. P_{ee} varies with time. This leads to a non-stationary expected value of $\tilde{h}_m$. However, the expected value of $\tilde{h}_m$ in a normally functioning cortex is much smaller numerically than peak $\tilde{h}_m$ values observed during the seizure state. We can thus neglect the estimated value and calculate control effort based directly on the measured variable $\tilde{h}_m$.

The entire spatial domain of the model cortex is discretized with a Cartesian mesh to perform numerical simulations. The measured potential and intensity are calculated as piecewise constant approximations at every grid point, and we do not account for the electrodes' spatial profiles, or the spatial variation of illumination in this first study of the efficacy of the control law and the dynamics of the combined cortico-optogenetic model during closed loop stimulation.

3.1.1 Triggering and deploying control

In the previous chapter, the model cortex was hyperexcited by increasing the excitatory subcortical inputs to a magnitude 50 times higher than during normal function. This led to travelling seizure waves that were suppressed by open loop optogenetic control, which was applied by depolarising inhibitory neurons that express ChR2 channels to increase inhibition. However, the measured potential, $\tilde{h}_m$, is related to the mean soma potential of the excitatory population, $\tilde{h}_e$, because surface electrode measurements are averaged readings from apical dendrites of pyramidal neurons, which are excitatory in nature. This means the light intensity required to illuminate the inhibitory population is also most closely related to $\tilde{h}_e$. In essence, to apply control, we measure the activity of the excitatory population, calculate intensity based on this measurement, which is then used to stimulate the inhibitory population. The effect of control is then measured again via the excitatory population and adjustments to the illumination intensity are made until seizures are suppressed.

Numerous methods of seizure detection using EEG/ECoG signals have been proposed over the last few years. Orosco et al. [70] used energy thresholds of instantaneous frequency data to detect seizures with around 60% accuracy. Spike features such as amplitude, width, rate and regularity, and changes in energy within specific frequency bands were taken into account while developing a seizure detection algorithm by Krook-Magnusson et al. [51]. Neural networks [67], entropy estimators [44], and a combination of neural networks and an entropy estimator [52] have been trained to detect seizures with more than 90% accuracy. The different methods currently available for seizure detection, and the pathway from acquiring data to closed loop applications can be found in [42]. Seizure prediction, on the other hand, has proven to be a more complicated task. Dynamical entrainment [37], accumulated signal energy [56] and phase synchronisation [64] are only a few examples of features of EEG data that were used in seizure prediction, but a fully satisfactory approach remains elusive. Realistically, given the wide variation in seizure pathologies and seizure types, a more subjective approach to detection [76] is required. This may entail a combination of detection methods including, but not limited to, electrode measurements, accelerometers, electrodermal activity and so on.

The aim of this work is to demonstrate the ability to calculate illumination intensity for optogenetic control directly from electrode measurements of cortical activity. The detection method merely serves as a trigger to turn on the controller, and does not play a role in the 'control law' itself. Therefore, we use a very straightforward trigger for seizure control based on the amplitude and rate of change of the measured potential, $\tilde{h}_m$, which has a mean value close to 0 during normal function, with fluctuations in amplitude that are much less than 0.1 in magnitude. Seizure activity is characterized by high amplitude oscillatory changes in the mean soma potential of neuron populations, and by extension, in $\tilde{h}_m$ as well. The amplitude and rate of change of amplitude thresholds that have to be surpassed for control to be triggered are based on the sensitivity of the controller, which in turn can be tuned differently for different paths to seizures. Again, this method of detection works well for the model seizures that we investigate in this work, but one can substitute any other detection method in its place to trigger the controller.

When control is triggered, the intensity of illumination is calculated based on the control law described in eq. 3.3. The proportional component contributes to changes in illumination intensity based on instantaneous changes in $\tilde{h}_m$, while the integral component is calculated over the past τ seconds and changes more gradually. The integral part of the control provides an offset for the proportional component resulting in the optimal amount of light intensity being used to inhibit seizures.

We have also included an off switch for the controller, which is based on the illumination intensity E and the amplitude of the measured potential h_m. This is a straightforward switch similar to the trigger used to turn on the controller, and facilitates studying the efficacy of the controller. One could substitute other switches in its place, which would work just as well with the controller.

3.1.2 Tuning the controller

In the next two sections, we demonstrate the efficacy of the PI controller for seizures in two different parameter spaces. The first space is associated with subcortical inputs from the excitatory populations (P_{ee}) and the influence of excitatory synaptic inputs on the mean soma potential (Γ_e). The second space is defined by the slope at the inflection point of the mean firing rate ($\tilde{g}_e$) and the influence of inhibitory synaptic inputs on the mean soma potential (Γ_i). Please see chapter 1 for the full set of equations that describe the dynamics of the meso-scale cortical model. In separate work, these parameter spaces were identified as being the most probable regions in which seizures produced using the mesoscale model have been shown to be directly, and quantifiably, compared with electrocorticogram (ECoG) readings of seizures from a human subject [23].

In both parameter spaces, seizures are induced in a normally functioning model cortex by gradually varying one of the parameters with time. In both parameter spaces, the model cortex produces the most robust seizures at the peak value of these parameters. The gains of the PI controller and the intensity for a comparable open loop controller, in turn, are tuned to suppress seizures induced at these peak values of the parameters.

Given the stochastic nature of the model cortex, we use numerical optimization to obtain the most optimal values of proportional and integral gains that successfully suppress seizures. We use the illumination intensity to define a cost function,

$$Cost = \int_{t_{on}}^{t_{off}} Edt \tag{3.4}$$

where E is the illumination intensity, t_{on} is the time at which control is switched on, and t_{off} is the time at which control is switched off. The cost, in terms of J/mm^2 is calculated for a range of proportional and integral gain terms. The response diagram for each pair of proportional and integral gains is examined for oscillations, and the pair which minimizes the total energy calculated by equation 3.4 while successfully suppressing seizures is chosen to calculate the control effort.

3.2 Seizures in the P_{ee}-Γ_e space

Seizures in this parameter space are simulated by increasing subcortical inputs that will lead to a hyperexcited model cortex, while simultaneously reducing the influence of excitatory synaptic input on the mean soma potential. We will explore seizures caused by a decrease in inhibition in section 3.3. An increase in subcortical inputs from the excitatory population, P_{ee}, leads to an increase in the post synaptic activation due to excitatory inputs ($\tilde{I}_{ee}$), which in turn increases the mean soma potential of both the excitatory ($\tilde{h}_e$) and inhibitory ($\tilde{h}_i$) cells that leads to higher firing rates in both populations. The post-synaptic activation due to the excitatory population in the seizing model cortex is lowered, while the post-synaptic activation due to the inhibitory population is held constant. This causes a net decrease in the post-synaptic influence of the excitatory population on itself and the inhibitory population. In addition, there are fewer inhibitory synapses than excitatory ones, leading to a net increase in excitation due to the hyper-excitatory subcortical inputs, that results in seizures in the model cortex. A more detailed analysis of the feedback and reciprocal synaptic connections in the model cortex that lead to seizures due to an increase in sub-cortical excitation can be found in [49].

When results from simulating cortical activity using the mesoscale model were compared with patient data [48], the magnitude of P_{ee} required to produce seizure like activity in the model cortex was almost 50 times the value of P_{ee} required for normal function. Here, we present two cases of epileptic seizures caused by excessive excitation with different values of Γ_e, the influence of the excitatory post-synaptic potential on the mean soma potential of a neuron population, and α, the amplitude of noise in the stochastic subcortical inputs[1]. The first case uses $\Gamma_e = 0.00066$ and $\alpha = 1.15$, while the second case uses $\Gamma_e = 0.0008$ and $\alpha = 1.6$. The excitatory inputs in the second case are higher and produces more robust seizures that require greater increases in inhibition to suppress seizures. These parameter values are within the physiologically acceptable range of Γ_e and α values that cause seizures for the range of P_{ee} used here.

3.2.1 Seizures with Γ_e = 0.00066 and $\alpha = 1.15$

A temporal distribution of P_{ee} with a maximum value of 548.0 as shown in fig. 3.1c ensures a gradual increase in the mean soma potentials of both neuron populations until the cortex is tipped into a state of seizures. Figure 3.1a depicts the variation of the mean soma potential of the excitatory population with time at a point in the model cortex, and figure 3.1b represents a one dimensional slice of the two dimensional domain illustrating travelling waves when seizure like activity is observed for the range of P_{ee} shown in fig. 3.1c. It should be noted here that the seizure waves may appear to be almost stationary in a 1D slice of the two dimensional cortex. These are, in fact, spiral waves with large radii of curvature as illustrated in chapter 1. The smaller cortex used in this work has dimensions of the order of a human cortex, making it difficult to appreciate the curvature of the travelling waves, which have radii of curvature of the order of the dimensions of the model human cortex. Interestingly, while high values of P_{ee} are required to initiate seizures, lower values of P_{ee} are able to sustain seizure like activity as seen in fig. 3.1. Oscillatory activity seizes when the magnitude of P_{ee} falls well below 450.0 despite starting only after P_{ee} has risen past a value of around 520, as shown in fig. 3.1a.

---

[1] Please refer to chapter 1 for details about the noise in the stochastic inputs

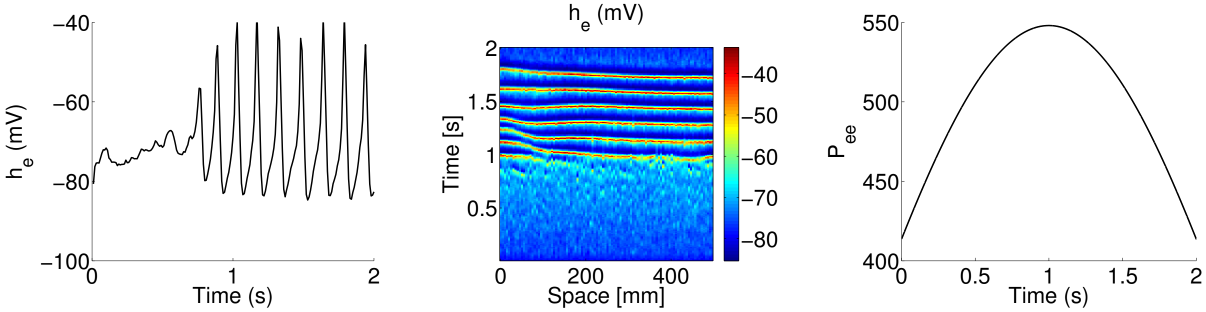

(a) Mean soma potential at a point (b) 1D slice of the 2D domain (c) P_{ee} at a point.

Figure 3.1: Seizures in the P_{ee}-Γ_e space. P_{ee} is gradually increased then decreased in time with a maximum value of 548.0 as shown in fig. 3.1c. Γ_e is held constant at 0.00066 with α = 1.15. All other parameters are similar to baseline parameters in [49].

Figure 3.2 shows the effect of closed loop optogenetic control on a seizing model cortex. Again, we use a temporal distribution of P_{ee} in time as shown in fig. 3.1c, and seizures are successfully suppressed. Control is effected by depolarising the inhibitory neurons. The increased inhibition suppresses the tendency of high subcortical inputs to hyperexcite the model cortex. Figure 3.2a shows that the mean soma potential is maintained around the rest potential of the excitatory population for the given values of Γ_e and P_{ee}. Figure 3.2b also shows the suppression of travelling seizure waves demonstrating a breakdown of oscillatory behavior.

Figure 3.2c shows the illumination intensity responsible for the mean soma potential of the excitatory population at the same point shown in fig. 3.2a. The intensity is calculated using eq. 3.3, and is triggered when $\tilde{h}_m$ surpasses a magnitude of 0.2, coupled with a 20 % change in $\tilde{h}_m$ over 20 ms. The controller gains are tuned to suppress a fully formed seizure with parameter values $P_{ee} = 548.0$, $\Gamma_e = 0.00066$ and $\alpha = 1.15$. The proportional and integral gain terms used in equation 3.3 ensure an optimal amount of light intensity will be used to quickly suppress oscillatory behavior. When the amplitude of measured potential $\tilde{h}_m$ and the intensity of light illuminating the

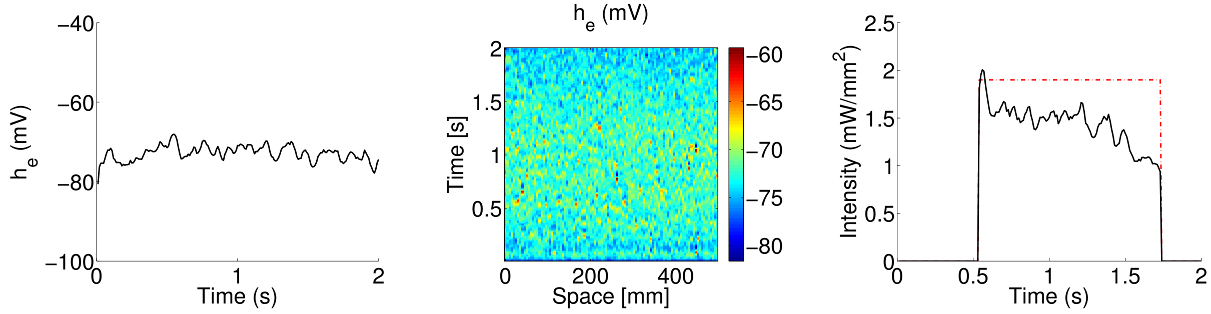

(a) Mean soma potential at a point (b) 1D slice of the 2D domain (c) Light intensity at a point

Figure 3.2: Effect of closed loop optogenetic control on seizures in the P_{ee}-Γ_e space using a temporal modulation of P_{ee} in time shown in fig. 3.1c. Γ_e is held constant at 0.00066 with $\alpha = 1.15$. All other parameters are similar to baseline parameters in [49]. Figures 3.2a and 3.2c show the variation with time of h_e and intensity, respectively at the same point. The red dot-dash line in figure 3.2c indicates the open loop intensity required to suppress a fully formed seizures at $P_{ee} = 548.0$. Gains used: $K_P = 3.0$ and $K_I = 0.12$.

model cortex fall below 0.1 and 1 mw/mm^2, respectively, control is switched off around 1.75s as shown in fig. 3.2c.

In contrast, An open loop illumination intensity of 1.9 mW/mm^2 will successfully suppress a fully formed seizure with parameter values $P_{ee} = 548.0$, $\Gamma_e = 0.00066$ and $\alpha = 1.15$. The red dot-dash line in fig. 3.2c shows the comparison between open loop and closed loop illumination required to suppress seizures if the light were switched on and off at the same time. However, as seen in figure 3.2c, lower intensities are required to maintain a state of normal function after an initial burst of 2 mw/mm^2, demonstrating the advantage of using a closed loop controller over an open loop controller using a constant illumination intensity. In fig. 3.1a, before the cortex seizes robustly with high amplitude changes in mean soma potential just before 1s, there are smaller oscillations around 0.5s that trigger control. When illumination is switched on just before the cortex starts seizing, the inhibitory population is depolarized. As stated earlier, this increases inhibition, which simultaneously suppresses excitation and the seizure waves.

This seizure is less robust than the one studied in the next subsection, requiring low intensities to successfully suppress oscillatory behavior. A high enough initial inhibitory stimulus is able to decrease excitation to levels that can be maintained with lower intensities. This is achieved by using a high proportional gain and a low integral gain. However, more robust seizures will require a greater offset in the proportional term to suppress oscillatory behavior, and this is achieved by using an integral term with a bigger contribution to the total calculated intensity.

3.2.2 Seizures with Γ_e = 0.0008 and $\alpha = 1.6$

Here we look at a more robust seizure with higher excitatory inputs. The seizure pathway is the same as the seizure studied in the previous subsection, however, the influence of the excitatory post synaptic potential (EPSP) denoted by Γ_e, and the amplitude of noise, α, in the stochastic subcortical inputs are both increased. Figures 3.4a and 3.3b show the variation of mean soma potential at a point and the travelling seizure waves in the model cortex, respectively. Again, the subcortical inputs from the excitatory population to itself is varied with time as shown in fig. 3.3c. As observed in fig. 3.1c, seizures start at a higher P_{ee} but are sustained even after the subcortical inputs have fallen below this initial value. However, we use a larger range of P_{ee} values here and this leads to two distinct differences with the seizures seen in section 3.2.1. One, for higher values of Γ_e and α seizures arise at a much lower value of P_{ee}. Two, we can clearly see the end of the seizure state in figures 3.3a and 3.3b, with oscillatory activity being suppressed around the 1.8 s mark.

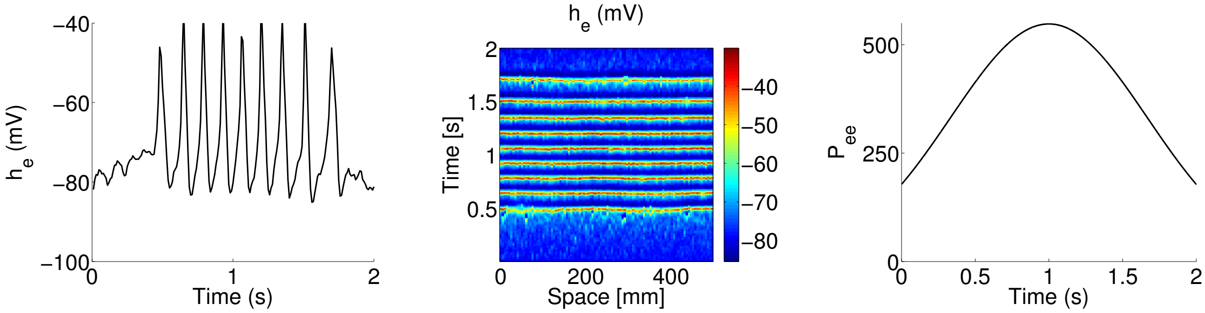

(a) Mean soma potential at a point (b) 1D slice of the 2D domain (c) P_{ee} at a point.

Figure 3.3: Seizures in the P_{ee}-Γ_e space. P_{ee} is gradually increased then decreased in time with a maximum value of 548.0 as shown in fig. 3.3c. Γ_e is held constant at 0.0008 with α = 1.6. All other parameters are similar to baseline parameters in [49].

Seizures arising with this set of parameters are successfully suppressed by using closed loop optogenetic stimulation as shown in fig.3.4. The proportional and integral gains for the controller are tuned to suppress a fully formed seizure at $P_{ee} = 548.00$, $\Gamma_e = 0.0008$ and $\alpha = 1.6$. An open loop intensity of 34 mW/mm^2 is required to control the same seizures. The red dot dash line in figure 3.4c compares open and closed loop intensity required to suppress the same seizure if the light were switched on and off at the same time. The on and off switch for the controller is based on the amplitude and rate of change thresholds used to detect seizures in section 3.2.1. Again, seizures are detected just as they begin to take shape, and control is triggered around 0.5s as seen in fig. 3.4c. As the strength of subcortical inputs peaks around 1s, there is a slight increase in the illumination intensity required to subdue oscillatory activity. Intensity continues to decrease almost monotonically after this increase at 1s.

The seizure in fig. 3.4 is rather robust and requires higher intensities to suppress oscillatory activity as compared to fig. 3.2. Furthermore, the proportional gain is lower in this case while

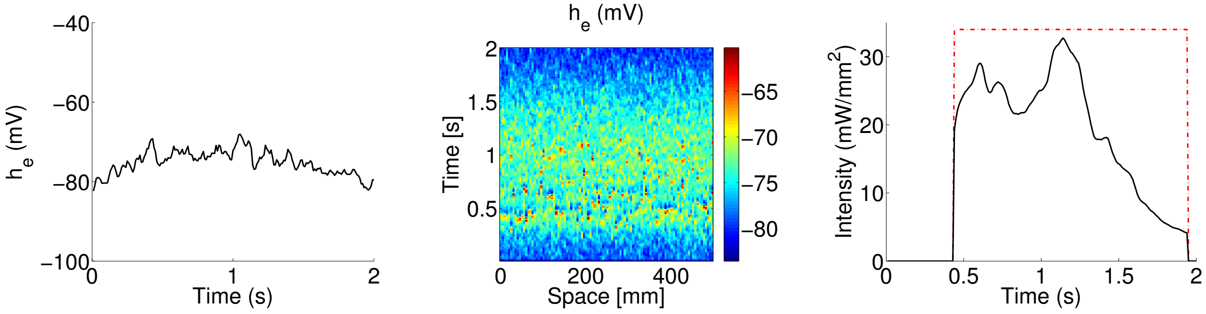

(a) Mean soma potential at a point (b) 1D slice of the 2D domain (c) Light intensity at a point

Figure 3.4: Effect of closed loop optogenetic control on seizures in the P_{ee}-Γ_e space using a temporal modulation of P_{ee} in time shown in fig. 3.3c. Γ_e is held constant at 0.0008 with $\alpha = 1.6$. All other parameters are similar to baseline parameters in [49]. Figures 3.4a and 3.4c show the variation with time of h_e and intensity, respectively at the same point. The red dot-dash line in figure 3.4c indicates the open loop intensity required to suppress a fully formed seizures at $P_{ee} = 548.0$. Gains used: $K_P = 0.4$ and $K_I = 3.6$.

the integral gain is much higher. This is because a high proportional gain will react more vigorously to the robust changes in mean soma potential caused by the higher excitatory inputs, and might synchronize the optogenetic and cortical dynamics leading to continued oscillatory activity. Additionally, high proportional gains might lead to rapid increases in illumination intensities well past physiologically safe values. The integral term provides the required offset to these drawbacks of purely proportional control. Higher integral gains lead to higher overall intensities, which are required to suppress robust oscillations in the model cortex.

3.2.3 Robust control

In each of the seizures presented above, the closed loop controller is tuned to suppress seizures arising at the peak values of parameters in the $P_{ee} - \Gamma_e$ plane, making it robust to temporal variations in parameter values. The controller also outperforms the open loop controller in each of the cases presented above using optimal intensity instead of a constant intensity to suppress seizures.

If the closed loop controller were tuned to suppress the most robust seizures, as seen in section 3.2.2, and were then used to suppress weaker seizures, as seen in section 3.2.1, it would easily outperform the open loop controller tuned under the same conditions. Fig. 3.5 clearly demonstrates the advantages of having a controller that calculates intensity based on the measured signal, as opposed to using an open loop approach. The use of a higher integral gain term results in intensities much higher than what would suffice to suppress a seizure of this nature, which results in inefficient use of illumination intensity. However, given the stochastic and dynamic nature of cortical dynamics, the sensitivity of the controller will have to be tuned subjectively to achieve optimal control.

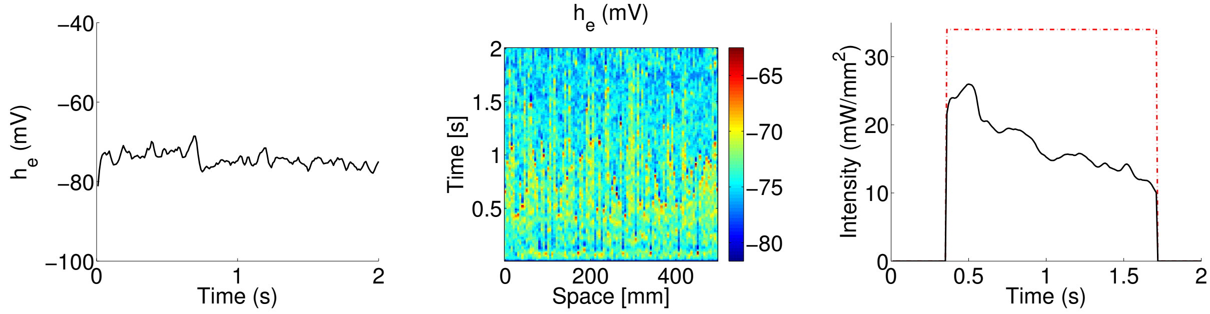

(a) Mean soma potential at a point (b) 1D slice of the 2D domain (c) Light intensity at a point

Figure 3.5: Effect of closed loop optogenetic control on seizures in the P_{ee}-Γ_e space using a temporal modulation of P_{ee} in time shown in fig. 3.3c. Γ_e is held constant at 0.00066 with $\alpha = 1.15$. All other parameters are similar to baseline parameters in [49]. This seizure is similar to the one presented in section 3.2.1. Figures 3.5a and 3.5c show the variation with time of h_e and intensity, respectively at the same point. The red line in figure 3.5c indicates the open loop intensity required to suppress fully formed seizures presented in section 3.2.2. The red dot-dash line in figure 3.2c indicates the open loop intensity required to suppress a fully formed seizures at $P_{ee} = 548.0$, $\Gamma_e = 0.0008$, and $\alpha = 1.6$. Gains used: $K_P = 0.4$ and $K_I = 3.6$, which are the same gains used to suppress the robust seizure presented in section 3.2.2.

3.3 Seizures in the g_e-Γ_i space

Another route to seizure using the meso scale cortical model is achieved by increasing the slope at the inflection point of the sigmoid function that represents the mean firing rate of the excitatory population, $\tilde{g}_e$, as it depends upon the mean soma potential of the excitatory population, $\tilde{h}_e$. This parameter models the effects of variance of depolarisation within a population of neurons [61]. By increasing $\tilde{g}_e$, small changes in $\tilde{h}_e$ could result in large changes in the firing rate $\tilde{S}_e$, a characteristic of oscillatory behavior. When Γ_i, the influence of synaptic input on mean soma potential, is also increased by a small amount, it leads to a small net increase in the rate of change of $\tilde{h}_e$. This rise in $d\tilde{h}_e/d\tilde{t}$ coupled with the higher $\tilde{g}_e$ leads to an abrupt onset of oscillatory behavior as observed in figure 3.6. We gradually increase, and then decrease, $\tilde{g}_e$ in time as shown in figure 3.6c, while Γ_i is held at a slightly higher values than during normal function. The value of $\tilde{g}_e$ at its peak is -12.5, which is within the physiological range of values for this parameter, but is much higher than its value during normal function.

Figure 3.6b is a one dimensional slice of the 2D domain illustrating travelling waves. The waves appear to be stationary because the radius of curvature of spiral waves produced is much larger than the dimensions of the model. When seizures are induced by increasing subcortical inputs and decreasing the influence of excitatory synapses on the mean soma potential, there is first a gradual increase in the post synaptic activation, which results in an increase in the firing rate that leads to highly oscillatory activity. However, when we change Γ_i and $\tilde{g}_e$, we directly increase

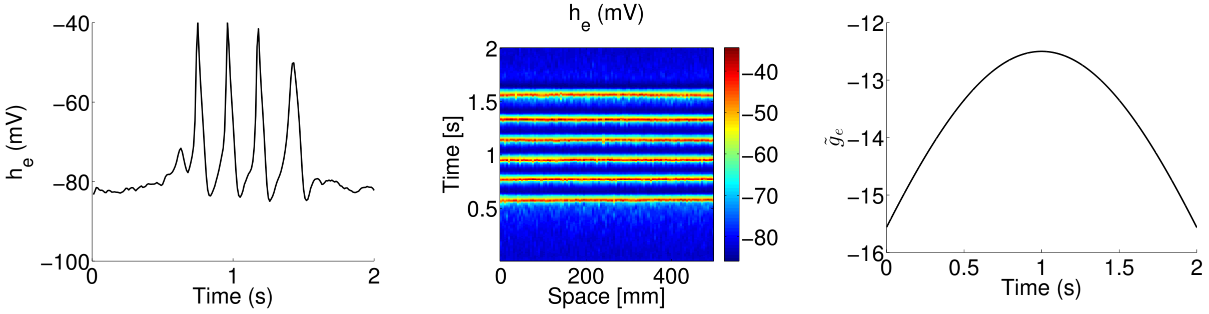

(a) Mean soma potential at a point (b) 1D slice of the 2D domain (c) $\tilde{g}_e$ at a point

Figure 3.6: Seizures in the $\tilde{g}_e$-Γ_i space using a variation of $\tilde{g}_e$ in time with a maximum value of -12.5 as shown in figure 3.6c. Γ_i is held constant at 0.085. All other parameters are similar to baseline parameters in [49].

the firing rate. This leads to a more abrupt onset seizure. Consequently, seizure like activity is quickly suppressed when $\tilde{g}_e$ is reduced.

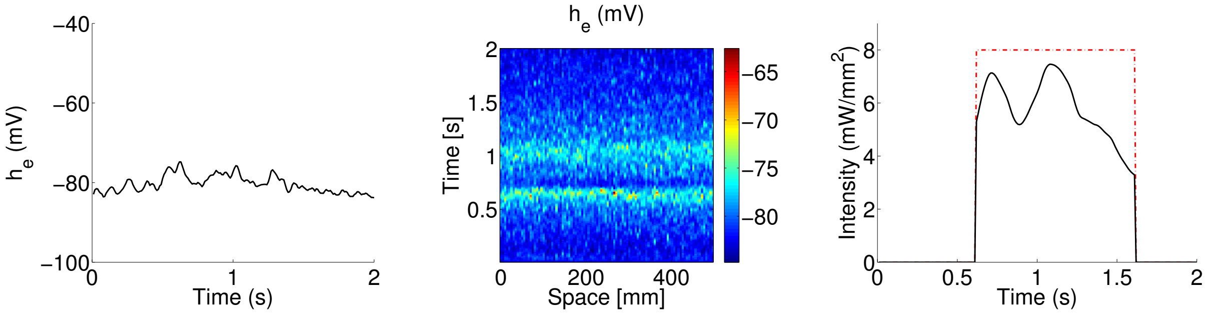

(a) Mean soma potential at a point (b) 1D slice of a 2D domain (c) Intensity of light at a point

Figure 3.7: Effect of closed loop optogenetic control on seizures in the $\tilde{g}_e$-Γ_i space. $\tilde{g}_e$ is varied in time with a maximum value of -12.5 as shown in figure 3.6c. Γ_i is held constant at 0.085 with $\alpha = 1.6$. All other parameters are similar to baseline parameters in [49]. Figures 3.7a and 3.7c show the variation with time of $\tilde{h}_e$ and intensity, respectively at the same point. The red dot-dash line in figure 3.7c indicates the open loop intensity required to suppress a fully formed seizures at $g_e = -12.5$. Gains used: $K_P = 1.0$ and $K_I = 0.64$.

To deal with the abruptness of seizure onset by quickly suppressing excessive excitatory activity, a strong initial control effort is required. This is achieved by using a relatively high proportional gain, $K_P = 1.0$, and a moderately high integral gain, $K_I = 0.64$. A higher intensity leads to higher optogenetic conductance, which in turn depolarizes inhibtory cells much faster. The gains are tuned for a fully formed seizure with parameters $\tilde{g}_e = -12.5$, $\Gamma_i = 0.085$ and $\alpha = 1.6$. An open loop intensity of 8 mW/mm^2 is required to suppress an equivalent fully formed seizure. The red dot-dash lines in figure 3.7c shows the comparison of open and closed loop control to suppress the same seizure if the light were turned on and off at the same time. The intensities used to suppress seizures in this space are lower than intensities observed in 3.2.2 because unlike constant high subcortical inputs, a high $\tilde{g}_e$ leads to rapid oscillations between high and low firing rates, which translates to the amplitude of total excitatory inputs in the model cortex oscillating between highs and lows. This gives the increased inhibition from optogenetic stimulation more opportunities for seizure suppression using lower intensities when the firing rate is low.

The delays associated with synaptic transmission make the rapidity in depolarization crucial to suppressing excessive excitatory activity before it reaches a state of synchronisation characteristic of seizures. As $\tilde{g}_e$ rises until it peaks at 1s, the firing rate increases and decreases more rapidly, and the controller accounts for these changes by adjusting the intensity of light as seen in figure 3.7c. We have used the same amplitude and rate triggers as in the previous section. Figure 3.7a shows how oscillations in h_e are suppressed, and figure 3.7b demonstrates the breakdown of travelling seizure waves.

3.4 Summary of original contributions

In this chapter, we present an energy efficient and robust method to stimulate the human cortex, which is the most accessible part of the brain. We define a closed loop control strategy for optogenetic control by basing the illumination intensity or ‘control effort’ on the measured signal, which is similar to clinical electrode recordings. Further, we successfully demonstrated the efficacy of our controller on two types of seizures that are found to be the most plausible when the meso-scale cortical dynamics are compared to patient data using statistical techniques.

We now turn towards bifurcation theory to provide more detailed insight into the effects of open and closed loop optogenetic control on the seizing model cortex. The combination of the optogenetic and cortical models presented in chapters 1 and 2 results in a highly non-linear set of stochastic partial differential equations with a rich structure of bifurcations and different states. By performing a dynamical systems analysis on the combined cortico-optogenetic dynamical model, we can qualitatively observe the effects of optogenetic stimulation on the seizing cortex in a manner that is not possible if one only considers neurophysiology.

Chapter 4

The combined cortico-optogenetic ODE model

The combined cortico-optogenetic model consists of a complex system of stochastic, non-linear equations that depend on a number of parameters. Dynamical systems analysis and bifurcation theory provide a means to qualitatively study the behavior of the system of equations when these parameters are changed. Depending on the values of those parameters, the behavior of the model can vary greatly. These changes can be observed in phase space, which is a multi dimension space that contains all possible states of the model, with each point in this space representing one possible state. The evolution of the solutions of the model when a parameter is changed is traced (phase space trajectory) through this multi dimension space. For example, changes in one parameter can lead to a change in the number and/or stability of equilibria of the system at bifurcation points, which are defined as the parameter values where there is a change in the trajectory of the solutions of the model.

For the purposes of this chapter, we will only define a few terms related to bifurcation theory, however, the reader is referred to the book by Hale and Koçak [33] for a mathematically rigorous introduction to bifurcation theory, to the book by Strogatz [98] for an application based approach, and to the book by Abraham and Shaw [1] for an excellent visual and geometric interpretation of bifurcation theory. In this chapter, using numerical simulations that map out bifurcation points at which the cortex goes from a state of normal function to a seizure state, we study the role optogenetic control plays in moving the system away from these points. A dramatic or gradual transition to synchronous activity in the cortex is determined by the presence of a limit cycle arising from Hopf bifurcations. The Hopf bifurcation indicates the start or end of periodic solutions (oscillations) or limit cycles surrounding an equilibrium point when a parameter associated with the model is varied. There are two types of Hopf bifurcations, subcritical and supercritical. Subcritical Hopf bifurcations occur when an unstable limit cycle arises from a stable equilibrium point, while a supercritical Hopf bifurcation occurs when an unstable equilibrium point gives rise to a stable limit cycle. Folds in the bifurcation diagram indicate the existence of multiple stable states of the cortex for a given set of parameter values associated with the connectivity and functioning of the cortex.

Significantly, all of this connects back to the neurophysiology captured in the model, so knowledge of these features and an understanding of the role of fluctuations on a bifurcating model will help perfect closed loop feedback optogenetic control to make the abruptness of seizure onset more manageable for patients.

4.1 The ODE model

The stochastic and spatial terms in the set of stochastic partial differential equations (SPDEs) that describe the meso-scale cortical model make bifurcation analysis a challenging task. To gain a preliminary insight into the rich dynamics of this system via bifurcation analysis, the stochastic inputs and spatial terms from the SPDEs, which can be found in chapter 1, that describe the cortical model are ignored, and a simpler ordinary differential equation (ODE) system is considered. The combined optogenetic and cortical ODE system is stated here:

$$\frac{d\tilde{h}_e}{d\tilde{t}} = 1 - \tilde{h}_e + \Gamma_e(h_e^0 - \tilde{h}_e)\tilde{I}_{ee} + \Gamma_i(h_i^0 - \tilde{h}_e)\tilde{I}_{ie} \tag{4.1}$$

$$\frac{d\tilde{h}_i}{d\tilde{t}} = 1 - \tilde{h}_i + \Gamma_e(h_e^0 - \tilde{h}_i)\tilde{I}_{ei} + \Gamma_i(h_i^0 - \tilde{h}_i)\tilde{I}_{ii} - u \tag{4.2}$$

$$\left(\frac{1}{T_e}\frac{d}{d\tilde{t}} + 1\right)^2 \tilde{I}_{ee} = N_e^{\beta}\tilde{S}_e\left[\tilde{h}_e\right] + \tilde{\phi}_e + P_{ee} \tag{4.3}$$

$$\left(\frac{1}{T_e}\frac{d}{d\tilde{t}} + 1\right)^2 \tilde{I}_{ei} = N_e^{\beta}\tilde{S}_e\left[\tilde{h}_e\right] + \tilde{\phi}_i + P_{ei} \tag{4.4}$$

$$\left(\frac{1}{T_e}\frac{d}{d\tilde{t}} + 1\right)^2 \tilde{I}_{ie} = N_i^{\beta}\tilde{S}_i\left[\tilde{h}_i\right] + P_{ie} \tag{4.5}$$

$$\left(\frac{1}{T_e}\frac{d}{d\tilde{t}} + 1\right)^2 \tilde{I}_{ii} = N_i^{\beta}\tilde{S}_i\left[\tilde{h}_i\right] + P_{ii} \tag{4.6}$$

$$\left(\frac{1}{\lambda_e}\frac{d}{d\tilde{t}} + 1\right) \tilde{\phi}_e = N_e^{\alpha}\tilde{S}_e\left[\tilde{h}_e\right] \tag{4.7}$$

$$\left(\frac{1}{\lambda_i}\frac{d}{d\tilde{t}} + 1\right) \tilde{\phi}_i = N_i^{\alpha}\tilde{S}_e\left[\tilde{h}_e\right] \tag{4.8}$$

$$\frac{dN_{O1}}{d\tilde{t}} = K_{a1}.N_{C1} - (K_{d1} + e_{12}).N_{O1} + e_{21}.N_{O2} \tag{4.9}$$

$$\frac{dN_{O2}}{d\tilde{t}} = K_{a2}.N_{C2} + e_{12}.N_{O1} + (K_{d2} + e_{21}).N_{O2} \tag{4.10}$$

$$\frac{dN_{C2}}{d\tilde{t}} = K_{d2}.N_{O2} - (K_{a2} + K_r).N_{C2}, \tag{4.11}$$

Eqs. 4.1-4.8 represent the cortical model and eqs. 4.9-4.11 describe the dynamics of populations of ChR2 optogenetic channels. This system has been recast in dimensionless variables and all variables are functions of dimensionless time $\tilde{t}$ only. The subscripts e and i represent excitatory and inhibitory populations respectively, and variables with two subscripts in the cortical model represent the transfer of energy from one population to another. The mean soma potential of each population is denoted by $\tilde{h}$, post-synaptic connections by $\tilde{I}$, and long range connections by $\tilde{\phi}$. N represents the fraction of ChR2 channels in each of the four states, while K is the rate of transition from one state to another as described in chapter 2. Again, tildes represent non-dimensionalized variables in the cortical model. The control term u is given by,

$$u = \tilde{h}_i . G_{ChR2} . R_m . \tag{4.12}$$

In equation 4.12, $\tilde{h}_i$ is the mean soma potential of the inhibitory population, G_{ChR2} is the channel conductivity described in equation 5.3, and the membrane resistance R_m is obtained from voltage clamp experiments and has a value of $7.1 G\Omega$ [97]. The values of all constants connected to the cortical model can be found in [49] and values of rate constants associated with the optogenetic model can be referenced in chapter 2. We use AUTO [25], a software package for continuation and bifurcation problems in ordinary differential equations, to study this system of equations and to determine the associated fixed points, bifurcations, limit cycles and their stability type.

Figure 4.1a shows the comparison between the SPDE and ODE models for a hyperexcited model cortex with subcortical input $P_{ee} = 548.0$. Red represents the maximum and minimum values of h_e over 2 seconds for a given Γ_e using the SPDE model while black represents the bifurcation diagram of the ODE model. In figure 4.1a, the amplitude of noise from the stochastic subcortical inputs, defined in chapter 1, is set at 0.1 to demonstrate the effect of the spatial terms on the SPDE model, and how the dynamics compare to the ODE model. This is an order of magnitude lower than the amplitude used in other simulations presented in this dissertation using the SPDE model where $\alpha = 1.15$ or 1.6. Apart from high amplitude oscillations occurring at a lower Γ_e using the SPDE model, the dynamics of the SPDE model follow that of the ODE model closely in stable regions (solid lines). This agreement between the SPDE and ODE models makes it reasonable to use the simpler ODE model to perform a dynamical systems analysis on the cortical model. Figure 4.1b shows the region of P_{ee}-Γ_e space that leads to oscillatory behavior in the ODE and SPDE models denoted by dark grey and light grey regions, respectively. In this figure, $\alpha = 1.6$ is used to account for the full effect of noise in the SPDE model. Except at the boundaries, the seizure causing region using the ODE model overlaps that of the SPDE model almost entirely. The SPDE model has boundaries for the seizure regions that are slightly broader and less distinct than the boundaries of the ODE model.

4.2 Bifurcations in the P$_{ee}$-Γ_e space

In section 3.2, P_{ee} was gradually varied until a high enough magnitude of excitatory subcortical inputs induced seizures in the model cortex. Here, we study the response of the cortical model by observing the features of the mean soma potential of the excitatory population when the magnitude

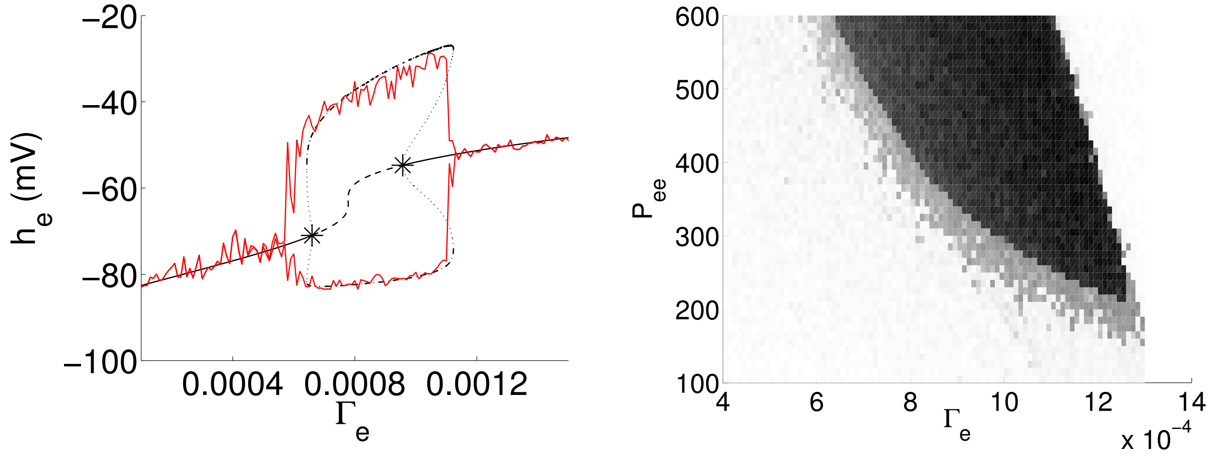

(a) (b)

Figure 4.1: Comparison between the full SPDE model and the simpler ODE model. **Left:** Response diagram for the hyperexcited cortex with subcortical input $P_{ee} = 548.0$. Amplitude of noise from stochastic subcortical inputs was reduced by an order of magnitude to 0.1 to demonstrate the effect of spatial terms on the dynamics of the model. The red jagged lines indicate maximum and minimum values of h_e over 2 seconds for different Γ_e, which is the influence of the synaptic input on the mean soma potential of the excitatory population, using the SPDE model. Black lines indicate the bifurcation diagram for the ODE model. Dashed and solid lines indicate unstable and stable fixed points, respectively. Maximum and minimum values of h_e during stable (dot-dashed) and unstable (dashed) limit cycles arising from a subcritical Hopf bifurcation (asterisk) are also shown. **Right:** Comparison of the SPDE and ODE models in parameter space, with grey regions indicating seizure causing areas. As one might expect, the stochastic inputs in the SPDE model enhance the seizure area (indistinct boundary marked in grey) in parameter space when compared to the ODE model (darker region with sharp boundaries). Here, we use $\alpha = 1.6$ which corresponds to the amplitude of noise used with the SPDE model elsewhere in the manuscript.

of excitatory subcortical inputs is varied. Fig. 4.2a shows the response of the ODE model when no optogenetic stimulation is applied at $\Gamma_e = 0.00066$ with all other parameters held at baseline values [49]. Asterisks at $P_{ee} = 548.0015$ and $P_{ee} = 1510.9635$ indicate subcritical Hopf bifurcations that give rise to unstable limit cycles, which stabilize at the turning points on the branch. Maximum and minimum values of h_e achieved during stable and unstable limit cycles are indicated by dot-dashed lines and dotted lines, respectively. We do not explore the dynamics past $P_{ee} = 2000.0$, which is well above the physiological limit of P_{ee}. Stable oscillations (dot-dashed lines) occur between $P_{ee} = 527.004$ and $P_{ee} = 1829.712$.

To evaluate the efficacy of open loop optogenetic control, we use an intensity of 1.9 mW/mm^2, which is the minimum intensity required to suppress successfully a fully formed seizure when $\Gamma_e = 0.00066$, and P_{ee} is within the physiologically acceptable range of values. When open

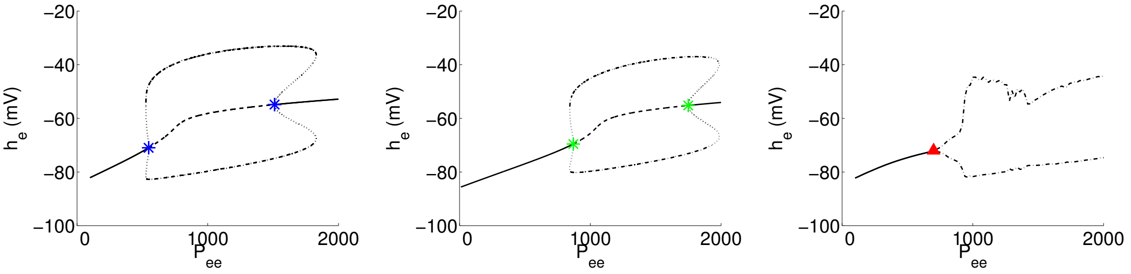

(a) No control

(b) Open loop

(c) PI

Figure 4.2: Bifurcation analysis using an unstimulated cortex (figure 4.2a) and a cortex stimulated with light of constant 10 mW/mm^2 intensity in the open loop configuration (figure 4.2b). Asterisks indicate subcritical Hopf bifurcations that lead to unstable limit cycles. Time integration of the combined cortico optogenetic model with PI control to track the maximum and minimum values of the excitatory mean soma potential is shown in figure 4.2c. The red triangle ($P_{ee} = 710$), which is shifted further away from the first blue Hopf bifurcation ($P_{ee} = 548.0015$) in figure 4.2a, indicates the start of oscillatory activity despite closed loop control being triggered. The dashed black lines in fig. 4.2c indicate minimum and maximum values of $\tilde{h}_e$ during oscillatory activity arising despite the use of closed loop control. Gains used $K_P = 3.0$ and $K_I = 0.12$.

loop optogenetic control is applied via the inhibitory population using an illumination intensity of 1.9 mW/mm^2 the first and second subcritical Hopf bifurcations, marked with green asterisks, shift to higher values of $P_{ee} = 870.45$ and $P_{ee} = 1749.0$, respectively. These Hopf bifurcations also lead to an unstable limit cycle, and demonstrate how even a low illumination intensity can delay seizure activity until much higher excitatory inputs are available to elicit seizures.

In the case with triggered PI control, we cannot perform a bifurcation analysis because the trigger renders the system discontinuous in time. Instead, we time integrate the ODE system to obtain the maximum and minimum values of the mean soma potential for various values of P_{ee}, as shown in figure 4.2c. After control is triggered, we simulate cortical activity for a further 2 seconds. This is done to allow the system to reach a steady state, which in turn allows us to track the maximum and minimum value of the mean soma potential for the excitatory population after the control effort has attained maximum strength. The black solid line indicates no oscillatory activity in the cortex when control is switched on (stable fixed points), while the black dot dashed lines indicate oscillations in the mean soma potential of the excitatory population despite control being turned on. The red triangle around $P_{ee} = 710.0$ indicates the lowest value of subcortical excitatory inputs that will produce dynamics approaching seizure but with a lower amplitude onset seizure in the ODE model despite the use of closed loop optogenetic control. Here, we use $K_P = 3.0$ and $K_I = 0.12$. In both the open and closed loop cases, we do not explore higher intensities or gains because they successfully delay oscillatory activity well past the physiological range of parameters.

4.2.1 Seizures in parameter space

To illustrate the effect of open loop and closed loop control on the entire P_{ee}-Γ_e parameter space we turn to figure 4.3.

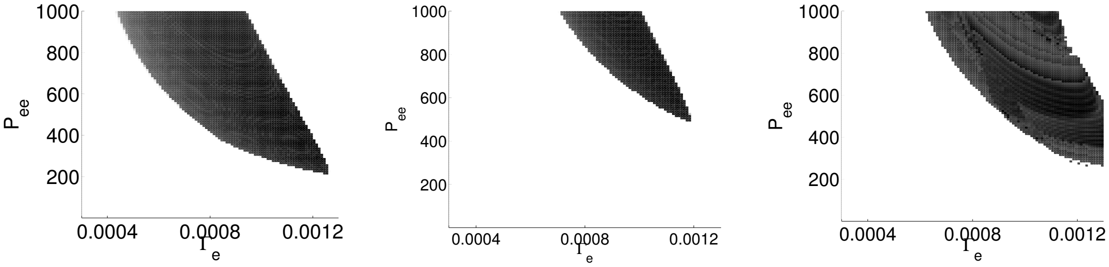

(a) No control (b) Open loop (c) PI

Figure 4.3: From left to right: Seizure prone areas in the $\mathrm{P}_{ee} - \Gamma_e$ parameter space with no control, using open loop control with an illumination of 1.9 mW/mm^2, and PI control using $K_P = 3.0$ and $K_I = 0.12$. Here, dark regions represent values of P_{ee} and Γ_e which produce oscillations in the mean soma potential h_e. These results were obtained using the dimensionless ODE system of equations.

Figure 4.3a shows the values of P_{ee} and Γ_e that lead to oscillatory behavior in the model cortex when no control is applied. The seizure causing area is dramatically reduced when open loop control is applied via a constant illumination of 1.9 mW/mm^2. In the case with closed loop control, we use $K_P = 3.0$ and $K_I = 0.12$. The seizure area is not noticeably decreased, but it does push the seizure causing areas to higher values of P_{ee} and Γ_e. Again, we simulate the effects of open and closed loop control using the lower values of intensities and gains used in section 3.2.1 because higher values of these control parameters will successfully suppress seizures in the region of physiologically acceptable values of P_{ee} and Γ_e. The tendency of closed loop control merely to move the seizure causing area and not reduce it is because of the use of high proportional control and low integral control. The controller is able to respond to rapid increases in mean soma potential of the excitatory population, but is not effective in suppressing oscillatory activity when more robust excitatory inputs are involved. A higher contribution from the integral component will be able to address this shortfall in control effort as shown in section 3.2.2.

4.3 Seizures in the g_e-Γ_i space

Figure 4.4 illustrates the region of the $\tilde{g}_e$-Γ_i space that leads to seizure like activity in the model cortex. Open loop control via an 8 mW/mm^2 illumination and closed loop PI control with K_P = 1.0 and K_I = 0.64 successfully suppress oscillatory activity throughout the entire range of values of $\tilde{g}_e$ and Γ_i shown in figure 4.4, and so we have not shown this parameter space here with illumination turned on; the plot looks pure white. Again, the SPDE model will lead to less distinct boundaries of the seizure area in parameter space.

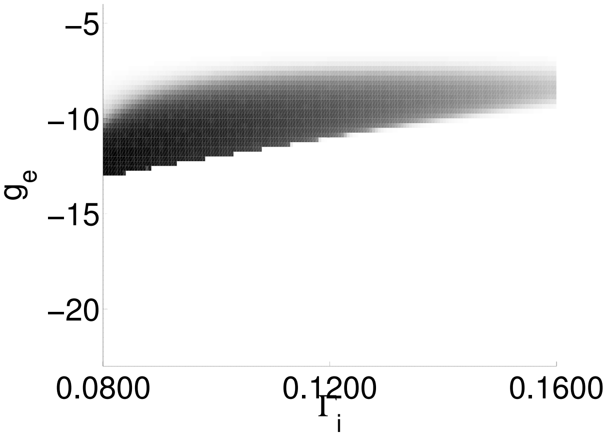

Figure 4.4: Seizure prone areas in the $\tilde{g}_e - \Gamma_i$ parameter space with no optogenetic stimulation. Here, dark regions represent values of $\tilde{g}_e$ and Γ_i which produce oscillations in the mean soma potential h_e. The grayscale shading indicates the variation in h_e during oscillatory behavior. These results were obtained using the dimensionless ODE system of equations.

4.4 Summary

In this chapter, we reduced the combined cortico-optogenetic model from chapters 1 and 2 to a set of ordinary differential equations (ODEs) by leaving out the stochastic and spatial terms from the set of stochastic partial differential equations (SPDEs) that describe the model. This enables us to use bifurcation theory to study the behavior of the combined cortico-optogenetic model during the unstimulated and open loop stimulated states, and to compare these results to results from the time integration of the discontinuous closed loop system. While the bifurcation and time integration diagrams for the open and closed loop systems behave similarly by delaying the start of oscillations in the model until stronger excitatory inputs are available, there is a stark contrast in how they affect the areas of parameter space that cause seizures. The illumination intensity is decoupled from the model in the open loop system, while it is entirely dependent on the output of the cortical model in the closed loop case. This added coupling between optogenetic and cortical dynamics serves only to move the seizure causing area to a different part of parameter space in the closed loop case instead of reducing it as seen in the open loop case. More importantly, however, the seizure causing area of parameter space is moved out of the range of physiologically relevant values with closed loop stimulation.

Bifurcation analysis is a powerful technique that can be used to analyze and understand the dynamics of a non-linear system of differential equations, and we employ it again in the next chapter, where we explore the use of optogenetic stimulation to induce seizures in a normally functioning model cortex.

Chapter 5

Stimulating seizures using optogenetics

In seizure research, cortical stimulation has been used as a means to study the pre-seizure state, epileptogenesis, the epileptic state and seizure control. In vivo stimulation using radial electric fields [79], and high frequency [99] and low frequency [40] *in vitro* electrical stimulation are some of the methods that have been used to modulate epileptiform activity.

Optogenetics offers another modality of cortical stimulation with high spatial, temporal and cell type specificity. In chapters 2 - 4, we demonstrated the use of optogenetics to inhibit epileptic seizures *in silico*. In this chapter, we explore the use of optogenetics as a stimulation strategy to hyper-excite a patch of otherwise normally functioning model cortex to produce travelling seizure waves that cause the entire cortical model to seize. The intensity of light illuminating the cortical model determines the opening and closing rates of the optogenetic channels, which in turn lead to seizure waves of different frequencies. We use bifurcation analysis presented in chapter 4 to analyze the relation between illumination intensity and seizure frequency. Much of this material was previously published in [86].

5.1 Optogenetic stimulation of the excitatory population in a normally functioning model cortex

To study the effects of optogenetic stimulation on the cortex, we use the four state model of Channelrhodopsin-2 (ChR2) proposed in [31]. A meso-scale version of this model was combined with the cortical model presented in chapter 1 by modifying the inhibitory cell population to express light sensitive ChR2 ion channels as seen in chapter 2. Here, the excitatory population of the cortical model expresses ChR2 channels, which changes the equation describing the dynamics of the mean soma potential of the excitatory population to:

$$\frac{\partial \tilde{h}_e}{\partial \tilde{t}} = 1 - \tilde{h}_e + \Gamma_e(h_e^0 - \tilde{h}_e)\tilde{I}_{ee} + \Gamma_i(h_i^0 - \tilde{h}_e)\tilde{I}_{ie} - u. \tag{5.1}$$

The term u is the stimulation applied to the excitatory population, and is given by,

$$u = \tilde{h}_e . G_{ChR2} . R_m . \tag{5.2}$$

$\tilde{h}_e$ is the membrane potential for the excitatory population, R_m is the membrane resistance of the cells, and the conductance of ChR2 channels, G_{ChR2}, is defined as

$$G_{ChR2} = G_{max} \cdot g_{ChR2} \cdot \frac{(1 - exp(-h_e/U_0))}{h_e/U_1} . N_{ChR2}, \tag{5.3}$$

where g_{ChR2} is the total conductance of the optogenetic channels in the $O1$ and $O2$ states. U_0 and U_1 are empirical constants and N_{ChR2} is the number of ChR2 channels per representative neuron. The expression for g_{ChR2}, and values and explanations for all parameters can be found in [85].

5.2 Constant illumination

Here, we apply optogenetic stimulation of a portion of model cortex of dimensions 1400 × 1400 mm^2, which is divided into 100×100 cells or representative neurons.[1] We stimulate an area of model cortex of the order of spatial scales of clinical recordings. In figure 1.2, a square region in the middle of the cortex of approximate dimensions 280 × 280 mm^2 (1/25 the total area of the cortex) is modified to express ChR2 ion channels in the excitatory population, and this region is illuminated with blue light of wavelength 470 *nm* with a constant intensity of 50 mW/mm^2 starting at 0.5s. An ion channel density of 10^9ChR2's$/m^2$ is used to keep illumination intensities within physiologically permissible values and still ensure optimal stimulation of the cortex.

Fig. 5.1 depicts the birth of a seizure like wave within the square patch of stimulated cortex. Neighboring regions are then excited by the outward propagation of travelling seizure waves, and the effects of the stimulation spread to the entire cortical area. Hyper-excitation in chapters 2 and 3 was achieved by increasing subcortical inputs to the excitatory population throughout the model cortex. This meant the entire cortex was on the verge of seizing, and a small increase in subcortical inputs to a column could cause a region of cortex to seize. These seizures originated from a cortical column, and propagated outwards in spiral waves. Here, spatially uniform travelling waves are formed by the equal hyper-excitation of cortical macrocolumns within a patch of cortex using optogenetic channels, and subcortical inputs do not play as important a role in starting seizures as illumination intensity increases.

It should be noted here that the entire model cortex is functioning normally, with inhibitory and excitatory inputs of comparable magnitudes balancing each other out. However, when adequate optogenetic stimulation is applied to the excitatory population, it depolarizes these cells, increasing

---

[1] The average human cortex has dimensions of 500 × 500 mm^2 if it were laid open like a sheet. However, to remain consistent with previous work, and because dynamics in this model of undifferentiated cortex are scale-free, we have used a larger cortical domain to illustrate seizure waves.

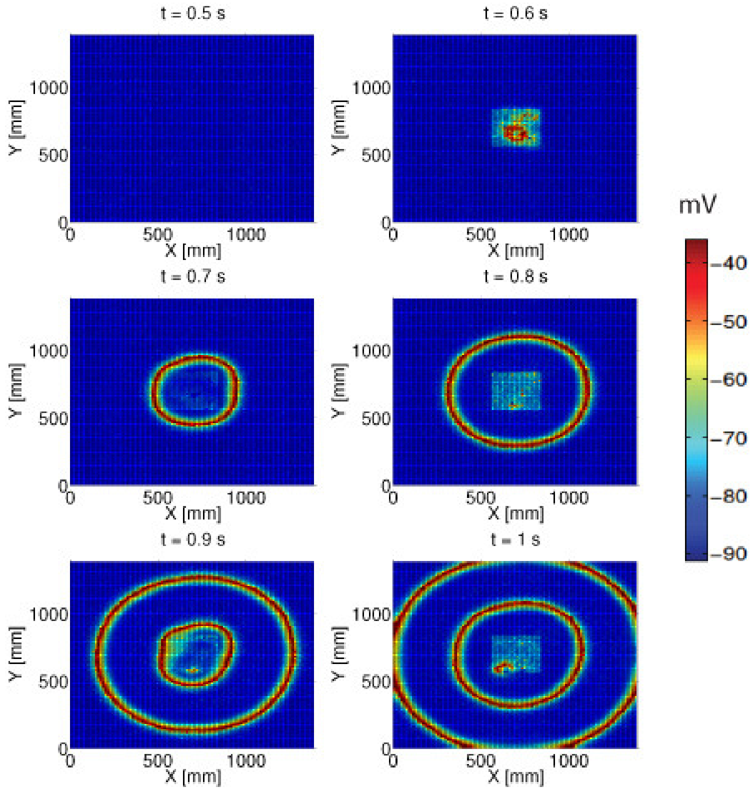

Figure 5.1: Propagation of seizure waves in a 2D model of a normally functioning human cortex when optogenetic stimulation is applied to a 280×280 mm^2 patch in the centre of the cortex. Snapshots are taken from time t = 0.5s to t = 1s. The traveling waves are tracking the values of the mean soma potential of the excitatory population (h_e) in mV. Normal cortical function is characterized here by the baseline parameters of [49] with $P_{ee} = 11.0$ and $\Gamma_e = 0.0012$. The model cortex is stimulated with a constant light intensity of 50 mW/mm^2 at 0.5s.

their mean soma potential, which immediately increases their firing rate. The local excitatory and long range contributions to post synaptic activation are increased because of the higher firing rate, producing a further rise in the mean soma potential of both populations, which ultimately leads to even higher firing rates in both excitatory and inhibitory cells. Increases in inhibitory firing rates trail excitatory ones within a macrocolumn by 1-2 ms because stimulation is applied directly to the excitatory population, and because of the time delays associated with synaptic transmission. Spatial connectivity between columns transfers synchronous activity to neighboring columns of neurons outside the stimulated cortical patch, exciting them into synchronous states facilitating propagation of seizure activity. Again, only neurons within the stimulated area are hyperexcited while the rest of the cortex is functioning normally. This constrains the minimum area of stimulated region in our model that will excite the rest of the cortex into an epileptic state to about 1/25 the total area of the cortex. Smaller stimulated regions are not able to support seizure activity for cortical and optogenetic parameters mentioned above.

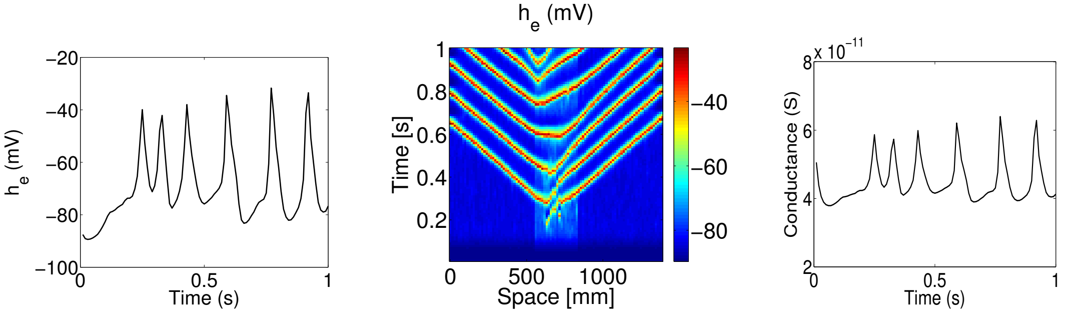

(a) Mean soma potential at a point (b) 1D slice of a 2D domain (c) Conductance at a point

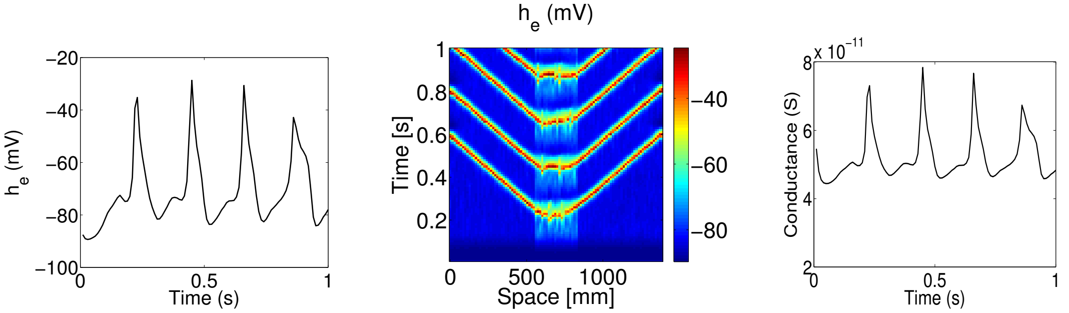

(d) Mean soma potential at a point (e) 1D slice of a 2D domain (f) Conductance at a point

Figure 5.2: Optogenetic stimulation of a normally functioning cortex with an illumination source of constant intensity. Figures 5.2a - 5.2c are for a stimulation intensity of 30 mW/mm^2 and figures 5.2d - 5.2f are for a stimulation intensity of 60 mW/mm^2.

In fig. 5.2, we look at the variation of mean soma potential of the excitatory population at a point within the stimulated patch of cortex, and take a one dimensional cross section of the two dimensional spatial domain to study how different illumination intensities and illumination profiles lead to travelling seizure waves of varying frequencies. For both illumination profiles presented in fig. 5.2, stimulation is turned on at t = 0s. Figures 5.2a and 5.2d show the variation of mean soma potential with time when the cortical patch is constantly illuminated with intensities of 30 mW/mm^2 and 60 mW/mm^2, respectively. Figures 5.2b and 5.2e depict travelling waves in a one dimensional slice of the two dimensional domain, and comprises both stimulated cortex between 560 mm and 840 mm, and normally functioning cortex. Higher illumination intensities result in higher conductances, as shown in figures 5.2c and 5.2f, resulting in cells being depolarized more quickly. Counter-intuitively, though, while a higher intensity depolarizes cells more quickly, it reduces the frequency of seizure waves as seen by comparing figures 5.2a and 5.2d. One possible explanation is that the rate of change of mean soma potential given in eq. 5.1 is lower for higher intensities because the stimulation term, u, is always positive on account of using ChR2, a cation pump. A higher rate of change decreases the time required to change from a lower to a higher firing rate and back. In other words, the rate of change of firing rate increases, which results in higher frequency oscillations.

5.3 Pulsed illumination

The frequency of travelling waves induced by optogenetic stimulation can also be influenced by the illumination protocol used as shown in figure 5.3 where a different pulsing profile is used in each row. Figures 5.3a - 5.3c depict a 200 ms on 100 ms off pulsed illumination of 50 mW/mm^2 intensity, the mean soma potential at a point in the stimulated patch of cortex and travelling waves in a 1D cross section of the 2D domain, respectively. Figures 5.3d - 5.3f depict a 200 ms on 200 ms off pulsed illumination of 60 mW/mm^2 intensity, the mean soma potential at a point in the stimulated patch of cortex and travelling waves in a 1D cross section of the 2D domain, respectively. Figures 5.3c and 5.3f comprise both stimulated cortex between 560 mm and 840 mm, and normally functioning cortex.

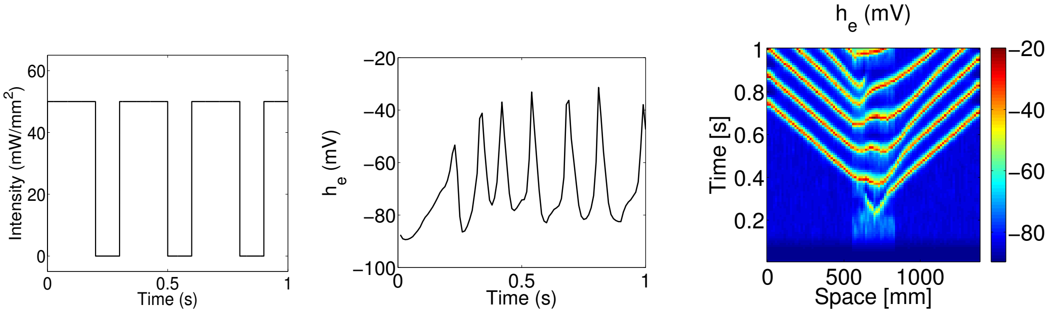

(a) Intensity (b) Mean soma potential at a point (c) 1D slice of a 2D domain

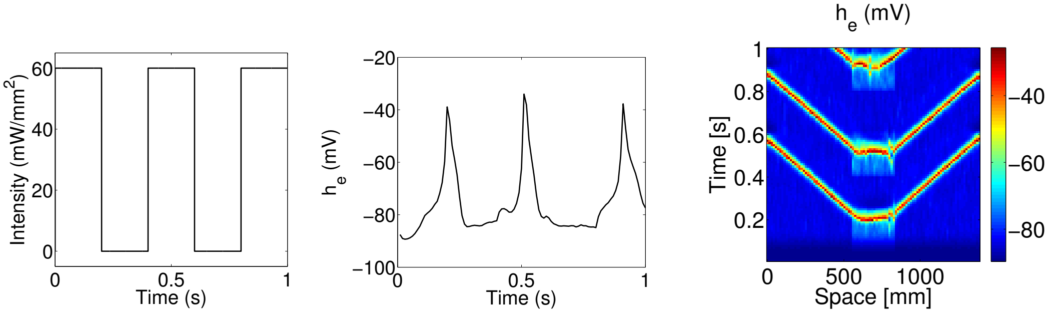

(d) Intensity (e) Mean soma potential at a point (f) 1D slice of a 2D domain

Figure 5.3: Optogenetic stimulation of a normally functioning cortex with an illumination source of constant intensity. Figures 5.3a - 5.3c are for a stimulation intensity of 50 mW/mm^2 and figures 5.3d - 5.3f are for a stimulation intensity of 60 mW/mm^2.

By using a higher intensity in figures 5.3b and 5.3c, synchronous behavior with a frequency comparable to the 30 mW/mm^2 constant illumination case can be achieved. However, by using a higher intensity, synchronous behavior is induced more quickly. Figures 5.3e and 5.3f show how the frequency of the travelling wave can be further reduced by using a pulsed profile of 60 mW/mm^2 intensity because of the periods when illumination is turned off and the cortex goes back to functioning normally. For a given illumination intensity, pulsed light can reduce the frequency of seizure waves because the stimulatory input rapidly drops to zero when light is turned off, sending the cortex back to a normally functioning state. So increasing the time of no illumination when using a pulsed light source decreases seizure frequency. This difference can be seen between fig. 5.2d, where constant illumination is used, and fig. 5.3e, where pulsed illumination is used.

5.4 Seizure stimulation in parameter space using the ODE model

We turn to bifurcation analysis to give us a picture of what happens in the cortex when illumination of a certain intensity is used. To perform a bifurcation analysis, as in chapter 4, we turn off the stochastic and spatial terms in the cortical model to obtain an underlying set of deterministic ordinary differential equations (ODEs), which helps us gain insight into the complete system of stochastic partial differential equations (SPDEs) that describe the mesoscale cortical model in a simpler way. It has been shown that Hopf bifurcations in the dimensionless ODEs can correspond to travelling waves in the SPDE system [49]. Here, we combine this ODE system with the optogenetic model to study the dynamics of the combined system.

Figure 5.4a shows the values of Γ_e and P_{ee} that cause oscillatory behavior in the ODE model when not stimulated (black) and when stimulated (grey) by optogenetic channels using an illumination intensity of 60 mW/mm^2. The red dot in the figure is located at $\Gamma_e = 0.0012$ and $P_{ee} = 11.0$, which are used in the full SPDE system simulations shown in figures 5.1 - 5.3. These values lie well outside the region of epilepsy in the unstimulated cortex. The seizure prone area in parameter space is vastly increased when optogenetic stimulation is applied. It has been observed, but not shown here, that this area is slightly larger with less distinct boundaries (as expected) for the SPDE system owing to stochasticity.

A bifurcation analysis of the ODE system yields a bifurcation diagram depicting the salient features for the mean soma potential of the excitatory population, h_e, for different illumination intensities as shown in fig. 5.4b. Again, we use $P_{ee} = 11.0$ and $\Gamma_e = 0.0012$ for this analysis. Solid lines indicate stable fixed points, while dashed lines represent unstable ones. Dot-dashed lines and dotted lines indicate maximum and minimum values of h_e achieved during stable and unstable limit cycles, respectively. The asterisk represents a subcritical Hopf bifurcation at 5.1352 mW/mm^2, which gives rise to an unstable limit cycle. At 4.7908 mW/mm^2 the limit cycle stabilizes after going through a saddle node bifurcation, and becomes unstable again after going through another saddle node bifurcation at 33.8682 mW/mm^2. While fig. 5.4b is truncated at 40 mW/mm^2, the limit cycle remains unstable and does not terminate well beyond 100 mW/mm^2,

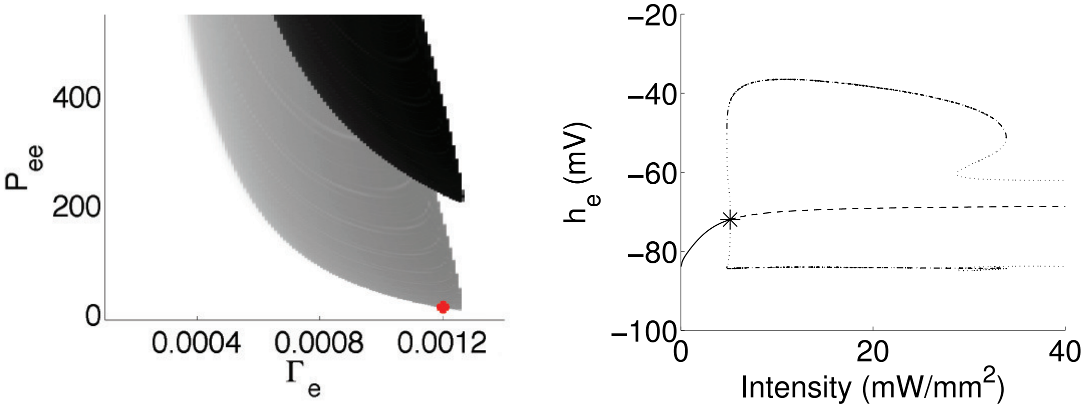

(a) Seizures in parameter space (b) Variation of h_e with intensity

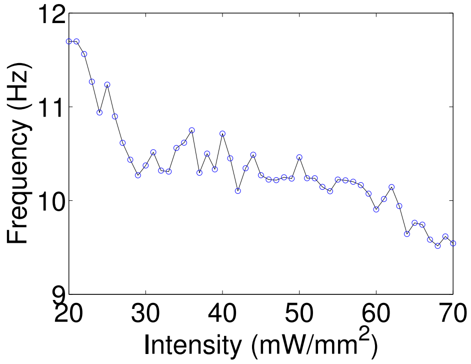

(c) Frequency response

Figure 5.4: Top left: effect of optogenetic stimulation on oscillatory behavior in the Γ_e - P_{ee} parameter space, using a 60 mW/mm^2 illumination intensity (grey) and in an unstimulated cortex (black). The red dot indicates $\Gamma_e = 0.0012$ and $P_{ee} = 11.0$, which are used in the full SPDE system simulations shown in figures 5.1 - 5.3. Top right: Bifurcation diagram for the underlying deterministic ODE system showing the variation of h_e for different illumination intensities. Dashed and solid lines indicate unstable and stable fixed points, respectively. Maximum and minimum values of h_e during stable (dot-dashed) and unstable (dashed) limit cycles arising from a subcritical Hopf bifurcation (asterisk) are also shown. Bottom: Frequency of seizure waves for a given illumination intensity.

which is around the limit of physiologically acceptable illumination intensities[2]. This suggests the combined cortical-optogenetic model is unable to support stable oscillations past 34 mW/mm^2, and so for higher intensities we might be observing a succession of independent columnar spiking events and not entrained spiking seen during stable oscillatory behavior. In the case of an individual spike in mean soma potential, a cortical column relaxes to its resting potential before firing again. This takes longer to produce a spike than the case with continuous oscillatory behavior, where a column can be excited to spike again before reaching resting state. This explains why lower frequency seizure waves are observed when higher illumination intensities are used, a trend which is shown in fig. 5.4c after averaging frequency over multiple simulations of the full SPDE system. For lower intensities, subcortical inputs may aid in exciting or suppressing the system, so the probability of producing seizures decreases for intensities lower than 25 $\mathrm{mW/mm^2}$. For higher intensities, the system will almost always produce seizures, but the frequency of seizure waves is dependent on the magnitude of subcortical and long range inputs. Overall, however, a tendency to produce lower seizure wave frequencies for higher illumination intensities is seen.

---

[2] Prolonged exposure (> 0.5s) at an intensity of 100 mW/mm^2 caused significant tissue damage in animal models [11].

5.5 Summary of original contributions

Epilepsy is a network disorder, and the ability to stimulate individual network elements to determine their role in the function and malfunction of networks would be invaluable to seizure research. Optogenetics offers unparalleled specificity in targeting individual neuron types with high spatial and temporal resolution. In this chapter, we present a way of specifically depolarising the excitatory population in a patch of normally functioning model cortex to produce seizures that generalize. With the help of bifurcation theory, we clearly outline stimulation parameters like illumination intensity that will lead to seizures of a particular frequency and strength. Eventually, this method holds the promise of identifying specific seizure pathways in individuals suffering from epilepsy.

We now provide preliminary insights into the link between metabolic demand and cortical activity. This link will help quantitatively define the relationship between fast time scale neural activity measured by electrodes, and slow time scale, high spatial resolution measurement techniques like positron emission tomography (PET) and functional magnetic resonance imaging (fMRI). In terms of seizure research, this link will be invaluable in understanding the role of cortical energy demands in epileptogenesis, and in maintaining the seizure state.

Chapter 6

Cortical metabolic demands

Among mammalian brains, the human brain stands out in terms of metabolic demand. It consumes the highest share of the body's total energy demands at 20%, despite contributing only about 2% to the total mass of the body [46; 80; 91]. Studies have shown a strong correlation between blood flow and metabolic demand of the brain [74; 75], and consequently, the effect of blood flow on neural activity has also been a topic of intense research [5; 57; 89; 104]. Glucose is the primary source of energy, and is metabolized both oxidatively [46; 89] and non-oxidatively [28], producing ATP, the basic currency of energy in metabolic processes.

The calculation of ATP consumption rates is one way to estimate the total energy demands of the brain, and understand the underlying mechanisms coupling blood flow, metabolic rate and neural activity. Bottom-up approaches, where the energy consumption of individual neurons is calculated by summing up ATP use per neuronal or glial electrical or neurostransmission process, have been presented in [6; 54]. A top-down approach [36] demonstrated that cortical energy demands of mammalian brains is conserved across species and activity levels.

Knowledge of the ATP consumption rate aids in the estimation of the amount of glucose consumed in the cortex, which has been the basis of numerous studies on brain metabolic demands using nuclear magnetic resonance imaging (NMR) [15; 32; 62] and positron emission tomography (PET) [77] in humans. In terms of research on epilepsy, the ketogenic diet has been proposed as a method to stem the effects of epilepsy [8; 94]. A link between a glycolysis model and the meso scale model will facilitate testing this method of seizure suppression, and the role of cortical metabolic dynamics in determining the seizure state. However, to gain further insight into how neural activity levels influence oxidative and non-oxidative consumption of glucose, a measurement of blood oxygen levels, and the cerebral blood flow are also necessary. A mathematical model, based on oxygen phosphorescence quenching readings from rats [4], mimicked the the link between oxygen consumption and blood flow. In humans, models based on PET imaging results [38; 87], and using near-infrared spectroscopy [9] have also tried to simulate the same link. Models connecting the cerebral metabolic rates of oxygen and glucose to cerebral blood flow have also been proposed [53; 88]. In the hyper-excited state associated with diseases like epilepsy and Parkisnon's, studies have tried to understand the role of blood flow [7; 39], and energy metabolism [17; 63; 83; 92].

Here, we aim to estimate the energy demands in terms of ATP and glucose consumption rates in a meso scale mathematical model of the human cortex. For example, in terms of seizure research, the use of a high fat, low carbohydrate diet in epileptic patients where the dietary sources of glucose is restricted, has been shown to be an effective and non-pharmacological treatment modality [93; 90]. This study will help improve the accuracy of cortical models in simulating measured cortical activity, and also help to understand the dynamics and metabolic demands of the cortex during various activity levels.

6.1 Calculating energy demands of the model cortex

Meso-scale models of brain activity offer a practical way of simulating the collective dynamics of millions of neurons without having to take into account the activity of, and the connections between, individual neurons in a region of the brain. Here, we will be looking at the energy demands of the model cortex in terms of ATP and glucose consumption via the cortical model described in chapter 1,

6.1.1 Model for ATP consumption

The energy needed to support cellular metabolism in the mammalian cortex can be attributed to either signaling events (P_s) like depolarisation, and non-signaling events (P_{ns}) like ion movements. The number of adenosine triphosphate (ATP) molecules produced during the oxidation of acetates to generate energy, can be used as a measure of energy consumption in the cortex. From previous bottom-up approaches [6; 54], the total energy (E_{tot}), in units of units of ATP per unit cortical volume per unit time, was calculated by summing the energy demands of signaling and non-signaling events:

$$E_{tot} = E_s + E_{ns} \tag{6.1}$$

Non-signaling energy consumption, which is attributed to ion movement associated with maintaining the resting potentials of neuronal and glial cells is calculated using:

$$E_{ns} = P_{ns,N} \times \eta_N + P_{ns,A} \times \eta_A, \tag{6.2}$$

where N and A represent neurons and astrocytes, $P_{ns,x}$ is the number of ATP molecules consumed per cell (neuron or astrocyte) per second during non-signaling events, and η_x is the concentration of each cell type (neuron or astrocyte) in a given volume of cortex (number of cells/cm^3).

Signaling events like depolarisation, axonal propagation, neurotransmitter cycling etc. contribute to E_s, the energy of signaling events in the cortex.

$$E_s = P_s \times f \times \eta_N \tag{6.3}$$

where P_s is the number of ATP molecules consumed per neuron per spike during signaling events, f is the firing rate in units of spikes per second, and η_N is the concentration of neurons per unit volume.

The top-down approach in [36] showed energy requirements per cell per signaling and non-signaling event is independent of the state of neuronal activity (e.g., sensory activation, awake, asleep, or anesthetized), and are conserved across species. That is, P_s (ATP/(neuron.spike)) and P_{ns} (ATP/(neuron.second) remain constant over a range of activity levels and species. Energy consumption in terms of ATP/s per cm^3 using this method is also estimated via equations 6.1-6.3.

6.1.2 Calculating glucose consumption ($\mathbf{CMR_{glc}}$) from calculated ATP consumption

From the total energy consumed in terms of ATP/s per cm^3, the cerebral metabolic rate (CMR) of glucose oxidation can be calculated by,

$$\mathrm{calcCMR}_{\mathrm{glc(ox)}} = kE_{tot}, \tag{6.4}$$

where k is given by

$$k = \frac{\mathrm{CMR}_{\mathrm{glc}} \times 10^7}{N_A \mathrm{CMR}_{O_2} \rho} = \frac{10^7}{N_A \mathrm{OGI} \rho}, \tag{6.5}$$

N_A is the Avogadro constant and has a value of 6.023×10^{23}/mole, ρ is the tissue density (1.05 g/mL), and OGI is the oxygen to glucose index, also defined as the ratio of cerebral metabolic rate of oxygen CMR_{O_2} to the cerebral metabolic rate of glucose $\mathrm{CMR}_{\mathrm{glc}}$.

Under awake resting conditions, OGI in humans has been measured using PET imaging, and found to be around 5.6 [89]. However, this value changes when the activity level of the cortex changes. For example, during high activity levels associated with epileptic seizures, OGI drops, indicating a higher non-oxidative use of glucose [88].

In [36] P_s and P_{ns} were calculated by comparing calculated $\mathrm{CMR}_{\mathrm{glc}}$ with measured $\mathrm{CMR}_{\mathrm{glc}}$ obtained from PET scans in humans, and 2-deoxyglucose (2DG) measurements in rats. It should be noted that the differences in values of P_s and P_{ns} in [6], [54] and [36] are due to the assumed values of membrane rest potentials [36].

6.2 Preliminary results

The data used to arrive at the results presented in [36] were obtained from studies of rats and humans under normal awake resting conditions, or some form of an anesthetized state. Under these conditions, there is an almost stoichiometric relation between the metabolic rates of glucose and oxygen, suggesting that the ATP produced is mostly from the oxidative use of glucose. Stoichiometric conditions would give us an OGI of 6, while the measured OGI during the activity levels discussed in [36] is around 5.6. To this end, we first calculate the use of ATP in the model cortex

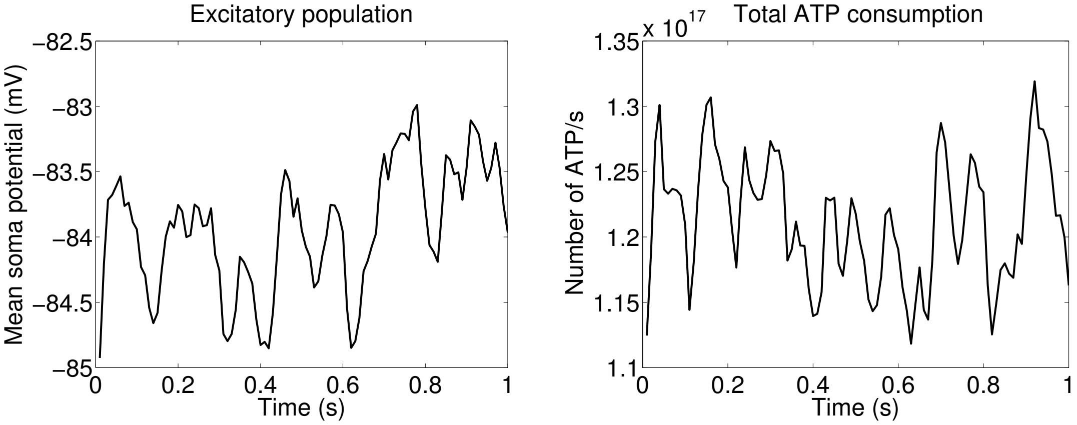

(a) Mean soma potential at a point

(b) Total ATP consumption per cm^3

Figure 6.1: Mean soma potential of the excitatory population and energy consumption in terms of number of ATP per second per unit volume in the model cortex during normal function. The mean firing rate of the excitatory population is calculated using the mean soma potential via a sigmoid function as described in [58]. The ATP consumption of signaling events, in turn, is directly calculated from the firing rate using equation 6.3. Non-signaling events have a total ATP consumption rate of 2.9372×10^{16} per second per cm^3 which remains constant. Total ATP consumption in figure 6.1b includes both signaling and non-signaling events. Parameters: $P_{ee} = 11.0$, $\gamma_e = 0.0012$, $\alpha = 1.15$.

under normal function, which is presented in figure 6.1a in terms of the mean soma potential of the excitatory population of neurons.

In figure 6.1b the total number of ATPs consumed per second per cm^3 of cortex is presented as a function of time at a point in the cortex. This is the total energy consumption rate of both signaling and non-signaling events combined. The consumption rate is calculated at normal function, which means OGI is around 5.6. The amount of glucose consumed oxidatively can be calculated using equation 6.4.

The total (oxidative + non-oxidative) amount of glucose consumed can then be calculated by:

$$\text{calcCMR} = \frac{\text{calcCMR}_{\text{glc(ox)}} \times 6}{OGI} \tag{6.6}$$

Specific measurements of blood oxygen levels, and the cerebral blood flow at different activity levels will aid in defining a quantitative relationship between firing rate and OGI.

While there is still a long way to go before a complete quantitative link between electrode measurements and imaging techniques can be established, the meso-scale model offers an excellent means to explore this relationship, and we have provided an outline of the steps involved in achieving this goal. Additionally, this is also a first step in building a physiologically relevant model of the cortex that takes into account both neural activity and its dependence on the cardiovascular supply system.

Chapter 7

Conclusion

7.1 Summary

Optogenetics is a highly specific, targeted stimulation technique offering a unique way to study brain function at levels ranging from individual neurons to complex neural circuits. With respect to epilepsy, it has the potential to extend significantly the understanding of epileptogenesis (seizure initiation), and has the potential to improve the specificity, safety, and efficacy of a novel treatment modality for epilepsy that could pave the way to alleviating human suffering. While testing of optogenetics for use in humans is still a few years away given the intricacies of the technology, we are able to explore the effects of this cortical stimulation technique via a physiologically relevant, meso-scale mathematical model of the human cortex. With the help of the model, we were able to make novel contributions that demonstrate the efficacy of optogenetics as both a seizure control and seizure stimulation technique.

First, we demonstrated the birth and propagation of seizure waves in a two dimensional model of the human cortex when subject to hyperexcited subcortical inputs. We then expressed the essentially single cell level dynamics of channelrhodopsin-2 (ChR2) ion channels at the meso-scale using a probabilistic formulation. The probabilistic formulation is scale free, and facilitates simulation of channel activity at any scale. By using these channels on the inhibitory population of the meso-scale model, we were able to depolarize the inhibitory population at a higher rate, which suppressed the excessive excitatory neural activity characteristic of seizures. This work demonstrated the potential of optogenetics as a robust seizure control modality in an open loop configuration for various parameter ranges that gave rise to weak and strong seizures in the meso-scale model.

Next, we developed a closed loop controller that uses the measured potential calculated from the excitatory mean soma potential to determine the intensity of light required to optimally illuminate the ChR2 expressing inhibitory population. We successfully suppressed seizures in two parameter spaces that were identified as being the most likely model parameter ranges that correspond well with patient seizure data. In addition, comparisons with tuned open loop controllers clearly showed the advantages and efficiency of our close loop strategy. The ability to optimally calculate control effort from clinical recordings is of great importance if optogenetics is to be adopted as a strategy for seizure inhibition in patients.

Using a simpler ODE model obtained by discarding the spatial and stochastic terms from the full SPDE cortical model, we performed a bifurcation analysis of the combined cortico-optogenetic system under unstimulated, open loop, and closed loop stimulated conditions for two parameter spaces. In the parameter space defined by the subcortical excitatory inputs P_{ee} and the gain on the excitatory post-synaptic potential Γ_e, both open and closed loop systems delayed the start of seizure activity until much higher excitatory inputs were available, the closed loop method did so using optimal effort. In the second parameter space defined by the gain on the inhibitory post-synaptic potential Γ_i and the slope at the inflection point of the sigmoid function describing the excitatory firing rate $\tilde{g}_e$, seizure activity was successfully suppressed for the entire range of physiologically relevant parameter values. This part of our work further demonstrates the efficacy of our closed loop control strategy, and also highlights the potency of optogenetics as a spatially, temporally and cell type specific seizure control strategy.

We demonstrated the use of optogenetics as a seizure stimulation mechanism by expressing the ChR2 ion channels in the excitatory population. We depolarized the excitatory cells in a patch of normally functioning model cortex, and were able to drive the entire model cortex into a seizure state. Interestingly, we observed that higher intensities of illumination produced seizure waves of lower frequency, and determined via bifurcation analysis that the stable limit cycle signifying sustained synchronous oscillatory activity in the model cortex was rendered unstable at higher illumination intensities. The spatial, temporal, and cell type specificity this stimulation technique offers would be invaluable for use in epilepsy surgery to determine seizure causing areas, or to study the origins and propagation of seizure waves in the human cortex.

Finally, we made a start in exploring the connection between cortical activity and metabolic demand through a further development in the meso scale model. An understanding of this connection would not only help us build more physiologically relevant models of brain activity, but also help specify the link between fast temporal activity measured by electrodes and slow, spatially refined measurements of brain activity obtained from imaging techniques like PET and fMRI. For seizure research, this link will help tailor dietary based treatment strategies that would be invaluable in cases of pharmacologically resistant epilepsy, or treating epileptogenic zones that are physically hard to reach.

7.2 Future work

While this study suggests the use of optogenetics to inhibit seizure waves is possible, there are a number of improvements that can be made. The light cone produced by a light source will render variable illumination in the spatial domain [11]. This can be exploited for better spatial and temporal control of the activation of optogenetic channels. We can also account for the spatial electrode profile in our measurements to improve the accuracy of the measured potential, and also account for spatial variations of the cortical model, for example the presence of gyri and sulci, making only a region of model cortex easily accessible to optogenetic stimulation. In chapter 2 we showed optogenetic control is still effective when only parts of the cortical model are illuminated.

However, a limited region of stimulation might require higher illumination intensities, and a more refined tuning of the gain terms.

Second, as stated in chapter 1, different types of inhibitory neurons could be responsible for specific types of seizures. Previous work [85], has explored the consequences of stimulating only a fraction of the neurons in the meso-scale model to inhibit seizure activity. Using constant illumination, control was achieved when only a third of the inhibitory population in the area of a seizure hotspot was stimulated with higher illumination intensities. It would be interesting to investigate how stimulation via different neuron subtypes influences the dynamics of seizures in the human cortex. While we currently do not have sufficient data on different types of human interneurons to include them in our model, in rats [45; 13] and in mice [82], inhibitory neurons can be divided into three main subtypes, fast spiking, latent spiking and another group containing burst spiking and regular spiking neurons. The meso-scale model offers a very suitable platform to incorporate the dynamics of these neurons because the layout of the equations of the model facilitates the inclusion of more sub-types of neurons.

Third, we have seen seizures can be more abrupt in the $\tilde{g}_e - \Gamma_i$ parameter space, which suggests exploring control actuation via the excitatory population to mitigate the effect of synaptic delays by suppressing excessive excitation at the source. One way of doing this is to use halorhodpsin, which is an anion pump that is activated by light of wavelength around 570 nm [24], to hyperpolarize the excitatory neurons. Apart from avoiding synaptic delays, another advantage of using this method in conjunction with our current method of control is the option of selectively stimulating either inhibitory or excitatory neurons, or stimulating both together to provide more flexible control. In the same vein, while chapter 5 only explores the use of cation pumps in the excitatory population of the meso-scale cortical model, the wide variety of illumination options, light activated ion channels, and their temporal and spatial specificity could provide more interesting insights into seizures and cortical dynamics in general. Clearly, numerical simulations will provide a much less expensive way to investigate these possibilities.

Fourth, it will be interesting to study the effects of optogenetic stimulation of subcortical brain structures. Some seizures specifically arise because of the dynamic interplay between the cortex and subcortical regions. For example, in [72], seizures arising from cortical injury, and maintained by the interplay between the thalamus and cortical regions were identified in rats. Additionally, in the same paper, thalamocortical neurons were stimulated via closed loop optogenetic control to inhibit seizures caused by cortical injury. The meso-scale mathematical model of the cortex used in this work does not yet include detailed equations describing the dynamic interplay between subcortical and cortical regions, which may only be a feature in some seizures. Instead, we explore whether seizures caused by higher excitatory subcortical inputs or changes in the inflection point of the sigmoid function that describes the mean excitatory firing rate could be controlled with optogenetics in the cortex, which is a much more accessible part of the brain to stimulate than subcortical regions. The control of specific seizures might entail other, more involved strategies. This first attempt at exploring whether cortical feedback stimulation could work has proven successful even when the precipitating cause is subcortical inputs. In the future, a complex mathematical model of dynamic cortico-subcortical interactions, will aid in studying the effect of applying optogenetic control to subcortical regions, and also provide insight into the effects of cortical stimulation when the pathway to seizures is the dynamic interplay between the cortex and subcortical regions.

Finally, a measure of the cerebral metabolic rate gives us another way of verifying the meso scale model. First, model parameters can be obtained by the path tracing method described in [22; 23] for various activity levels. Next, the cerebral metabolic rate of glucose can be calculated using equations 6.1-6.4. Finally, we can compare calculated values of $\mathrm{CMR}_{\mathrm{glc}}$ with measured values of $\mathrm{CMR}_{\mathrm{glc}}$ obtained from PET imaging, which gives us averaged consumption rates, or NMR imaging for the instantaneous rate of use of glucose. Dynamic models of brain energy metabolism have been presented in a number of articles, for example [71] and [18]. Models of the cerebral metabolic rates of glucose, oxygen and blood flow are also available: cerebral blood flow (CBF) & CMR_{O_2} [87; 38; 9]; CMR_{O_2}, $\mathrm{CMR}_{\mathrm{glc}}$ and CBF [53; 88]; only $\mathrm{CMR}_{\mathrm{glc}}$ [77; 15; 62; 60]. However, there is no direct link between the measurable variables of the meso-scale model (e.g. measured potential h_m [58]) and the cerebral metabolic rates for glucose and other metabolites. The link might be via the mean firing rate of the meso-scale model, which would now be a function of the mean soma potential and the available energy in terms of ATP.

Bibliography

[1] Abraham RH, Shaw CD (1992) Dynamics: The Geometry of Behavior, 2nd edn. Addison-Wesley Publishing Company, Redwood City, CA, USA

[2] Adamantidis A, Carter MC, Lecea L (2009) Optogenetic deconstruction of sleepwake circuitry in the brain. Frontiers in Molecular Neuroscience 2(31):1–9

[3] Ahmari SE, Spellman T, Douglass NL, Kheirbek MA, Simpson HB, Deisseroth K, Gordon JA, Hen R (2013) Repeated cortico-striatal stimulation generates persistent OCD-like behavior. Science 340(6137):1234–1239

[4] Ances BM, Wlison DF, Greenber JH, Detra JA (2001) Dynamic changes in cerebral blood flow, O_2 tension, and calculated cerebral metabolic rate of O_2 during functional activation using oxygen phosphorescence quenching. Journal of Cerbral Blood Flow and Metabolism 21:511–516

[5] Attwell D, Iadecola C (2002) The neural basis of functional brain imaging signals. Trends in Neuroscience 25(12):621–625

[6] Attwell D, Laughlin SB (2001) An energy budget for signalling in the grey matter of the brain. Journal of Cerebral Blood Flow and Metabolism 21(10):1133–1145

[7] Attwell RA, Zubal IG, Stokking R, Studholme C, Corsi M, Seibyl JP, Spencer SS (2000) Decreased cerebral blood flow during seizures with ictal SPECT injections. Epilepsy Research 40(1):53–61

[8] Barañano BW, Hartman AL (2008) The ketogenic diet: uses in epilepsy and other neurologic illnesses. Current Treatment Options in Nerology 10(6):410–419

[9] Boas DA, Strangman G, Culver JP, Hoge RD, Jasdzewski G, Poldrack RA, Rose BR, Mandeville JB (2003) Can the cerebral metabolic rate of oxygen be estimated with near-infrared spectroscopy? Physics in Medicine and Biology 48:2405–2418

[10] Bojak I, Liley DTJ (2005) Modeling the effects of anesthesia on the electroencephalogram. Physical Review E 71(2):041,902

[11] Cardin JA, Carlén M, Meletis K, Knoblich U, Zhang F, Deisseroth K, Tsai LH, Moore CL (2010) Targeted optogenetic stimulation and recordings of neurons *in vivo*, using cell type specific expression of channelrhodopsin-2. Nature Protocols 5(2):247–254

[12] Cascino GD (2004) Surgical treatment for epilepsy. Epilepsy Research 60(2-3):179–186

[13] Cauli B, Audinat E, Lambolez B, Angulo MC, Ropert N, Tsuzuki K, Hestrin S, Rossier J (1997) Molecular and physiological diversity of cortical nonpyramidal cells. Journal of Neuroscience 17(10):3894–3906

[14] Chen TW, Wardill TJ, Sun Y, Pulver SR, Renninger SL, Baohan A, Schreiter ER, Kerr RA, Orger MB, Jayaraman V, Looger LL, Svoboda K, Kim DS (2013) Ultrasensitive fluorescent proteins for imaging neuronal activity. Nature 499:295–300

[15] Chen W, Novotny EJ, Zhu XH, Rothman DL, Shulman RG (1993) Localized 1H NMR measurement of glucose consumption in human brain during visual stimulation. Proceedings of the National Academy of Sciences USA 90:9896–9900

[16] Chuong AS, Miri ML, Busskamp V, Matthews GAC, Acker LC, Soresnsen AT, Young A, Klapoetke NC, Henninger MA, Kodandaramaiah SB, et al (2014) Noninvasive optical inhibition with a red-shifted microbial rhodopsin. Nature Neuroscience 17:1123–1129

[17] Cloix JF, Hévor T (2009) Epilepsy, regulation of brain energy metabolism and neurotransmission. Current Medicinal Chemistry 16(7):841–853

[18] Cloutier M, Bolger FB, Lowry JP, Wellstead P (2009) An integrative dynamic model of brain energy metabolism using in vivo neurochemical measurements. Journal of Computational Neuroscience 27(3):391–414

[19] Cobos I, Calcagnotto ME, Vilaythong AJ, Thwin MT, Noebels JL, Baraban SC, Rubenstein JL (2005) Mice lacking Dlx1 show subtype-specific loss of interneurons, reduced inhibition and epilepsy. Nature Neuroscience 8(8):1059–1068

[20] Cossart R, Dinocourt C, Hirsch JC, Merchan-Perez A, De Felipe J, Ben-Ari Y, Esclapez M, Bernard C (2001) Dendritic but not somatic GABAergic inhibition is decreased in experimental epilepsy. Nature Neuroscience 4(1):52–62

[21] Covington III HE, Lobo MK, Maze I, Vialou V, Hayman JM, Zaman S, LaPlant Q, Mouzon E, Ghose S, Tamminga CA, Neve RL, Deisseroth K, Nestler EJ (2010) Antidepressant effect of optogenetic stimulation of the medial prefrontal cortex. Journal of Neuroscience 30(48):16,082–16,090

[22] Dadok V, Kirsch HE, Sleigh JW, Lopour BA, Szeri AJ (2013) A probabilistic framework for a physiological representation of dynamically evolving sleep state. Journal of Computational Neuroscience DOI 10.1007/s10827-013-0489-x

[23] Dadok V, Kirsch HE, Sleigh JW, Lopour BA, Szeri AJ (2015) A probabilistic method for determining cortical dynamics during seizures. To appear in the Journal of Computational Neuroscience

[24] Deisseroth K (2011) Optogenetics. Nature Methods 8:26–29

[25] Doedel EJ, Paffenroth RC, Champneys AR, Dercole F, Fairgrieve TF, Kuznetsov YA, Oldeman BE, Sandstede B, Wang X, Zhang C (2008) Continuation and Bifurcation Software for Ordinary Differential Equations. Available via http://www.python.org/ftp/python/2.7.2/python-2.7.2-macosx10.3.dmg

[26] Doyle JC, Francis BA, Tannenbaum AR (1990) Feeddback control theory. Macmillan Publishing, London, UK

[27] Fisher RS, van Emde Boas W, Blume W, Elger C, Genton P, Lee P, Engel J (2005) Epileptic seizures and epilepsy: Definitions proposed by the international league against epilepsy (ILAE) and the international bureau for epilepsy (IBE). Epilepsia 46(4):470–472

[28] Fox PT, Raichle ME (1986) Focal physiological uncoupling of cerebral blood flow and oxidative metabolism during somatosensory stimulation in human subjects. Proceedings of the National Academy of Sciences USA 83(4):1140–1144

[29] Franklin GF, Powell JD, Emami-Naeni A (2002) Feeddback control of dynamics systems, 4th edn. Prentice Hall, New Jersey, USA

[30] Gluckman B, Nguyen H, Weinstein S, Schiff S (2001) Adaptive electric field control of epileptic seizures. Journal of Neuroscience 21(2):590–600

[31] Grossman N, Nikolic K, Toumazou C, Degenaar P (2011) Modeling study of the light stimulation of a neuron cell with channelrhodopsin-2 mutants. IEEE Transactions on Biomedical Engineering 58(6):1742–1751

[32] Gruetter R, Novotny EJ, Boulware SD, Rothman DL, Mason GF, Shulman GI, Shulman RG, Tamborlan WV (1992) Direct measurement of brain glucose concentrations in humans by 13C NMR spectroscopy. Proceedings of the National Academy of Sciences USA 89(3):1109–1112

[33] Hale JK, Koçak H (1991) Dynamics and Bifurcations. Springer-Verlag, New York, USA

[34] Hegemann P, Ehlenbeck S, Gradmann D (2005) Multiple photocycles of channelrhodopsin. Biophysical Journal 89:3911–3918

[35] Hight DF, Dadok VM, Szeri AJ, Garcia PS, Voss L, Sleigh JW (2014) Emergence from anesthesia and the sleep-manifold. Frontiers in Systems Neuroscience 8(146):1–14

[36] Hyder F, Rothman DL, Bennett MR (2013) Cortical energy demands of signaling and nonsignaling components in brain are conserved across mammalian species and activity levels. Proceedings of the Natoinal Academy of Sciences 110(9):3549–3554

[37] Iasemidis LD, Pardalos P, Sackellares JC, Shiau DS (2011) Quadratic binary programming and dynamical system approach to determine the predictability of epileptic seizures. Journal of Combinatorial Optimization 5(1):9–26

[38] Ibaraki M, Shinohara Y, Nakamure K, Miura S, Kinoshita F, Kinoshita T (2010) Interindividual variations of cerebral blood flow, oxygen delivery, and metabolism in relation to hemoglobin concentration measured by positron emission tomography in humans. Journal of Cerebral Blood Flow and Metabolism 30:1296–1305

[39] Ingvar M (1986) Cerebral blood flow and metabolic rate during seizures relationship to epileptic brain damage. Annals of the New York Academy of Sciences 462:194–206

[40] Jerger K, Schiff SJ (1995) Periodic pacing an in vitro epileptic focus. Journal of Neurophysiology 73:876–879

[41] Jette N, Beghi E, Haesdorffer D, Moshé SL, Zuberi SM, Medina MT, Bergen D (2015) ICD coding for epilepsy: Past, present, and future - A report by the international league against epilepsy task force on ICD codes in epilepsy. Epilepsia 56(3):348–355

[42] Jouny CC, Franaszczuk PJ, Bergey GK (2011) Improving early seizure detection. Epilepsy and Behavior 22 (Suppl 1):544–548

[43] Kandel ER, Schwartz J, Jessell T (2000) Principles of neural science (4th edn). McGraw-Hill, New York, USA

[44] Kannathal N, Choo ML, Acharya UR, Sadasivan PK (2005) Entropies for detection of epilepsy in EEG. Computer Methods and Programs in Biomedicine 80(3):187–194

[45] Kawaguchi Y, Kubota Y (1997) GABAergic cell subtypes and their synaptic connections in rat frontal cortex. Cerebral Cortex 7(6):476–486

[46] Kety SS (1957) The general metabolism of the brain in vivo In: Metabolism of the nervous system. Pergammon, London, UK

[47] Kim T, McCall JG, Jung YH, Huang X, Siuda ER, Li Y, Song J, Song YM, Pao HA, Kim RH, Lu C, Lee SD, Song I, Shin GC, Al-Hasani R, Kim S, Tan MP, Huang Y, Omenetto FG, Rogers JA, Bruchas MB (2013) Injectable, cellular-scale optoelectronics with applications for wireless optogenetics. Science 340(6129):211–216

[48] Kramer MA, Kirsch HE, Szeri AJ (2005) Pathological pattern formation and cortical propagation of epileptic seizures. Journal of the Royal Society Interface 2:113–127

[49] Kramer MA, Szeri AJ, Sleigh JW, Kirsch HE (2007) Mechanisms of seizure propagation in a cortical model. Journal of Computational Neuroscience 22(1):63–80

[50] Kravitz AV, Freeze BS, Parker PRL, Kay K, Thwin MT, Deisseroth K, Kreitzer AC (2010) Regulation of parkinsonian motor behaviors by optogenetic control of basal ganglia circuitry. Nature 466:622–626

[51] Krook-Magnuson E, Armstrong C, Oijala M, Soltesz I (2013) On-demand optogenetic control of spontaneous seizures in temporal lobe epilepsy. Nature Communications 4(1376):1–8

[52] Kumar Y, Dewal ML, Anand RS (2012) Epileptic seizures detection in EEG using DWT-based ApEn and artificial neural network. Signal, Image and Video Processing DOI 10.1007/s11760-012-0362-9

[53] Kuwabara H, Ohta S, Brust P, Meyer E, A G (1992) Density of perfused capillaries in living human brain during functional activation. Progress in Brain Research 91:209–215

[54] Lennie P (2003) The cost of cortical computation. Current Biology - Cell 13(6):493–497

[55] Liley DTJ, Cadusch PJ, Dafilis MP (2001) A spatially continuous mean field theory of electrocortical activity. Network: Computation in Neural System 13:67–113

[56] Litt B, Esteller R, Echauz J, D'Alessandro M, Shor R, Henry T, Pennell P, Epstein C, Bakay R, Dichter M, Vachtsevanos G (2001) Epileptic seizures may begin hours in advance of clinical onset: a report of five patients. Neuron 30(1):51–64

[57] Logothetis NK (2002) The neural basis of the blood-oxygen-level-dependent functional magnetic resonance imaging signal. Philosophical Transactions of the Royal Society of London B - Biological Sciences 357(1424):1003–1037

[58] Lopour BA, Szeri AJ (2010) A model of feedback control for the charge-balanced suppression of epileptic seizures. Journal of Computational Neuroscience 28:375–387

[59] Lopour BA, Tasoglu S, Kirsch HE, Sleigh JW, Szeri AJ (2011) A continuous mapping of sleep states through association of EEG with a mesoscale cortical model. Journal of Computational Neuroscience 30:470–481

[60] Lund-Andersen H (1979) Transport of glucose from blood to brain. Physiological Reviews 59(2):305–352

[61] Marreiros AC, Daunizeau J, Kiebel SJ, Friston KJ (2008) Population dynamics: Variance and the sigmoid activation function. Neuroimage 42:147–157

[62] Mason GF, Behar KL, Rothman DL, Shulman RG (1992) NMR determination of intracerebral glucose concentration and transport kinetics in rat brain. Journal of Cerebral Blood Flow and Metabolism 12(3):448–455

[63] Meldrum BS, Nisson B (1976) Cerebral blood flow and metabolic rate early and late in prolonged epileptic seizures induced in rats by bicuculline. Brain 99(3):523–542

[64] Mormann F, Kreuz T, Andrzejak RG, David P, Lehnertz K, Elger CE (2003) Epileptic seizures are preceded by a decrease in synchronization. Epilepsy Research 53(3):173–185

[65] Mutter M, Munch TA (2013) Strategies for expanding the operational range of channelrhodopsin in optogenetic vision. PLoS One 8(11):e81,278

[66] Nagel G, Szellas T, Huhn W, Kateriya S, Adeishvili N, Berthold P, Ollig D, Hegemann P, Bamberg E (2003) Channelrhodopsin-2, a directly light-gated cation-selective membrane channel. Proceedings of the National Academy of Sciences 100(24):13,940–13,945

[67] Nigam VP, Graupe D (2004) A neural-network-based detection of epilepsy. Neurological Research 26(1):55–60

[68] Nordli DR (2005) Idiopathic generalized epilepsies recognized by the international league of against epilepsy. Eplepsia 46(9):48–56

[69] Nunez PL, Srinivasan R (2006) Electric fields of the brain: The neurophysics of EEG, 2nd edn. Oxford University Press, New York

[70] Orosco L, Laciar E, Correa AG, Torres A, Graffigna JP (2009) An epileptic seizures detection algorithm based on the empirical mode decomposition of EEG. In: Conference Proceedings of IEEE Engineering in Medicine and Biology Society, pp 2651–2654

[71] Patel AB, de Graaf RA, Mason GF, Kanamatsu T, Rothman DL, Shulman RG, Behar KL (2004) Glutamatergic neurotransmission and neuronal glucose oxidation are coupled during intense neuronal activation. Journal of Cerebral Blood Flow and Metabolism 24(9):972–985

[72] Paz TP, Davidson TJ, Frechette ES, Delord B, Parada I, Peng K, Deisseroth K, Huguenard JR (2013) Closed-loop optogenetic control of thalamus as a tool for interrupting seizures after cortical injury. Nature Neuroscience 16:64–70

[73] Peled A (2011) Optogenetic neuronal control in schizophrenia. Medical Hypotheses 76(6):914–921

[74] Pellerin L, Magistretti PJ (1994) Glutamate uptake into astrocytes stimulates aerobic glycolysis: a mechanism coupling neuronal activity to glucose utilization. Proceedings of the National Academy of Sciences USA 91(22):10,625–10,629

[75] Pellerin L, Bouzier-Sore AK, Aubert A, Serres S, Merle M, Costalat R, Magistretti PJ (2007) Activity-dependent regulation of energy metabolism by astrocytes: an update. Glia 55(12):1251–1262

[76] Ramgopal S, Thome-Souza S, Jackson M, Kadish NE, Ferná IS ndez, Klehm J, Bosl W, Reinsberger C, Schachter S, Loddenkemper T (2014) Seizure detection, seizure prediction, and closed-loop warning systems in epilepsy. Epilepsy and Behavior 37:291–307

[77] Reivich M, Kuhl D, Wolf A, Greenberg J, Phelps M, Ido T, Casella V, Fowler J, Hoffman E, Alavi A, Som P, Sokoloff L (1979) The [18F]fluorodeoxyglucose method for the measurement of local cerebral glucose utilization in man. Circulation Research 44(1):127–137

[78] Richardson K, Schiff S, Gluckman B (2005) Control of travelling waves in mammalian cortex. Physical Review Letters 94(2):028,103

[79] Richardson KA, Gluckman BJ, Weinstein SL, Glosch CE, Moon JB, Gwinn RP, Gale K, Schiff SJ (2003) In vivo modulation of hippocampal epileptiform activity with radial electric fields. Epilepsia 44(6):768–777

[80] Rolfe DFS, Brown GC (1997) Cellular energy utilization and molecular origin of standard metabolic rate in mammals. Physiological Review 77:731–758

[81] Romanin C (2011) Extending optogenetics to a Ca(2+)-selective channel. Chemistry and Biology 18(7):820–821

[82] Rudy B, Fishell G, Lee S, Hjerling-Leffler J (2011) Three groups of interneurons account for nearly 100% of neocortical GABAergic neurons. Developmental Neurobiology 71(1):45–61

[83] Sakamoto S, Takami T, Tsuyuguchi N, Morino M, Ohata K, Inoue Y, Ide W, Hashimoto I, Kamada H, Tanaka H, Hara M (2009) Prediction of seizure outcome following epilepsy surgery: asymmetry of thalamic glucose metabolism and cerebral neural activity in temporal lobe epilepsy. Seizure 18(1):1–6

[84] Schacter SC, Saper CB (1998) Vagus nerve stimulation. Epilepsia 39(7):677–807

[85] Selvaraj P, Sleigh JW, Freeman WJ, Kirsch HA, Szeri AJ (2014) Open loop optogenetic control of simulated cortical epileptiform activity. Journal of Computational Neuroscience 36(3):515–525

[86] Selvaraj P, Sleigh JW, Freeman WJ, Kirsch HA, Szeri AJ (2015) Optogenetic induced epileptiform activity in a model human cortex. Springer Plus 4(155)

[87] Shulman RG, Hyder F, Rothman DL (1997) A model for the coupling between cerebral blood flow and oxygen metabolism during neural stimulation. Journal of Cerebral Blood Flow and Metabolism 17:64–72

[88] Shulman RG, Hyder F, Rothman DL (2001) Cerebral energetics and the glycogen shunt: Neurochemical basis of functional imaging. Proceedings of the National Academy of Sciences USA 98(11):6417–6422

[89] Siesjo B (1978) Brain Energy Metabolism. Wiley, New York, USA

[90] Sinha SR, Kossoff EH (2005) The ketogenic diet. Neurologist 11(3):161–170

[91] Sokoloff L (1960) The metabolism of the central nervous system in vivo In: Handbook of Physiology, Section I, Neurophysiology, vol 3. American Physiological Society, Washington DC, USA

[92] Spanaki MV, Kopylev L, DeCarli C, Gaillard WD, Liow K, Fazilat S, Reeves P, Sato S, Kufta C, Theodore WH (2000) Postoperative changes in cerebral metabolism in temporal lobe epilepsy. Archives of Neurology 57(10):1447–1452

[93] Stafstrom CE (2004) Dietary approaches to epilepsy treatment: Old and new options on the menu. Epilespy Currents 4(6):215–222

[94] Stafstrom CE, Rho JM (2012) The ketogenic diet as a treatment paradigm for diverse neurological disorders. Frontiers in Pharmacology 3:59

[95] Steyn-Ross DA, Steyn-Ross ML, Sleigh JW, Liley DTJ (1999) Theoretical electroencephalogram stationary spectrum for a white-noise-driven cortex: Evidence for a general anesthetic-induced phase transition. Physical Review E 60:7299

[96] Steyn-Ross ML, Steyn-Ross DA, Sleigh JW, Whiting DR (2003) Theoretical predictions for spatial covariance of the electroencephalographic signal during the anesthetic-induced phase transition: Increased correlation length and emergence of spatial self-organization. Physical Review E 68:021,902

[97] Steyn-Ross ML, Steyn-Ross DA, Wilson MT, Sleigh JW (2007) Gap junctions mediate large-scale turing structures in a mean-field cortex driven by subcortical noise. Physical Review E 76:011,916

[98] Strogatz SH (1994) Nonlinear dynamics and chaos. Perseus Books, Reading, Massachussetts, USA

[99] Su Y, Radman T, Vaynshteyn J, Parra LC, Bikson M (2008) Effects of high-frequency stimulation on epileptiform activity in vitro: ON/OFF control paradigm. Epilepsia 49(9):1586–1593

[100] The Epilepsy Foundation (accessed 2014) Epilepsy Stats and Facts. World Wide Web http://www.epilepsy com/connect/forums/living-epilepsy-adults/epilepsy-stats-and-facts

[101] The Epilepsy Foundation (accessed 2014) Who Gets Epilepsy. World Wide Web http://www.epilepsy com/learn/epilepsy-101/who-gets-epilepsy

[102] Tønnesen J, Sørensen A, Deisseroth K, Lundberg C, Kokaia M (2009) Optogenetic control of epileptiform activity. Proceedings of the National Academy of Sciences, USA 106:12,162–12,167

[103] Ursino M, LaCara GE (2006) Travelling waves and EEG patterns during epileptic seizure: Analysis with an integrate-and-fire neural network. Journal of Theoretical Biology 242(1):171–187

[104] Vafaee MS, Vang K, Bergersen LH, Gjedde A (2012) Oxygen consumption and blood flow coupling in human motor cortex during intense finger tapping: implication for a role of lactate. Journal of Cerebral Blood Flow and Metabolism 32:1859–1868

[105] Yizhar O, Fenno LE, Davidson TJ, Mogri M, Deisseroth K (2011) Optogenetics in neural systems. Neuron 71(1):9–34

[106] Zhang F, Wang LP, Brauner M, Liewald JF, Kay K, Watzke N, Wood PG, Bamberg E, Nagel G, Gottschalk A, Deisseroth K (2007) Multimodal fast optical interrogation of neural circuitry. Nature 446(7136):633–639